tRNA modifications during translation

The roles of dihydrouridine and queuosine

Dissertation zur Erlangung des Grades

“Doktor der Naturwissenschaften”

im Promotionsfach Pharmazie

am Fachbereich Chemie, Pharmazie, Geographie und Geowissenschaften

der Johannes Gutenberg-Universität Mainz

Lea-Marie Kilz, geb. Vogt

geboren in [redacted]

Mainz, Mai 2024

JOHANNES GUTENBERG UNIVERSITÄT MAINZ

JG|U

Dekanin: Prof. Dr. Eva Rentschler

1. Berichterstatter: [redacted]
2. Berichterstatterin:

D77 (Dissertation Mainz)

Die vorliegende Arbeit wurde am Institut für Pharmazeutische und Biomedizinische Wissenschaften der Johannes Gutenberg-Universität in Mainz zur Erlangung des Grades „Doktor der Naturwissenschaften“ unter der Betreuung von [redacted] angefertigt.

1. Berichterstatter:
[redacted]
Fachbereich Chemie, Pharmazie, Geographie und Geowissenschaften
Institut für Pharmazeutische und Biomedizinische Wissenschaften
Johannes Gutenberg-Universität Mainz

2. Berichterstatterin:
[redacted]
Fachbereich Chemie, Pharmazie, Geographie und Geowissenschaften
Institut für Pharmazeutische und Biomedizinische Wissenschaften
Johannes Gutenberg-Universität Mainz

Hiermit versichere ich eidesstattlich:

a) Ich habe die jetzt als Dissertation vorgelegte Arbeit selbst angefertigt und alle benutzten Hilfsmittel (Literatur, Apparaturen, Material) in der Arbeit angegeben.

b) Ich habe oder hatte die jetzt als Dissertation vorgelegte Arbeit nicht als Prüfungsarbeit für eine staatliche oder andere wissenschaftliche Prüfung eingereicht.

c) Ich hatte weder die jetzt als Dissertation vorgelegte Arbeit noch Teile davon bei einer anderen Fakultät bzw. einem anderen Fachbereich als Dissertation eingereicht.

_____ _____

Ort, Datum Unterschrift

Danksagung

[redacted]

Contents

Abstract

The high and still increasing variety of tRNA modifications is crucial for all roles tRNA is playing in biological systems. tRNA modifications have been shown to modulate translational processes, thereby regulating gene expression, especially as reaction to stress stimuli. The dihydrouridine (D) modification affects tRNA flexibility and is thus thought to play an important role in the overall tRNA structure and function. However, it is still largely unknown whether D is involved in translation and whether the NADPH-dependent synthesis of D is affected by stress stimuli. Here, the intracellular redox state in *Escherichia coli (E. coli)* was altered using the bipyridine salt paraquat which resulted in different sensitivities of the three tRNA-dihydrouridine synthases (Dus) towards oxidative stress. The activities of DusB and DusC were severely affected by paraquat, whereas DusA was highly active even under paraquat treatment. The analysis of *E. coli* polysome preparations did not reveal an indication that D plays a specific role in translation, although D-modified tRNAs were found on actively translating polysomes. Whereas D is a rather simple structured modification of the nucleobase, another project focused on the hypermodification queuosine (Q), which is located at the wobble position in the tRNA anticodon loop and was reported to modulate mRNA translation. In this work, an increase of Q modifications on tRNAs was detected in *E. coli* polysome preparations in comparison to the cytosolic tRNA pool, confirming that Q is playing a role in the translational process. Further, a non-natural azide-containing analogue of the precursor $preQ_1$ was efficiently incorporated into tRNA via transglycosylation *in vitro* and *in vivo* in *E. coli*, *Schizosaccharomyces pombe* (*S. pombe*) and human cells. The resulting semi-synthetic modification, termed Q-L1, was also present in tRNAs on actively translating ribosomes, indicating the functional integration into translational processes. Q-L1 was also functionally integrated into an RNA modification circuit in *S. pombe*, replacing the natural Q in its stimulation of further methylation of cytosine 38 in $tRNA^{Asp}$. This functional and minimally invasive replacement of Q with non-natural derivatives enables the incorporation of clickable conjugates in RNA *in vivo* and opens up for new opportunities investigating the biological role of Q.

Zusammenfassung

Die große und stetig wachsende Vielfalt der tRNA-Modifikationen ist von entscheidender Bedeutung für alle biologischen Funktionen der tRNA. Es hat sich gezeigt, dass tRNA-Modifikationen die Genexpression regulieren, indem sie die mRNA-Translation modulieren, insbesondere als Reaktion auf Stressimpulse. Die Modifikation Dihydrouridin (D) beeinflusst die Flexibilität der tRNA und ihr wird demnach eine wichtige Rolle für die Gesamtstruktur der tRNA und deren Funktion zugeschrieben. Es ist jedoch noch weitgehend unbekannt, ob D an der Translation beteiligt ist und ob die NADPH-abhängige Synthese von D durch Stressstimuli beeinflusst wird. In dieser Arbeit wurde der intrazelluläre Redoxstatus in *Escherichia coli (E. coli)* mit dem Bipyridinsalz Paraquat verändert. Hierbei wurde festgestellt, dass die drei tRNA-Dihydrouridinsynthasen (Dus) unterschiedliche Sensitivitäten gegenüber oxidativem Stress aufweisen. Die Aktivitäten von DusB und DusC wurden durch Paraquat stark beeinträchtigt, während DusA auch bei der Behandlung mit Paraquat eine hohe Aktivität zeigte. Die Analyse von *E. coli* Polysompräparationen ergab keinen Hinweis darauf, dass D eine spezifische Rolle in der Translation spielt, obwohl D-modifizierte tRNAs auf aktiv translatierenden Polysomen gefunden wurden. Während D eine einfach strukturierte Modifikation der Nukleobase ist, befasste sich ein anderes Projekt mit der Hypermodifikation Queuosin (Q), die in der Wobble-Position des Anticodon-Loops vorkommt und Berichten zufolge die mRNA-Translation moduliert. In dieser Arbeit wurden vermehrt Q-Modifikationen auf *E. coli* tRNAs auf Polysomen im Vergleich zum cytosolischen tRNA-Pool detektiert, wodurch die Beteiligung von Q am Translationsprozess bestätigt wird. Darüber hinaus wurde ein synthetisches Azid-haltiges Derivat von $preQ_1$ (Azido-propyl-$preQ_1$) über eine Transglykosylierung *in vitro* und *in vivo* in *E. coli*, *Schizosaccharomyces pombe (S. pombe)* und humanen Zellen effizient in die tRNA eingebaut. Die daraus resultierende semi-synthetische Modifikation, die als Q-L1 bezeichnet wird, war ebenfalls auf tRNAs auf aktiv translatierenden Ribosomen vertreten, was auf eine funktionelle Integration des Analogons in die Translationsprozesse hinweist. Q-L1 wurde auch in einen Modifikationskreislauf in *S. pombe* integriert und ersetzt das natürliche Q bei der Anregung zur Methylierung von Cytosin 38 in $tRNA^{Asp}$. Dieser funktionelle und minimal-invasive Ersatz von Q durch synthetische Derivate ermöglicht den Einbau von klickbaren Konjugaten in RNA *in vivo* und eröffnet neue Möglichkeiten zur Untersuchung der biologischen Funktion von Q.

Abbreviations

8-oxo-G	8-oxoguanosine
A	adenine
aa-AMP	aminoacyl-adenylate
AAS	AlkAniline sequencing
ac^4C	N^4-acetylcytidine
ACN	acetonitrile
ADPRase	adenosine diphosphate ribose pyrophosphatase
Ahp	alkyl hydrogen peroxide reductase
ALKBH1	AlkB homolog 1
APS	ammonium persulfate
Asn	asparagine
Asp	aspartatic acid
bTGT/eTGT	bacterial / eukaryotic tRNA guanine transglycosylase
C	cytosine
Ccp	cytochrome c peroxidase
cDNA	complementary DNA
CDS	coding sequence
CID	collision induced dissociation
CMC	*N*-cyclohexyl-*N'*-(2-morpholinoethyl)carbodiimide-methyl-*p*-toluenesulfonate
D	dihydrouridine
DHOD	dihydroorotate dehydrogenase
DHPDH	dihydropyrimidine dehydrogenase
dMRM	dynamic multiple reaction monitoring
DNA	deoxyribonucleic acid
Dnmt2	DNA methyltransferase 2
DTT	dithiothreitol
Dus	tRNA-dihydrouridine synthase
E. coli	*Escherichia coli*
EDTA	ethylenediaminetetraacetic acid
EIC	extracted ion chromatogram
ELP1 / ELP3	elongator complex proteins 1 / 3
ESI	electrospray ionisation
F0	free RNA fraction
F1	fraction containing ribosomal subunits
F2	monosome fraction
F3	polysome fraction

FastAP	fast alkaline phosphatase
fMet	*N*-formylmethionine
$FMNH_2$	reduced flavin mononucleotide
G	guanine
GCH I	GTP cyclo hydrolase I
GDP	guanosinediphosphate
Gly	glycine
Gm	2'-*O*-methylguanosine
GTP	guanosinetriphosphate
H_2NTP	7,8-dihydroneopterin triphosphate
H_2O_2	hydrogen peroxide
HEPES	4-(2-hydroxyethyl)-1-piperazineethanesulfonic acid
His	histidine
hm^5C	5-hydroxymethylcytidine
$HO^{\cdot}$	hydroxyl radicals
ho^5C	5-hydroxycytidine
HPLC	high performance liquid chromatography
I	inosine
IC	initiation complex
IF	initiation factor
k_{cat}	catalytic constant
k_{cat}/K_m	efficiency constant
K_m	Michaelis-Menten constant
KO	knockout
L1	3-azidopropyl-$preQ_1$
L2	4-azidobutyl-$preQ_1$
L3	2-(2-azidoethoxy)ethyl-$preQ_1$
LB	lysogeny broth
LC-MS	liquid chromatography coupled mass spectrometry
LC-MS/MS	liquid chromatography coupled tandem mass spectrometry
lncRNA	long non-coding RNA
m/z	mass-to-charge ratio
m^1A	1-methyladenosine
m^1G	1-methylguanosine
m^3C	3-methylcytidine
m^3U	3-methyluridine
m^5C	5-methylcytidine
m^5U	5-methyluridine
m^6A	N^6-methyladenosine

m^6Am	N^6,2'-*O*-dimethyladenosine
m^7G	7-methylguanosine
mcm^5s^2U	5-methoxycarbonylmethyl-2-thiouridine
MELAS	mitochondrial myopathy, encephalopathy, lactic acidosis, stroke-like episodes
Met	methionine
METTL1	methyltransferase like 1
miRNA	micro-RNA
mnm^5s^2U	5-methylaminomethyl-2-thiouridine
mRNA	messenger RNA
NAD	nicotinamide adenine dinucleotide
NADP	nicotinamide adenine dinucleotide phosphate
NAIL-MS	nucleic acid isotope labelling coupled mass spectrometry
NLS	neutral loss scan
Nm	2'-*O*-methylation
NPPDAG	*N*-((2-amino-4-oxo-4,7-dihydro-3H-pyrrolo[2,3-d]pyrimidin-5-yl)methyl)-3-phenylpropan-1-aminium chloride
NSUN2	NOL1/NOP2/Sun domain family member 2
$O_2^{\cdot-}$	superoxide anion
OD_{600}	optical density
oQ	epoxyqueuosine
PAGE	polyacrylamide gelelectrophoresis
PCR	polymerase chain reaction
PIC	preinitiation complex
piRNA	PIWI-interacting RNA
Pmt1	pombe methyltransferase 1
PNPase	polynucleotide phosphorylase protein
PQ	paraquat
$preQ_0$	7-cyano-7-deazaguanine
$preQ_1$	7-aminomethyl-7-deazaguanine
PS	pentostatin
Q	queuosine
q	queuine
QQQ-MS	triple quadrupole mass spectrometry
QTRT1/QTRT2	queuine tRNA-ribosyltransferase subunit 1 / subunit 2
RBS	ribosomal binding site
RNA	ribonucleic acid
ROS	reactive oxygen species
RP	reversed-phase

rRNA	ribosomal RNA
RT	reverse transcription
S. pombe	*Schizosaccharomyces pombe*
SARS-CoV-2	severe acute respiratory syndrome coronavirus type 2
SD / aSD	Shine-Dalgarno / anti-Shine-Dalgarno
SILIS	stable isotope-labelled internal standard
snoRNA	small nucleolar RNA
snRNA	small nuclear
SOD	superoxide dismutase
T	thymine
TAG	transglycosylation at guanosine
TBE	Tris-borate-ethylenediaminetetraacetic acid
TEMED	*N,N,N',N'*-tetramethylethylenediamine
THU	tetrahydrouridine
tRNA	transfer RNA
Tyr	tyrosine
U	uracil
UTR	untranslated region
UV	ultraviolet
WT	wildtype
YB-1	Y box transcription factor 1
Ψ (Psi)	pseudouridine
τm^5U	5-taurinomethyluridine

1 Introduction

1.1 Nucleic acids

The central dogma of molecular biology, postulated by Francis Crick in 1970, describes the process of protein biosynthesis, emphasising the importance of ribonucleic acid (RNA) as the transmitter of genetic information.[1] The latter is saved in the form of deoxyribonucleic acid (DNA) which is transcribed into messenger RNA (mRNA), making the information accessible to the ribosomes for subsequent translation, which will be discussed in more detail for prokaryotes below (1.3). Of crucial importance for this process are ribosomes which are molecular machineries consisting of ribosomal RNA (rRNA) and proteins that read the mRNA and translate the genetic code into an amino acid sequence. Information about the correct amino acid sequence is given by the nucleobase sequence, which is encoded as base triplets, called codons, for each amino acid. Transfer RNAs (tRNAs), another non-coding RNA species besides rRNA, act as carriers of the amino acids, which are then attached to the nascent polypeptide and subsequently folded into the protein.[2–4]

The different types of RNA differ in their function and secondary structure, but their basic macromolecular structure is the same, consisting of a sugar-phosphate backbone carrying the nucleobase at the C1' position of the sugar. The sugar found in RNA is the eponymous ribose, as opposed to deoxyribose, which forms the backbone of DNA. Deoxyribose is less susceptible to alkaline hydrolysis than ribose because of the absence of a hydroxyl group at the C2' position, resulting in increased stability of the DNA, which preserves the genetic information. The canonical nucleobases attached to the sugar-phosphate backbone can be divided into two groups: the pyrimidines and the purines (Figure 1A). The pyrimidines cytosine (C) and uracil (U) and the purines guanine (G) and adenine (A) are found in RNA.[5] The only difference found in the canonical nucleobases in DNA is the pyrimidine uracil, which is methylated at position 5 and is called thymine (T) or 5-methyluracil. DNA forms a double helix, as reported by Watson and Crick in 1953.[6] They postulated that the strands are connected via two hydrogen bonds between the nucleobases A and T and three between C and G, as shown in Figure 1B. A few years after the postulate of Watson and Crick, Karst Hogsteen published an article reporting a variation of the base pairing. In line with the initial hypothesis, the pyrimidine positions N3 and C4 are involved in the hydrogen bonding interactions, whereas the purines are connected via their C6 and N7 positions, resulting in the formation of only two hydrogen bonds between C and G (Figure 1D).[7] It is worth noting that the combination of a nucleobase, a sugar and a phosphate is called a nucleotide, while the nucleobase bound to the sugar alone is termed a nucleoside (Figure 1C).

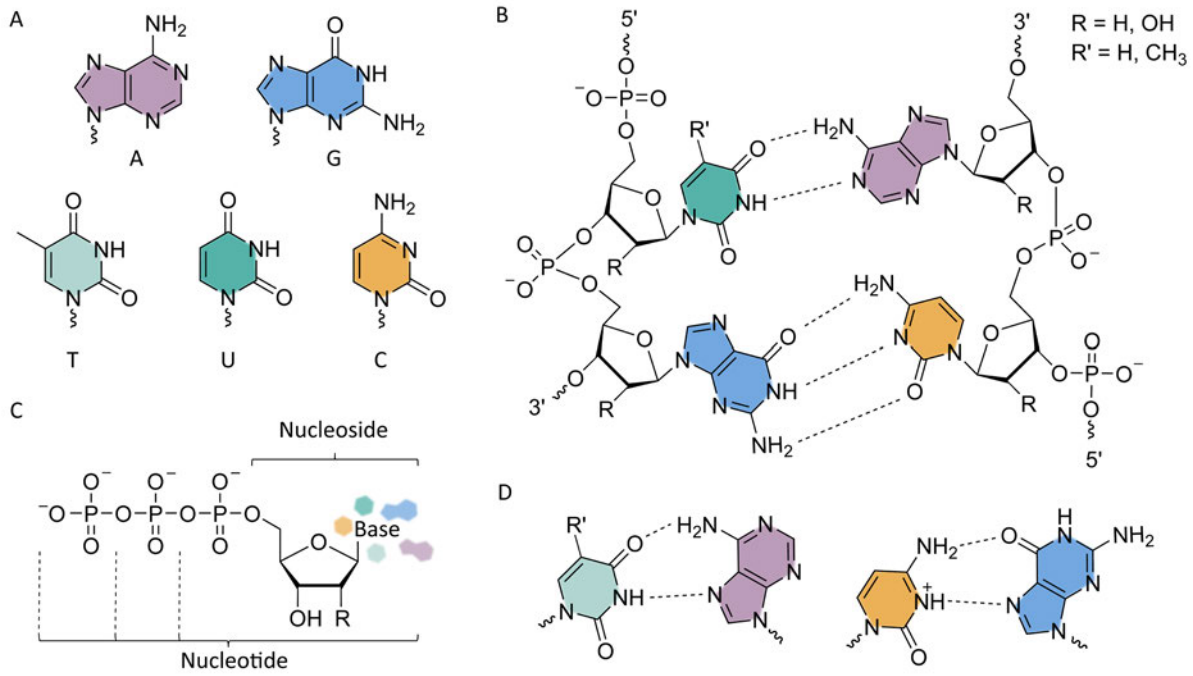

Figure 1: Structure of nucleic acids. A Structures of the purine nucleobases adenine (A) and guanine (G) as well as the pyrimidine nucleobases thymine (T), uracil (U) and cytosine (C). **B** Watson-Crick base pairing A-U/T and G-C of two RNA (R=OH, R'=H) or DNA (R=H, R'=CH_3) strands. Figure adapted from Clancy.[5] **C** Structure of nucleoside and nucleotide. **D** Hoogsteen base pairing. Figure adapted from Zhou *et al*.[8]

RNA is predominantly single-stranded, but can form double-stranded regions through hydrogen bonds between the nucleobases, leading to complex secondary and tertiary structures.[9,10] The tRNA nucleobases are occasionally decorated with chemical modifications, which play an important role in the stabilisation and formation of secondary structures.[11–14]

1.2 RNA modifications

The macromolecule RNA can assume a high variety of roles and functions, all of them requiring different functional and structural details. Chemical modifications of the canonical nucleosides, of which more than 170 are known today, contribute to this diversity.[11,15] These posttranscriptional modifications, also known as the epitranscriptome, add a second layer of information to the genetic code, which is based on the four canonical nucleobases.[16,17] The high chemical diversity of modifications is ranging from rather simple modifications such as methylations to highly decorated heterocycles and enables the RNA to perform its complex functions.[18]

tRNA is the most modified RNA species, with 80% of the modifications identified in this species. An average of 10 to 15% of tRNA nucleosides have been shown to be modified, varying between different organisms, with an average of 13 modifications per tRNA molecule in eukaryotes, while less residues are modified in bacteria, with an average of 8 modifications

per tRNA molecule in gram-negative bacteria and even less in gram-positive bacteria.[18–21] Around 33% of the known pool of modifications were reported in rRNA and around 10% in mRNA.[18]

In addition to modifications of tRNA, mRNA and rRNA, as well modifications of small nuclear and nucleolar RNA (snRNA and snoRNA), micro-RNA (miRNA), PIWI-interacting RNA (piRNA) and long non-coding RNA (lncRNA) have been reported to be involved in the biogenesis of small non-coding RNAs and to play important roles in cellular functions.[18,22,23]

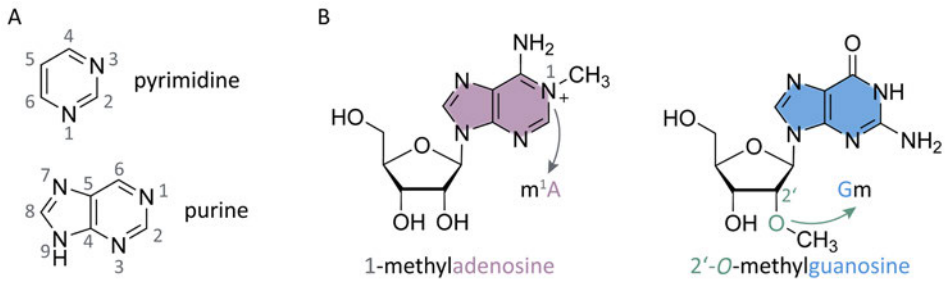

Figure 2: Nomenclature of RNA modifications. A Purine and pyrimidine ring numbering serves as basis for RNA modification nomenclature. **B** RNA modification nomenclature and abbreviations illustrated by the modifications 1-methyladenosine (m^1A) and 2'-*O*-methylguanosine (Gm).

The nomenclature of the modifications is based on the numbering of the underlying nucleobase, which in turn is similar to the numbering of pyrimidines and purines (Figure 2A), resulting in a one or two letter code, in which the base abbreviation is preceded by a superscript indicating the position of the modification. For example, 1-methyladenosine is referred to m^1A, with m representing the methyl group and the superscripted 1 denoting that the methyl group is attached to position 1 of the adenosine ring. Modifications linked to the ribose are indicated after the base, as for example 2'-*O*-methylguanosine is abbreviated as Gm (Figure 2B). There are also exceptions to this nomenclature for special modifications, which are abbreviated by individual letters, such as queuosine (abbreviated as Q), dihydrouridine (abbreviated as D) or pseudouridine (abbreviated as Ψ).[18,24] The latter one is outstanding because of its C-C bond between the sugar and the base instead of the typical *N*-glycosidic bond.[25]

1.2.1 tRNA modifications

tRNA is the RNA species with the highest diversity of modifications, as mentioned above. Some examples of these are shown in Figure 3 with their location in the schematic cloverleaf tRNA structure. The latter is caused by internal base pairing of the tRNA strand, forming four double-stranded arms, namely the acceptor stem, D arm, anticodon arm and T (TΨC) arm, as well as four single-stranded loop regions: D loop, anticodon loop, variable loop and T (TΨC) loop. The 3' end of the acceptor stem is single stranded and contains the CCA end which serves as the

acceptor for aminoacylation. The D loop is called after the dihydrouridine modification that occurs here, while the loop containing the anticodon is referred to as the anticodon loop. As the name suggests, the variable loop is variable in its length. The T arm or TΨC arm is named according to the conserved modified bases thymidine, pseudouridine and cytidine. Through tertiary interactions of the T and the D arms, the tRNA folds into a three-dimensional L-shape structure.[26–29] The tRNA positions are numbered consecutively from the 5' end, with positions that are not present in each tRNA, such as positions in the variable loop or in the D loop, being labelled with an additional letter, for example e1 (variable loop) or 20a (D loop).[30]

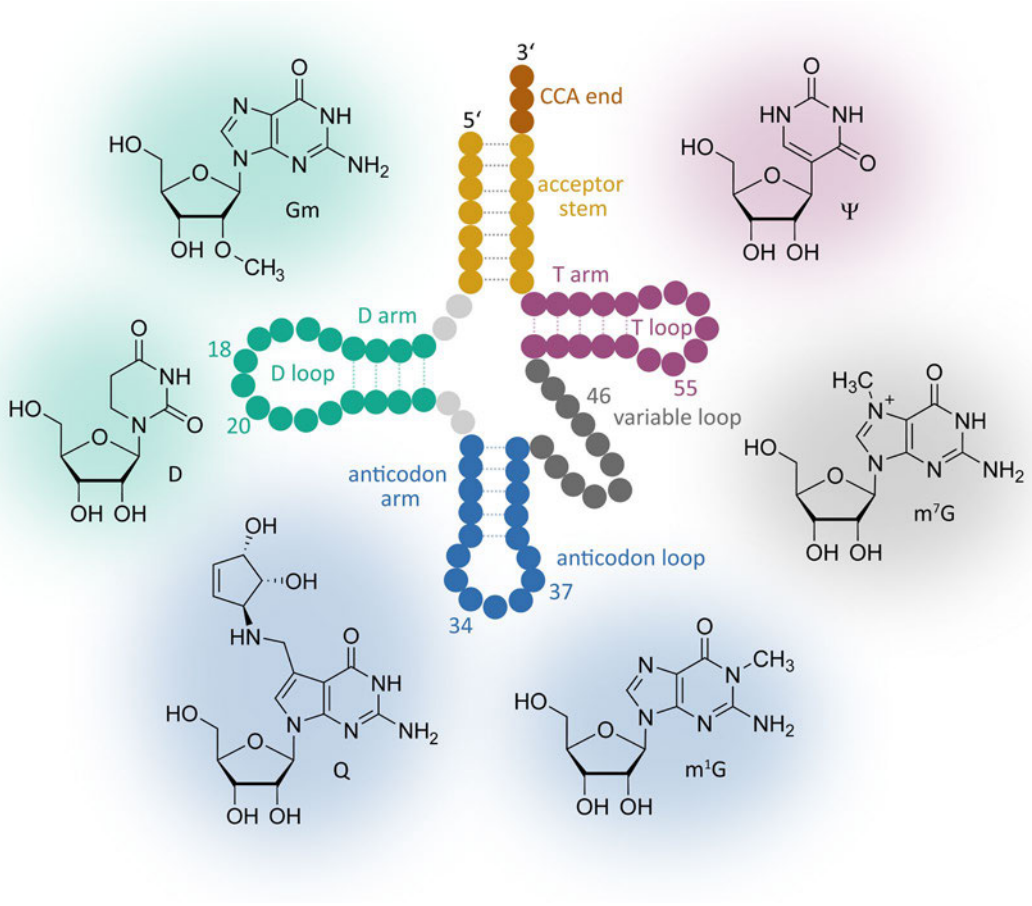

Figure 3: Examples of tRNA modifications. Scheme of the tRNA cloverleaf structure with the following examples of modified nucleosides: 2'-*O*-methylguanosine (Gm), dihydrouridine (D), queuosine (Q), 1-methylguanosine (m^1G), 7-methylguanosine (m^7G) and pseudouridine (Ψ). Figure adapted from Suzuki, Lorenz *et al.* and Crécy-Lagard *et al.*[31–33]

In tRNA, most of the modifications are located in or adjacent to the anticodon loop, allowing for optimal stacking and hydrogen bonding interactions for correct binding to the ribosome during translation.[18,34] The wobble hypothesis states that the third base of the codon can vary during base pairing of codon and anticodon, increasing the flexibility during decoding, as for example an unmodified U at position 34, the so-called wobble position, allows for the recognition of A or G.[31,35,36] Interestingly, in some bacteria and organelles a U at position 34 is

able to recognise all four nucleotides, a phenomenon called four-way wobbling or superwobbling.[37,38] The wobbling is fine-tuned by posttranscriptional modifications at position 34, as for example, the four-way wobbling is limited to the recognition of A or G when U34 is modified with a derivative of 5-methyluridine. In contrast, the modified position 34 can also lead to an extended decoding, as the inosine (I) modification resulting from adenosine deamination, for example, allows the base pairing with U, C and A, whereas the unmodified A only permits pairing with U.[31] Interestingly, the tRNA binding site of the ribosome leaves enough space for the different wobble base pairings.[31,36] Reports by Zinshteyn *et al.* and Nedialkova *et al.* highlight the role of m^5U derivatives at position 34, observing reduced translation of A-ending codons with concomitant activation of stress response signalling pathways in the absence of the modification 5-methoxycarbonylmethyl-2-thiouridine (mcm^5s^2U) at position 34.[39,40] Furthermore, demethylation of the initiator tRNA by ALKBH1 was shown to attenuate translation initiation, presenting another regulatory mechanism of posttranscriptional gene expression.[41]

Since all tRNAs share the L-shaped structure, modifications that contribute to the identity of tRNAs and facilitate the correct recognition by the aminoacyl-tRNA synthetases are of considerable importance. In this context, 5-methylaminomethyl-2-thiouridine (mnm^5s^2U) and m^1G have been reported as identity elements for the glutamyl- and arginyl-tRNA synthetases, respectively.[42–45]

Since position 37, 3' adjacent to the anticodon, stabilises the anticodon region for correct codon binding, modifications at this position ensure an accurate decoding and correct reading frame, emphasising the role that tRNA modifications play directly during mRNA translation.[31,46,47] Besides the anticodon, tRNA is also modified in the D loop, T loop and the variable loop, which is important for stabilising the L-shaped structure of the tRNA.[15,31,48] It was shown that a lack of m^7G at position 46 and m^5C at position 49 in $tRNA^{Val}$(AAC) resulted in tRNA degradation, thus demonstrating the critical role of these modifications for tRNA stability.[49,50] Albeit not all tRNAs lacking modifications were degraded, Suzuki suggested a dynamic regulation mechanism, presumably by the metabolic status of the cell.[31] One example for metabolically regulated modifications is 5-taurinomethyluridine (τm^5U) in mitochondrial tRNA for whose synthesis 5,10-methylenetetrahydrofolate and the 2-aminoethanesulfonic acid taurine are required. Starvation of taurine showed reduced τm^5U modification levels, while interestingly glycine took the place of taurine, indicating a dynamic regulation in this case.[51] Taurine modifications were associated with mitochondrial diseases as a severe reduction of τm^5U and its 2-thiouridine derivative was observed in cells isolated from patients with mitochondrial dysfunctions.[52] This report resulted in a clinical trial analysing the supplementation of taurine as potential therapy of MELAS (mitochondrial myopathy, encephalopathy, lactic acidosis, stroke-like episodes) which was approved in Japan 2019.[53–55] The medical relevance of the U34 modifications is further emphasised by the finding

that the yeast elongator complex proteins 1 and 3 (ELP1 and ELP3), which have been implicated in familial dysautonomia, mental retardation and amyotrophic lateral sclerosis, are essential for the synthesis of mcm^{5}U derivatives.[31,56,57] tRNA-modifying enzymes were also linked to cancer, as deregulation of the methyltransferases NSUN2 and METTL1 was observed in various cancers, and targeting these modifications might be a promising tool in cancer chemotherapy.[31,58–60] In addition, loss of the NSUN2 gene resulted in growth retardation and neurodevelopmental defects.[61–63]

1.2.1.1 Dihydrouridine

Dihydrouridine is a rather simple structural modification that is omnipresent in all domains of life.[64–67] D is the second most abundant modification in tRNA and occurs in the eponymous D loop at positions 16, 17, 20 and 20a and in the variable loop at position 47.[21,67] Remarkably, in prokaryotes, dihydrouridylation at position 47 has only been reported in *Bacillus subtilis* tRNA^{Met}(CAU).[68] In ribosomal RNA the dihydrouridylation is not as common as in tRNA, but one modification site has been reported in *E. coli* 23S rRNA and two sites in rRNA isolated from *Clostridium sporogenes*. In the latter case, a methylation of dihydrouridine was reported.[65,69] Detection of D modification sites in mRNA was more difficult than in tRNA, as the detection by mass spectrometry often gave inaccurate results because of tRNA contamination in the samples. Sequencing methods using sodium borohydride to convert dihydrouridine to tetrahydrouridine (THU) facilitated the detection and enabled transcriptome-wide mapping, resulting in the detection of mRNA modification sites in eukaryotes, interestingly in stem-loop regions, similar to tRNA.[66,67]

Dihydrouridine modifications are introduced by dihydrouridine synthases (Dus), flavin-containing enzymes that reduce uridines at the 5,6-double bond by utilising the reduced nicotinamide adenine dinucleotide phosphate (NADPH) as a redox equivalent. Three different Dus enzymes are known in *E. coli*, each of them reducing uridines site-specifically. While DusA modifies U20 and U20a, U16 is reduced by DusC and U17 by DusB (Figure 4A).[70–72] In yeast, four site-specific Dus enzymes are known: Dus1p (U16 and U17), Dus2p (U20), Dus3p (U47) and Dus4p (U20a and U20b).[73]

Mechanistically, the redox equivalent NADPH transfers a hydride to the prosthetic flavin group, resulting in the formation of $FMNH_2$ (reduced flavin mononucleotide) and the dissociation of the oxidised $NADP^+$, leaving the free enzyme ready for catalysis.[74,75] By analysing the crystal structure of Dus from *Thermatoga maritima*, Yu *et al.* proposed the enzymatic mechanism to be similar to that of the flavin-dependent enzymes DHOD (dihydroorotate dehydrogenase) and DHPDH (dihydropyrimidine dehydrogenase) because of their structural similarity.[76] Here, the bound and reduced flavin mononucleotide transfers a hydride to the C6 of the uridine. Subsequently, the C5 is protonated by a cysteine residue

which is located in the active site of the enzyme (Figure 4B). While a cysteine residue has also been shown to be essential in the Dus2 enzyme in *Saccharomyces cerevisiae*, the *E. coli* DusA was reported to require additional five amino acids for its full activity.[75,77]

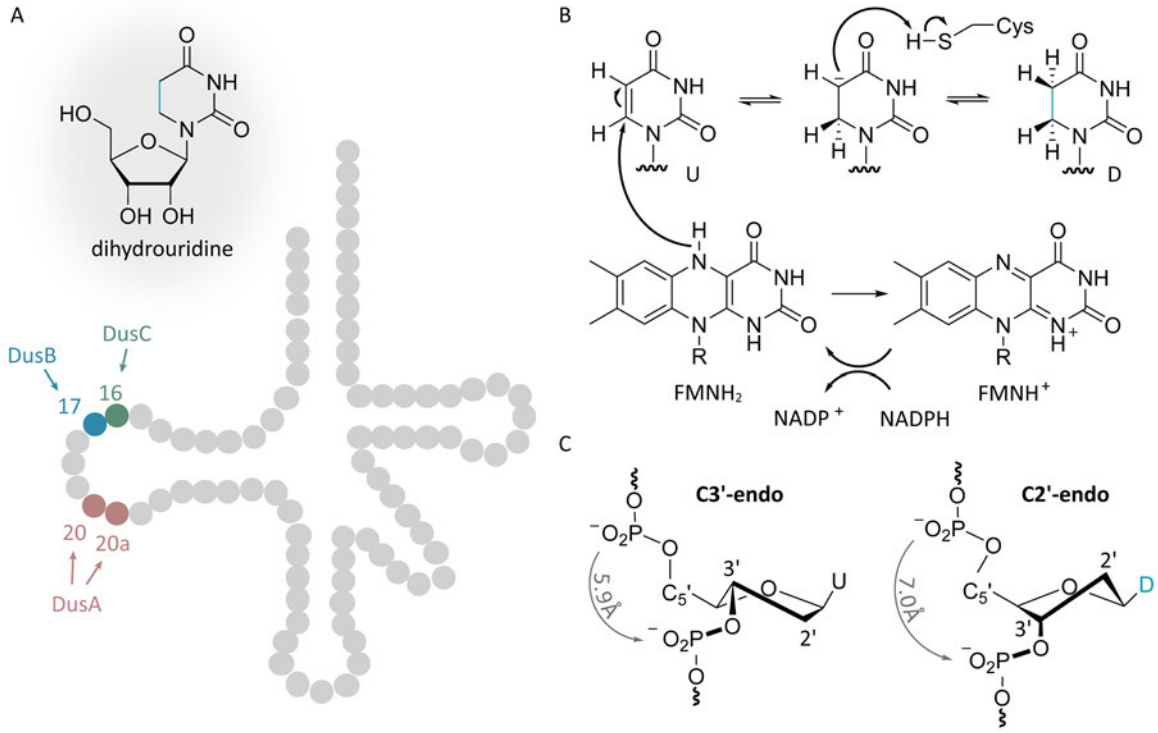

Figure 4: Dihydrouridine modification in tRNA. A Dihydrouridine positions in *E. coli* tRNA modified by three dihydrouridine synthases DusA, DusB and DusC. **B** Mechanism of the reduction of uridine to dihydrouridine. **C** Preferred ribose conformation of uridine and dihydrouridine. Figure adapted from Yu *et al.* and Bansal *et al*.[76,78]

Notably, the three different bacterial dihydrouridine synthases share strong structural similarities, but differ in their substrate specificities, which are achieved by tRNA binding in different orientations, enabled by specific amino acid clusters that define tRNA docking specifically for each Dus enzyme. In the case of DusB and DusC, which catalyse dihydrouridylation of the neighbouring positions 16 and 17, the polar and non-polar amino acids are reversed, resulting in a 180° rotation of the nucleobase.[70,71]

After reduction of the double bond, the dihydrouridine has lost its aromaticity and planarity, as measured by an increase in pK_a.[79–81] In contrast to other modifications such as ribose methylations, 2-thiolations or pseudouridylations, which improve the regional stability of RNA by stabilising the C3'-endo conformer, dihydrouridine stabilises the C2'-endoribose form (Figure 4C), leading to an enhanced flexibility.[82–87] Dyubankova *et al.* showed that dihydrouridine modifications in oligonucleotides trigger the folding into a hairpin suggesting that D is involved in the correct folding and stability of the tRNA D loop region.[81] Additionally, stabilisation of the C2'-endo conformation is important for RNA-protein recognition, since this conformation is bound by RNA recognition motifs.[88] Of note, Nomura *et al.* observed a

decrease in melting temperature when the dihydrouridine modification at position 20a in $tRNA^{Ser}$ was missing, leading to the suggestion that D might contribute to tRNA stability even though the structural flexibility is increased.[89]

In the 1990s, Dalluge *et al.* reported an up to 70% higher abundance of dihydrouridine on tRNAs in psychrophilic bacteria compared to their mesophilic counterparts, and suggested that higher dihydrouridylation allows the bacteria to preserve the L-shape structure of the tRNA at low temperatures.[90] This is consistent with the later reported temperature adaptations of the DusB homologue in *Clostridium botulinum* and Dus3 in *Bacillus manusensis*.[91,92] In *Lactobacillus agilis*, altered D levels have been observed after nutritional changes, leading to the suggestion that dihydrouridylation might be a tool for dynamic regulations.[93,94]

As early as the 1970s, dihydrouridine was linked to cancer and was discussed as a potential non-invasive biomarker for cancer diagnosis.[95,96] Over the years, further data has been published suggesting a correlation between altered D levels or Dus enzymes and various types of cancer.[97–100] Thus, suppression of Dus enzyme activity or the inhibition of Dus-tRNA complex formation might be a promising therapeutic strategy. In addition, Mittelstadt *et al.* observed the regulation of the interferon-induced protein kinase by human Dus2, which links dihydrouridine to innate immunity, stress signalling, cell proliferation and programmed cell death.[101]

Recently detected D modification sites in mRNA allow speculations about a potential role of dihydrouridine during translation. Dai *et al.* reported that the knockout of the human Dus3 resulted in reduced protein translation, indicating that hDus3 might be important for efficient translation, whereas Finet *et al.* observed that the translational speed of D-modified mRNA is reduced.[67,102] The latter results are in line with old data analysing the coding properties of D-containing oligoribonucleotides, causing loss of coding ability and repression of translation.[103–106] Although the main role during translation is played by tRNA modifications located in the anticodon loop, Cochella *et al.* observed that substitutions in the D arm of tRNA cause miscoding, probably induced by changes in the tRNA conformation, leading to the hypothesis that tRNA flexibility plays a critical role during decoding.[107] However, the role of dihydrouridine on tRNAs during translation has not yet been further analysed.

1.2.1.2 Queuosine

Queuosine is a so-called tRNA hypermodification consisting of a 7-deazaguanosine core with an amino-methyl side chain linked to a cyclopentanediol ring. Q occurs in eukaryotes and prokaryotes at position 34 of the four tRNAs containing a GUN anticodon sequence, namely $tRNA^{Asp}$, $tRNA^{Tyr}$, $tRNA^{His}$ and $tRNA^{Asn}$.[108,109] Eukaryotes are not able to synthesize the

hypermodified structure of queuosine themselves but have to salvage queuine (q) from their nutrition or higher eukaryotes from their gut microbiota.[110] In contrast to eukaryotes, prokaryotes are able to synthesise $preQ_1$, the precursor nucleobase of Q, *de novo*. Several enzymes are involved in the *de novo* biosynthesis (Figure 5, shown on grey background), the GTP cyclo hydrolase I (GCH I) catalyses the first step, the hydrolysis of guanosinetriphosphate (GTP) to 7,8-dihydroneopterin triphosphate (H_2NTP).[111] H_2NTP is further modified by QueD, QueE and QueC forming 7-cyano-7-deazaguanine, termed $preQ_0$. In a further step the cyano group is enzymatically converted into an amino group catalysed by QueF, resulting in the structure of $preQ_1$ (7-aminomethyl-7-deazaguanine).[112,113] The bacterial enzyme tRNA guanine transglycosylase (bTGT) exchanges $preQ_1$ with guanine at position 34 of the tRNA in a transglycosylation reaction, which is then further modified by QueA to epoxyqueuosine (oQ). *S*-adenosylmethionine serves as a cofactor, forming the precursor of the epoxycyclopentane moiety.[114] In a last step, the epoxyqueuosine reductase QueG reduces oQ to the final structure of queuosine.[115]

In eukaryotes the salvaged queuine is incorporated into the tRNA by the eukaryotic tRNA guanine transglycosylase (eTGT) comparable to the incorporation of $preQ_1$ in prokaryotes (Figure 5, shown on blue background). In contrast to the bacterial enzyme, the eTGT is a heterodimeric enzyme consistent of the catalytical subunit QTRT1 (queuine tRNA-ribosyltransferase subunit 1) and the non-catalytical subunit QTRT2.[116–119] Although bacteria are capable of the *de novo* biosynthesis of $preQ_1$, Yuan *et al.* showed that salvage of the precursors $preQ_0$ and $preQ_1$ also occurs in bacteria. In the case of mammals who salvage Q precursors from their gut microbiome, this is the first indication that host and bacteria of the gut microbiome might compete for Q precursors.[120]

Computational studies analysing the role of queuosine in the context of codon-anticodon binding showed that Q establishes a network of hydrogen bonds, resulting in a more stabilised and less flexible anticodon loop that supports optimal positioning for optimal Watson-Crick type associations.[121] This is consistent with the assumption that modifications at the wobble position can help to stabilise the codon-anticodon binding, leading to a better codon discrimination and strongly suggests an influence of the queuosine modification on the translation process.[122] Müller *et al*. reported that queuosine affects the translational speed in *S. pombe*. Within their study, ribosome profiling results revealed an enhanced translational speed of C-ending codons for aspartate and histidine, while the U-ending codons for asparagine and tyrosine were translated more slowly in the context of Q modification. Besides, it was shown that the queuosine modification suppresses second-position misreading of glycine codons, thus preventing translational errors.[123] Furthermore, Tuorto *et al*. showed that dietary Q levels play a role in controlling the translational speed of Q-containing codons in mammalian cell lines. By analysing the codon occupancy during translation elongation, they observed slower translation of the Q-decoded codons $tRNA^{Asp}$, $tRNA^{Tyr}$, $tRNA^{His}$ and $tRNA^{Asn}$ in

the absence of Q (q-free culture conditions).[124] To assess the phenotypic consequences of this observation, they extended their experiments to a mouse model by mutating the catalytically

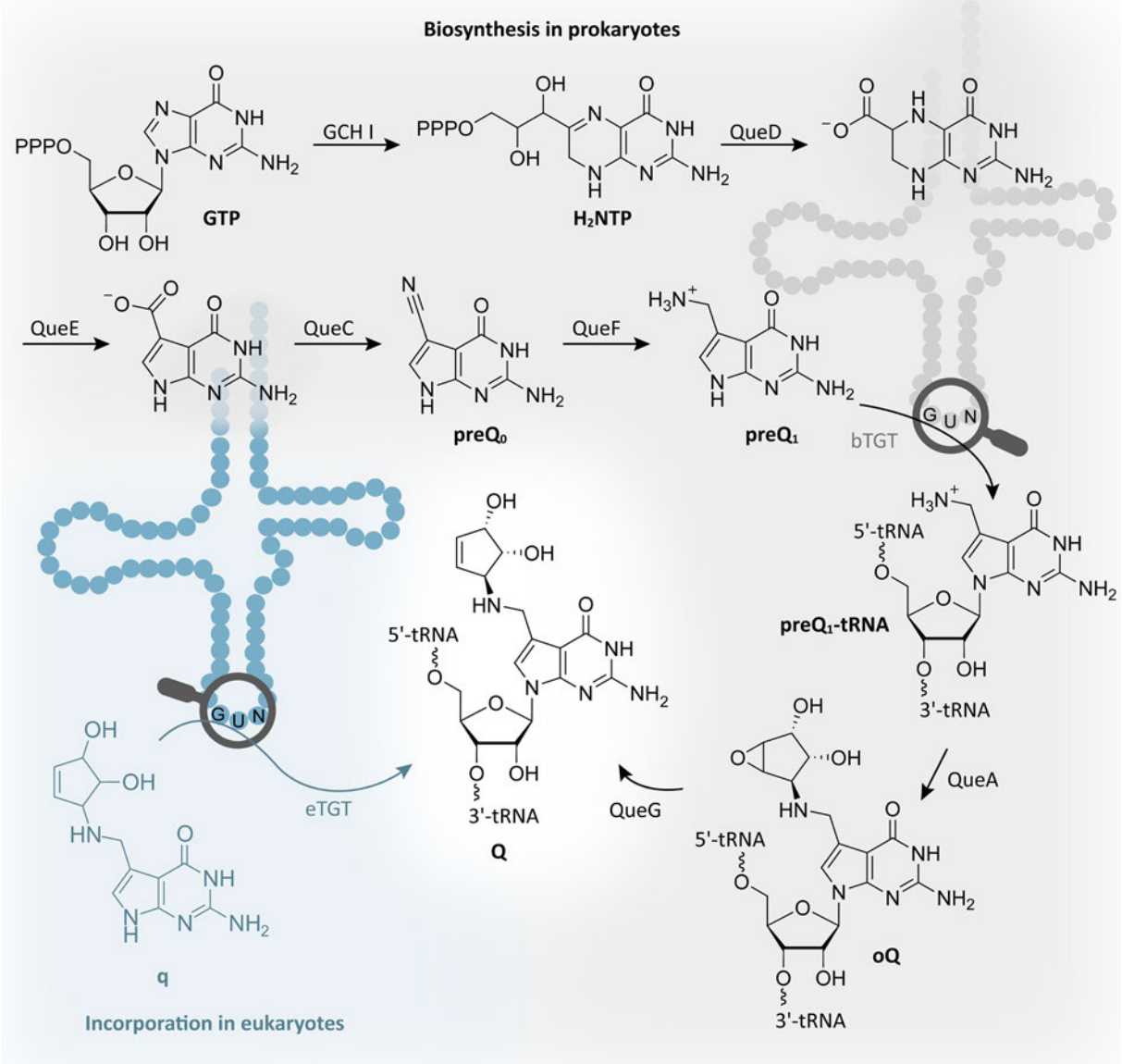

Figure 5: *De novo* biosynthesis of queuosine in prokaryotes and incorporation of queuine in eukaryotes. The biosynthesis in prokaryotes (shown on grey background) starts with guanosinetriphosphate (GTP) that reacts in four enzymatic steps, catalysed by the enzymes GTP cyclo hydrolase I (GCH I), QueD, QueE and QueC, to 7-cyano-7-deazaguanine ($preQ_0$). Further, QueF catalyses the conversion to $preQ_1$ (7-aminomethyl-7-deazaguanine) which is subsequently incorporated into tRNA by the bacterial tRNA guanine transglycosylase (bTGT). After incorporation of the precursor into the tRNA, QueA and QueG catalyse the final synthesis to Q. The mechanistic depiction is adapted from Dowling *et al.*[125] Eukaryotes incorporate the base queuine (q) into the tRNA catalysed by the eukaryotic tRNA guanine transglycosylase (eTGT) resulting in Q (shown on blue background).

active QRTR1 subunit of the eukaryotic TGT enzyme and observed that the Q-lacking knockout mice exhibited learning and memory deficits, linking tRNA modifications and in particular Q to brain function.[126] Similar correlations were observed before: Richard *et al.* showed that the addition of q to an *in vitro* model for Alzheimer's and Parkinson's disease led to an increase of

neuronal survival.[127] Moreover, a lack of Q-tRNA was linked to neurological and neuropsychiatric diseases. In a medical approach, Varghese *et al.* supplemented a synthetic substrate for TGT called NPPDAG (*N*-((2-amino-4-oxo-4,7-dihydro-3H-pyrrolo[2,3-d]pyrimidin-5-yl)methyl)-3-phenylpropan-1-aminium chloride) to a mouse model for multiple sclerosis and observed a reversal of the clinical symptoms. The data led to the suggestion that the exploitation of the TGT enzyme might be a promising approach for multiple sclerosis treatment.[128] To further investigate the biological role of queuosine and potential therapeutic approaches, one method is to use TGT to introduce analogues of Q precursors into tRNA, similar to the approach of Varghese *et al*. The eukaryotic as well as the bacterial enzyme were shown to tolerate diverse chemical variants with structures similar to Q precursors *in vitro*.[129,130] In this context, Devaraj and co-workers developed a method called RNA-TAG (transglycosylation at guanosine) using a short recognition motif of the bTGT to be introduced to different RNA transcripts resulting in a site-specific incorporation of $preQ_1$ analogues *in vitro*. Analogues containing fluorophores enable the visualisation of the respective transcripts, as it was shown for mRNA transcripts in a fixed cell environment. This approach was used to develop a light-activated mRNA translation system and to incorporate a tetrazine moiety that enables for further click chemistry.[131,132] Four years later, the group reported the development of RNA-CLAMP (clamping), a method to connect two stem loops within an RNA via a photocleavable crosslinker.[133]

In addition to its crucial role in translation, queuosine has been found to be involved in another molecular interaction outside the ribosome, referred to as a modification circuit. Using RNA bisulfite sequencing, Müller *et al*. showed that Q enhances the methylation of cytosine at position 38 in $tRNA^{Asp}$ in *S. pombe* which is catalysed by the Dnmt2 homologue Pmt1.[134,135] Further, Johannsson *et al.* reported a direct effect of queuosinylation on the methyltransferase activity of Dnmt2 *in vitro*: Q at position 34 optimises the positioning of the substrate tRNA and the relevant residues for the methyl transfer reaction in the active site of Dnmt2, thereby enhancing its catalytic activity, as revealed by cross-linking data and computational docking experiments.[136]

1.2.2 mRNA modifications

As coding RNA species, mRNA contains a coding sequence (CDS) flanked on both sides by untranslated regions (UTR) (Figure 6), which are important for regulating the localisation of mRNA, increasing its stability and controlling translation.[137] Protection from degradation is afforded by an m^7G cap structure at the 5' end of the eukaryotic mRNA, which was demonstrated to be important for RNA processing and translation initiation, as well as for the innate immune system, since the one to two 2'-*O*-ribose methylated nucleotides adjacent to the m^7G play a crucial role in the immune system's discrimination between self and non-self

mRNAs.[138–141] In addition to the canonical cap shown in Figure 6, cap structures derived from metabolites and cofactors have been reported, including the 5' nicotinamide adenine dinucleotide (NAD) cap structure, which affects RNA stability and mitochondrial functions, might play a role in translation and is involved in phage-host interactions during phage infection.[22,142,143]

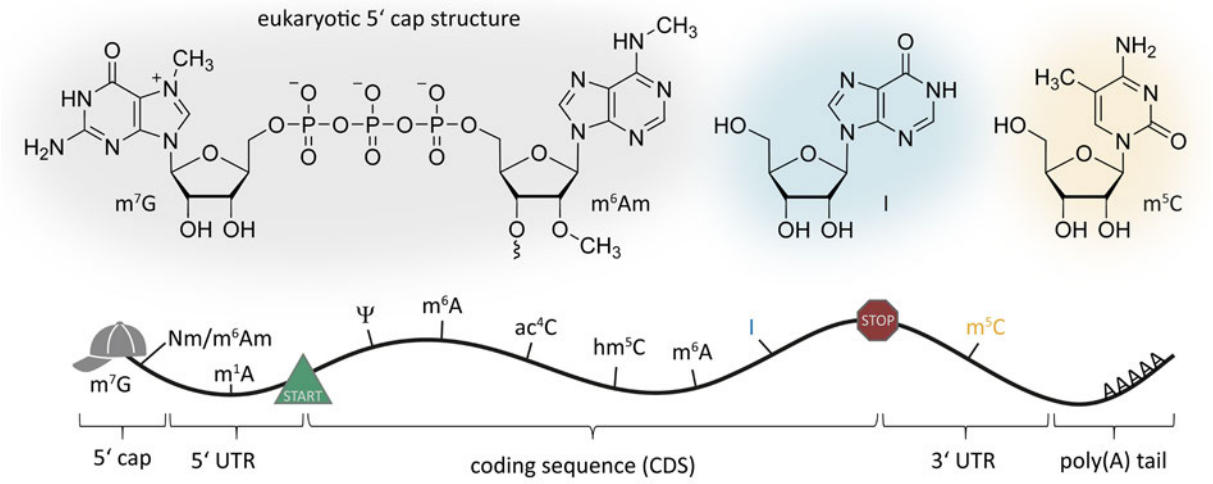

Figure 6: mRNA structure and modifications. Eukaryotic mRNA structure with the coding sequence (CDS) flanked by untranslated regions (UTR), a 5' cap and a 3' poly(A) tail. The structures of an exemplary 5' cap, inosine (I) and 5-methylcytidine (m^5C) are shown in the upper part. Figure adapted from Delaunay *et al*.[22]

Notably, the m^6Am cap modification was linked to metabolic diseases since variations in the m^6Am demethylase gene were associated with childhood obesity and severe adult obesity.[144,145] An important interaction of the 5' cap occurs with the 3' end of the mRNA, which is decorated with a poly(A) tail, forming a loop through interactions of cap-binding and poly(A)-binding proteins, thereby enhancing the translation in eukaryotes.[22,146,147] With ten types of modifications being reported in eukaryotic mRNA, the diversity of modifications within this RNA species is much lower compared to tRNA. While the 5' cap modifications and m^6A modifications are the most abundant ones in mRNA, pseudouridine and inosine have been reported to a smaller extent, as well as more scarce m^1A, hm^5C (5-hydroxymethylcytidine) and ac^4C (*N*^{4}-acetylcytidine).[22] It is worth noting that the deamination of adenosine to inosine results in an altered base pairing, as I pairs with C instead of U, thus directly affecting the genetic code.[18] The internal mRNA modifications have been associated with cancer, most notably the abundant m^6A modification whose biological role was summarised in a comprehensive review by Boulias and Greer.[148] Apart from that, m^1A and m^1G have been linked to cancer, since accumulation of m^1A resulted in poor clinical outcome in Hodgkin lymphoma cells. Moreover, Chen *et al.* reported that m^5C-modified RNA is involved in the regulation of oncogene activation in human urothelial carcinoma of the bladder.[149,150] Modified nucleosides play an essential role for stability, translational efficacy and low

immunogenicity of mRNA vaccines.[22,151,152] Apart from their prominent role in successfully fighting against the SARS-CoV-2 pandemic, mRNA vaccines are also potential therapies for infections, genetic disorders or cancer, encoding tumour antigens in antigen-presenting cells and stimulating immunity, with several candidates being currently in clinical trials.[22,153] This demonstrates the potential of mRNA vaccines, which provide the possibility of personalised therapies through individual mutanome vaccines.[154,155]

1.2.3 rRNA modifications

Besides tRNA, rRNA is also frequently modified, albeit in a much smaller structural variety than in tRNA, i.e. mainly 2'-*O*-methylations and pseudouridines, mostly introduced by small nucleolar RNAs, another non-coding RNA species.[156–158] Since rRNAs constitute the catalytically active parts of the ribosome with the ribosomal proteins contributing to the correct structure of the complex, it is reasonable to assume that rRNA modifications impact the translational control of gene expression.[159–161] rRNA modifications have been reported to play a crucial role in the translation accuracy, in particular pseudouridylation and 2'-*O*-methylation in the decoding centre, in intersubunit bridge regions or in rRNA domains at the tRNA binding site.[162] This is in line with other reports showing impaired translation as a consequence of combined deletions of two or three modifications in the tRNA binding regions, or deletion of snoRNPs that introduce pseudouridines at a tRNA binding site.[163,164] It has also been reported that the loss of m^5C at C2278 and Gm at G2288 in 25S rRNA in yeast causes structural changes, leading to ribosome instability.[165] By crystallising the structures of the *Thermus thermophilus* ribosome, Polikanov *et al.* highlighted the role of rRNA modifications in stabilising the folded rRNA by showing the interaction of modified rRNA residues with mRNA, tRNA or associated proteins.[165,166]

1.2.4 Detection of RNA modifications

The rapidly evolving field of RNA modification research is advancing with constantly improving tools for more accurate and precise detection of modified structures. The detection methods can be classified into LC-MS-based methods and sequencing-based approaches, which will be both discussed in the following sections.

1.2.4.1 Detection of nucleosides by liquid chromatography coupled mass spectrometry

Liquid chromatography coupled mass spectrometry (LC-MS) has established itself as the gold standard for the quantification of modified nucleosides, offering a unique combination of

specificity and sensitivity, and instrumentation has continuously been improved, increasing the ability to analyse complex biological samples.[167–169]

RNA analysis is most commonly performed at the nucleoside level, i.e. the RNA is digested with an enzyme mixture prior to analysis. As the nucleosides, both canonical and chemically modified, can react further, sample preparation plays a key role.[169] Pitfalls during LC-MS analysis with potential chemical instabilities or interactions of the modifications are discussed by Ammann *et al*.[170] In particular, the Dimroth rearrangement of m^1A to m^6A or chemical deaminations of m^3C to m^3U and adenosines to inosines. To avoid the latter, deaminase inhibitors such as pentostatin (PS) for purines and THU for pyrimidines are often added to the enzyme mixture.[171] Importantly, the addition of such reagents also bears potential pitfalls, as for example THU is often contaminated with dihydrouridine and therefore the addition of THU has to be avoided for correct quantification of D. However, not only enzyme impurities but also the enzyme buffer can be problematic, as demonstrated by the recently reported formation of a glycerol ester of t^6A, highlighting the importance of considering potential site reactions when preparing samples, even with chemicals thought to be mild.[172] An effective technique for the separation of digested nucleosides is reversed-phase high performance liquid chromatography (HPLC).[173–176] While nucleosides can also be identified by their UV absorbance and retention times, the combination with mass spectrometry provides highly sensitive and specific measurements.[173] The coupling of reversed-phase liquid chromatography with electrospray ionisation (ESI) mass spectrometry is a widely used method that allows quantification even in the low femtomole range.[177,178] Tandem mass spectrometry, often performed with triple quadrupole MS systems (QQQ-MS), allows the simultaneous detection of different analytes according to their specific fragmentation patterns. The sensitivity can be further improved by selecting retention time windows for the eluting analytes in the dynamic multiple reaction monitoring (dMRM) mode, reducing the number of analytes simultaneously reaching the detector.[177,179,180]

After chromatographic separation, the analyte to be analysed in dMRM mode is ionised and dissolved by electrospray ionisation and enters the first of three quadrupoles. The first mass analyser allows only precursor ions with the correct pre-defined mass-to-charge ratio (*m/z*) to pass through the quadrupole. Inside the collision cell, which is another quadrupole or hexapole in newer instruments, the precursor ions are fragmented induced by collisions of the latter with collision gas molecules (collision induced dissociation, CID) at their most labile bonds. The resulting product ions then enter a third quadrupole, which analyses the mass of the incoming product ions and selects only the pre-defined masses to pass to the electron multiplier and detector (Figure 7). This double selection step allows high sensitivity and reduces noise.[180]

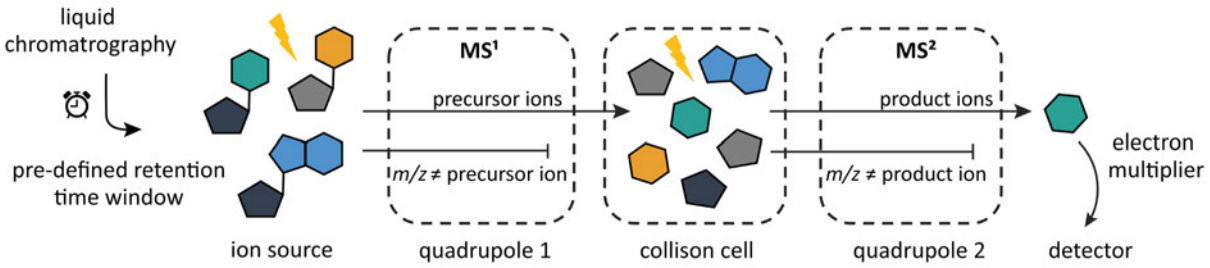

Figure 7: Scheme of nucleoside detection by liquid chromatography coupled tandem mass spectrometry (LC-MS/MS) in dynamic multiple reaction monitoring (dMRM) mode. After separation on a reversed-phase HPLC column, the analytes are ionised by electrospray ionisation (ESI) and subsequently enter the first mass analyser (quadrupole 1) in pre-defined retention time windows. After the first mass selection, the pre-defined precursor ions are allowed to pass into the collision cell. After collision induced dissociation, the resulting fragments are selected in the second mass analyser (quadrupole 2) for pre-defined product ions, which subsequently reach the electron multiplier and the detector. Figure adapted from Yoluç *et al.*[180]

LC-MS enables the detection of any chemically modified nucleoside by its characteristic fragmentation at the *N*-glycosidic bond, which results in a loss of -132 Da corresponding to ribose or -146 Da in the case of ribose methylation. However, there are exceptions to this common fragmentation pattern, such as pseudouridine because of its stable carbon-carbon bond, or queuosine.[169,177] For correct detection, it is important to avoid any cations other than H^+ or NH_4^+, as the cation adducts formed will lead to different mass values.[169]

A further important method for RNA nucleoside analytics is the neutral loss scan (NLS) mode, which detects all product ions after the loss of a pre-defined mass, such as the loss of ribose, enabling in principle the detection of all nucleoside structures that fragment at the *N*-glycosidic bond, except ribose-modified ones.[181] In addition, the pseudo-MS^3 scan mode allows the analysis of fragmentation patterns, which is a useful tool for the elucidation of unknown structures of RNA modifications, in particular in combination with isotope labelling or/and metabolic feeding.[177,179,182–185] The addition of stable isotope-labelled internal standard (SILIS) can be used to correct for potential instrumental variations during the analysis, as the analyte and SILIS are similarly affected by the analytical process. The SILIS is an isotopologue of the analyte, having the same physicochemical properties but containing stable isotopes (^{13}C, ^{15}N or ^{2}H) and is accessible by feeding labelled metabolites to prokaryotic or eukaryotic cultures.[171,186–189] The combination of isotope labelling and LC-MS/MS has been improved to nucleic acid isotope labelling coupled mass spectrometry (NAIL-MS), which enables the analysis of the dynamics of RNA modifications over time, overcoming the static measurement of modification levels by LC-MS.[190–193] Normalisation to the UV signal of one or all of the canonical nucleosides allows further correction for possible inaccuracies in the amount of RNA nucleosides injected. The use of external calibration allows the absolute quantification of modified residues but requires the modified nucleoside to be commercially available in weighable quantities. This step can be omitted for sample-to-sample comparisons.[170,186]

1.2.4.2 Detection of RNA modifications by sequencing-based methods

While mass spectrometric analysis of modified nucleosides allows very accurate quantification, this analytical approach does not provide any information on the modified sites as the RNA is digested to the nucleoside level prior to analysis. Sequencing-based approaches are able to overcome this limitation and provide information on the sequence context. The corresponding methods can be categorised into direct RNA sequencing and Illumina-based sequencing approaches. Avoiding the generation of a complementary DNA (cDNA), direct RNA sequencing methods are based on interruptions of the reverse transcription (RT stops) at the modified positions caused by truncation or misincorporation signatures, as for example reported for the detection of Ψ, m^1A, m^6A, ac^4C, Nm and m^7G.[168,194] To avoid interference of the reverse transcriptase with other modifications during library preparation and thus to incomplete detection of the modifications of interest, demethylation of m^1A, m^3C and m^1G by AlkB (or demethylase mixtures) prior to RT is required.[195,196] Another sequencing approach, belonging to the direct RNA sequencing approaches, is Nanopore sequencing, which allows the detection of modifications without reverse transcription by passing the RNA through a protein nanopore while monitoring the changes in electrical currents.[194] So far, Nanopore sequencing was used for the detection of m^6A, Ψ and 2'-*O*-methylations.[197–200] In contrast to direct RNA sequencing approaches, Illumina sequencing approaches require the RNA to be converted to DNA by reverse transcription, producing a cDNA for subsequent analysis. Here, the behaviour of the modifications during reverse transcription is of particular importance for their detection, since the different base pairing properties compared to the canonical nucleotides result in arrests, misincorporations or deletions during RT, thus forming certain RT signatures.[194] By adapting the RT reaction conditions and using reverse transcriptase enzymes with higher sensitivity for certain modifications, it was possible to detect modifications that had only shown weak RT signatures.[201–204] In particular, Huber *et al.* engineered an RT-active DNA polymerase variant that produces error RT signatures specific for Ψ and Q without the necessity of chemical treatment prior to analysis.[203] Since the RT signatures can be modulated by chemical treatment, sequencing methods are often based on chemical derivatisation of the modified nucleotides prior to their detection, such as bisulfite sequencing for the detection of m^5C.[22] In this case, treatment with bisulfite results in conversion of unmodified cytidine to uridine, while methylated cytidine is not deaminated, allowing differentiation between methylated and unmethylated cytidines.[205,206] Recently, Dai *et al.* published an improvement in bisulfite sequencing termed ultrafast bisulfite sequencing, using highly concentrated reagents and high reaction temperatures to accelerate the bisulfite reaction by 13-fold.[207] In another sequencing approach called PSI-seq, which uses derivatisation with CMC (*N*-cyclohexyl-*N'*-(2-morpholinoethyl)carbodiimide-methyl-*p*-toluenesulfonate) to detect pseudouridines, the formation of CMC-Ψ induces termination of the reverse transcription specifically at pseudouridylated sites.[194,208,209] Another sequencing approach for the detection of pseudouridines, called HydraPsiSeq, is based on the insensitivity

of Ψ to the reaction with hydrazine, which in turn reacts with uridine in a Michael addition, thus non-cleavage is measured to detect Ψ.[194,210] Notably, D, m^5U and some hypermodified uridines can also be detected using this approach.[194,211] The deamination of canonical adenosines to inosines, which behave as guanosines during reverse transcription, is used to detect m^6A, which, unlike adenosine, is not deaminated and therefore behaves as adenosine during reverse transcription.[212,213] Two recent sequencing-based detection methods for dihydrouridine have been reported, both based on chemical derivatisation. The D-Seq is based on sodium borohydride treatment which results in the reduction of dihydrouridine to tetrahydrouridine, thereby eliminating a hydrogen bond donor at the Watson-Crick site and causing RT stops, whereas Finet *et al.* reported RT stops as a consequence of a rhodamine labelling at the respective D sites.[66,67,214]

AlkAniline sequencing (AAS) is a sequencing method that is independent of RT signatures and instead relies on the generation of 5'-phosphates downstream of the targeted modification, which then serve as entry sites for library preparation. The alkaline conditions lead to cleavage of the *N*-glycosidic bond, forming an abasic site on the RNA strand, which can easily react with amines, such as aniline, forming a Schiff base and then leading to β-elimination under alkaline conditions.[215–217] This cleavage results in a downstream 5'-phosphate fragment and an upstream 3'-phosphate fragment (Figure 8). The use of a phosphatase prior to aniline addition removes pre-existing 5'-phosphates and 3'-phosphates resulting from alkaline hydrolysis, leading to a better signal-to-noise ratio in the subsequent sequencing run.[218–220] There are several scoring systems for AAS signals, all counting the 5'-reads' extremities, but differ in their subsequent calculation. While the normalised cleavage is defined as the reads starting at the respective N_{+1} position multiplied by 1000, related to all reads that were aligned to that RNA, and thus ranges from about 25 (depending on the background noise) to 1000, the stop ratio is calculated as the reads starting at the N_{+1} position in relation to all reads at that position (sum of starting reads and passing reads), with its value ranging from 0 to 1. The third calculation is called normalised count and defines the reads starting at the N_{+1} position in relation to the median in the selected window.[194,218] Originally developed for the detection of m^7G and m^3C, dihydrouridines can also be detected by AAS, as dihydrouridine undergoes ring opening under alkaline conditions, resulting in β-ureidopropionic acid, which is then comparable to a β-elimination and allows the detection by this sequencing protocol.[73,221] In addition, ho^5C (5-hydroxycytidine) has been detected by AAS and there is still potential to detect other modifications.[194]

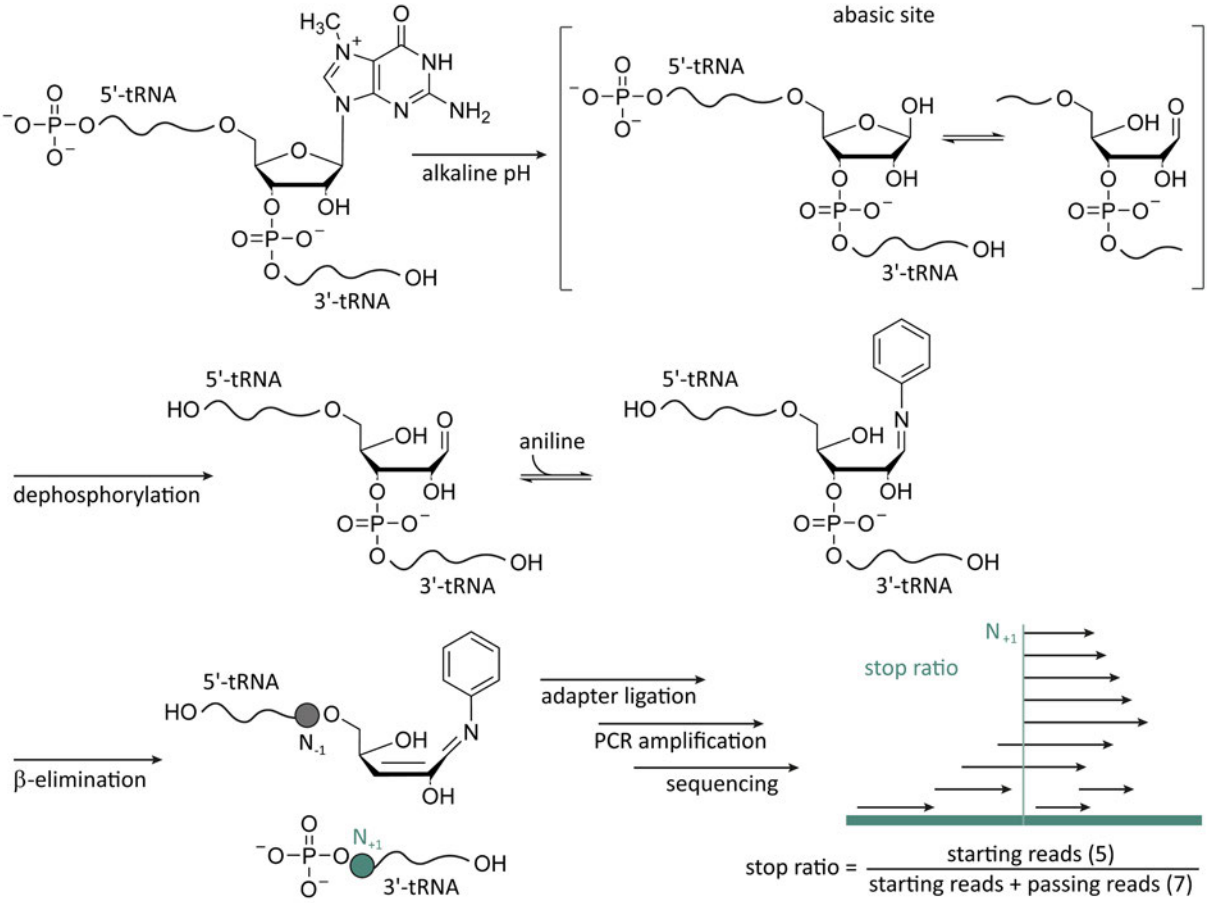

Figure 8: Principle of AlkAniline sequencing (AAS). Alkaline treatment leads to the formation of an abasic site. Subsequent dephosphorylation by alkaline phosphatase removes pre-existing 5'-phosphates and 3'-phospates that resulted from the alkaline hydrolysis. Aniline treatment results in the reaction of aniline with the abasic site, which leads to a β-elimination, inducing a strand break. The resulting phosphate group at the N_{+1} nucleotide (3'-tRNA fragment) is then ligated to sequencing adapters, amplified and subjected to Illumina high-throughput sequencing. The stop ratio scoring system is calculated by the reads starting at the N_{+1} position in relation to all reads at that position (sum of starting reads and passing reads) and its value is ranging from 0 to 1. Figure adapted from Marchand *et al.*[218]

1.3 Protein biosynthesis in prokaryotes

The translation takes place on ribosomes, which in prokaryotes consist of a 30S small subunit and a 50S large subunit, forming the 70S ribosome, with S being the abbreviation for the sedimentation coefficient given in Svedberg. While the 30S subunit is made up of one 16S rRNA and about 21 proteins, the 50S subunit is composed of two rRNAs, 5S and 23S, and 31 proteins. The ribosome has three integral tRNA binding sites: the aminoacyl site (A site), the peptidyl site (P site) and the exit site (E site), to which the tRNA is bound and transferred during the elongation cycle.[222–224]

In prokaryotes, the transcription of DNA into mRNA and the initiation of translation is a continuous process, as RNA polymerase and the ribosome interact, and the ribosome is bound directly to the ribosomal binding site (RBS) after mRNA transcription is complete.[225] While the

translation initiation can also occur with leaderless mRNAs or mRNAs that lack a Shine-Dalgarno (SD) sequence, translation initiation of mRNAs containing the latter has been described in detail and will be focused on in the following. The SD sequence is located upstream (8-10 nucleotides) of the start codon and interacts with the complementary anti-SD (aSD) sequence of the 16S rRNA, recruiting the small ribosomal subunit (30S) to the ribosomal binding site of the mRNA. This is promoted by the initiation factors IF1, IF2 and IF3, which form the preinitiation complex (30S PIC) after recruitment of the initiator $tRNA^{fMet}$ by IF2 and binding to the A site of the small subunit. Recognition of the start codon leads to a stabilisation of the labile 30S PIC, resulting in the more stable 30S IC (initiator complex). In a next step, the 50S large ribosomal subunit assembles with the 30S IC to form the 70S preinitiation complex (70S PIC). GTP is then hydrolysed by the GTPase IF2, leading to the dissociation of the initiation factors and the translocation of the $tRNA^{fMet}$ from the A site to the P site. GTP hydrolysis results in conformational changes that cause the ribosomal subunits to rotate relative to each other, allowing the ribosome to build intersubunit bridges, thus forming the mature 70S initiation complex (70S IC) ready for elongation (Figure 9).[226–229]

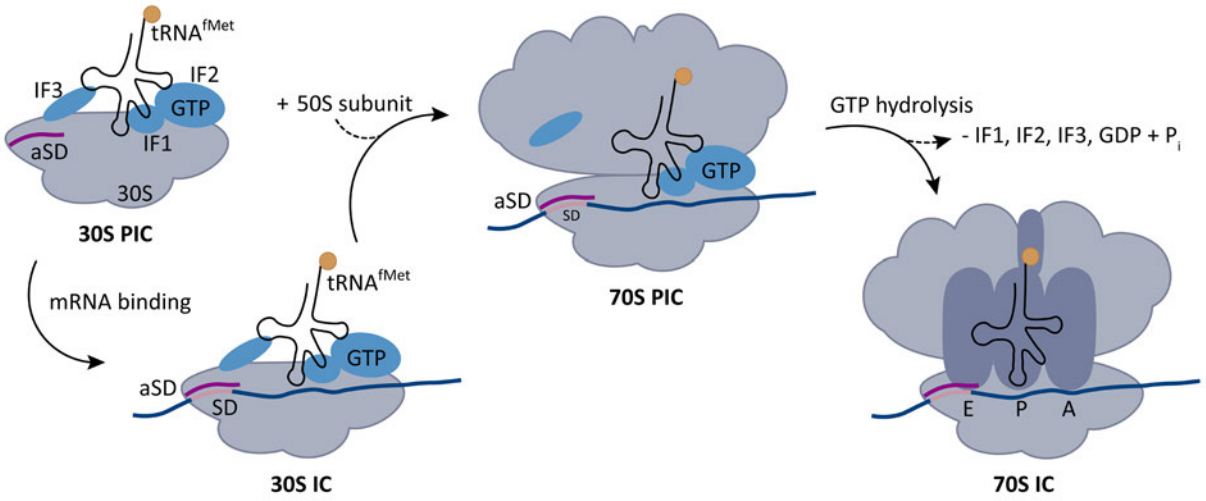

Figure 9: Translation initiation of mRNAs containing a Shine-Dalgarno (DS) sequence in prokaryotes. In a first step the 30S preinitiation complex (30S PIC) is formed consisting of the initiation factors IF1, IF2 and IF3, the initiator $tRNA^{fMet}$ and the small ribosomal subunit (30S). The anti-Shine-Dalgarno (aSD) sequence (coloured in pink) in the 30S subunit binds to the complementary SD sequence (coloured in rose) of the mRNA, forming the 30S initiation complex (30S IC). Addition of the 50S subunit leads to the formation of the 70S preinitiation complex (70S PIC) and subsequent GTP hydrolysis results in formation of the 70S initiation complex (70S IC). Schematic illustration is adapted from Rodnina.[226]

The tRNAs are selectively aminoacylated according to their structural and chemical identity by specific aminoacyl-tRNA synthetases, with the active site of the enzymes interacting with the acceptor stem loop of the tRNA.[230–232] The aminoacylated tRNAs are recognised by translation elongation factors and thus recruited to the A site of the ribosome (Figure 10). Here, hydrogen bonds between A1492, A1493 and G530 of 16S rRNA and the backbone of codon and anticodon stabilise the correct positioning.[31,233] In prokaryotes, the elongation factor EF-Tu

delivers the aminoacylated tRNAs together with GTP to the A site of the ribosome, coordinated by interactions with the stalk of the ribosome and leading to the codon-independent formation of an initial complex.[234–236] Subsequently, codon-anticodon recognition occurs, inducing conformational changes that lead to the interaction of rRNA with the minor groove of the codon-anticodon helix, resulting in an increase of EF-Tu's GTPase activity. Of note, the GTP hydrolysis is rapid for cognate codon-anticodon binding, while it is much lower for near-cognate codon recognitions (factor 650).[237] The conserved histidine residue in EF-Tu (His84) might function as base deprotonating the water molecule during catalytic GTP hydrolysis.[238] Subsequent to GTP hydrolysis, the phosphate is released and EF-Tu

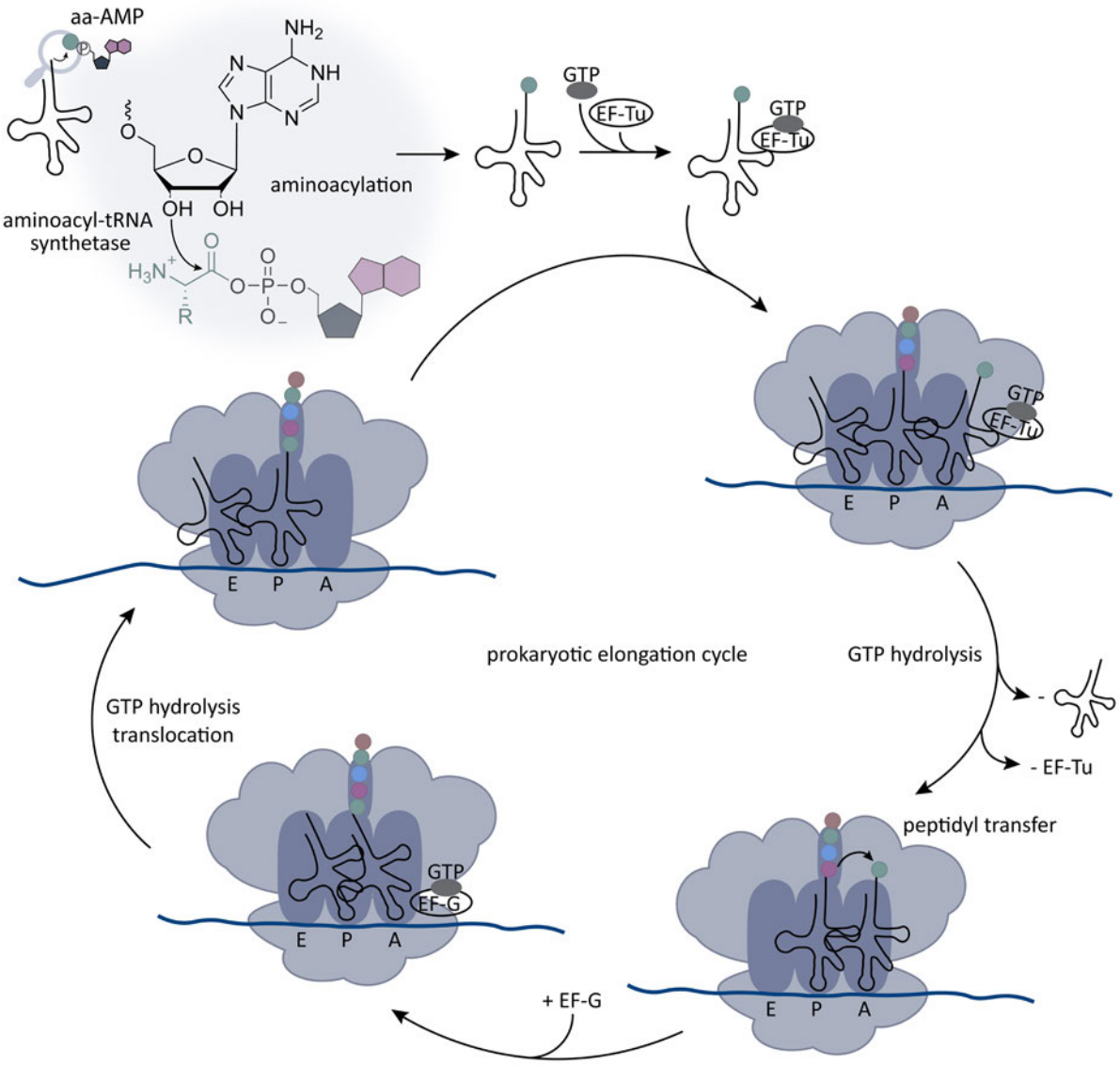

Figure 10: Aminoacylation and translation elongation cycle in prokaryotes. The 3'-terminal ribose moiety is linked to the aminoacyl-adenylate (aa-AMP) of the respective amino acid in the aminoacylation reaction catalysed by aminoacyl-tRNA synthetases. The elongation factor EF-Tu delivers the aminoacylated tRNA to the A site of the ribosome. GTP hydrolysis leads to the release of EF-Tu and the E site tRNA, and the nascent peptide chain is transferred to the aminoacylated tRNA in the A site. Subsequent to EF-G binding, the P and A site tRNAs are translocated, resulting in a free A-site, starting a new elongation cycle. Figure adapted from Voorhees *et al*. and Pang *et al*.[235,239]

undergoes conformational changes weakening its interactions with the ribosome and the tRNA, leading to dissociation of EF-Tu from the complex, while the aminoacylated tRNA remains on the ribosome through interactions with the decoding centre.[235] Cognate tRNAs are then faster accommodated into the peptidyl transferase centre compared to near-cognate tRNAs, which leads to a further discrimination between tRNAs.[237] In the peptidyl transferase centre, the peptide bond is formed and the tRNA and mRNA are then translocated via a hybrid state in which the 3' ends of the A and P site tRNAs are transferred to the P and E sites of the 50S subunit, while the anticodon ends of the tRNAs remain at the 30S subunit. EF-G then binds and GTP hydrolysis completes the translocation.[235] The nascent polypeptide chain moves from the peptidyl transferase centre to a tunnel in the 50S subunit, which allows the nascent peptide chain to pass through, emerge from the ribosome and subsequently fold, as the tunnel is mainly not large enough to pass polypeptide structures larger than alpha-helices.[240] It has been reported that some nascent peptide sequences are able to stall the ribosome, presumably by interacting with the tunnel, suggesting that this might be a form of regulation.[235,241]

1.4 Oxidative stress

As soon as reactive oxygen species (ROS) are present in the cell, they can oxidise various macromolecules as DNA, RNA, proteins and lipids, causing severe defects.[242] The exposure to oxidative agents as quinone-like compounds or bipyridine salts leads to the generation of ROS.[243–246] But there are also intracellular sources of ROS, as the autoxidation of enzymes such as NADH dehydogenase, glutathione reductase and cytochromes P450, which lead to the formation of $O_2^{\cdot-}$ (superoxide anion) and the subsequent dismutation to hydrogen peroxide (H_2O_2) and oxygen, catalysed by the superoxide dismutase (SOD).[247–250] H_2O_2, which can easily cross cell membranes (in contrast to $O_2^{\cdot-}$), reacts with iron ions (Fe^{2+}) in the Fenton reaction to form the highly reactive hydroxyl radical, which cannot be eliminated by an enzymatic reaction, thus leading to severe cell damage in the form of oxidations.[251–254] The oxidised macromolecules are affected in their structure and function which have serious consequences for the cell and might result in cell death.[242] Proteins are mostly oxidised at their thiol groups and aromatic side chains or carbonylated, resulting in conformational and functional changes or, in the case of highly carbonylated proteins, the formation of large aggregates, which are associated with a large number of neurodegenerative diseases.[255,256] The oxidation of lipids leads to the formation of lipid peroxides, which were reported to play a crucial role in signalling pathways in sublethal concentrations, but at higher concentrations affect membrane permeability and fluidity, causing disorders and diseases.[257–259]

The nitrogen and oxygen atoms in the nucleobases are prone to oxidation, making nucleic acids very susceptible to chemical damage.[260] In DNA, repair mechanisms are known, such as

the base excision repair, to prevent interference from oxidised nucleobases during transcription and replication.[261] Oxidative damage on RNA has not been studied as intensively as for DNA because of its shorter lifespan, and it has therefore been assumed not to cause severe defects, leading to an underestimation of its consequences.[262,263] However, RNA oxidation has been associated with several diseases such as Alzheimer's disease and Parkinson's disease, and rRNA oxidation in the active centre of the ribosome has been shown to affect translation.[264–266] Interestingly, Estevez *et al.* reported that unmethylated 23S rRNA is more susceptible to oxidative stress, and oxidation of tRNA was reduced in the presence of the mnm^5s^2U modification, suggesting a regulation by post-transcriptional modifications.[267] Furthermore, Leiva *et al.* reported that $tRNA^{Gly}$ was inactivated under oxidative stress, suggesting a possible translational control mechanism.[268] In 2022, the group further showed that under oxidative stress, translation initiation becomes much slower than the elongation, limiting the translational speed.[269]

8-Oxoguanosine (8-oxo-G) is the most common oxidative lesion on nucleosides because of the low redox potential of guanosine.[267,270,271] In *E. coli*, 8-oxo-G lesions in mRNA have been shown to affect the translational process by favouring base pairing of 8-oxo-G with adenosine instead of cytidine, resulting in misincorporation of amino acids or ribosome stalling.[272,273] Repair mechanisms as for oxidative damage on DNA have not yet been identified for RNA, but proteins were shown to specifically recognise and degrade oxidised RNA.[242] MutT converts 8-oxo-GTP to 8-oxo-GDP, which is then further degraded to the monophosphate by the adenosine diphosphate ribose pyrophosphatase (ADPRase) Rv1700, suggesting that this plays a crucial role in the viability of bacteria under oxidative stress.[274,275] The polynucleotide phosphorylase protein (PNPase) binds specifically to 8-oxo-G and is associated with survival under oxidative conditions, as PNPase-deficient cells were less viable upon peroxide treatment compared to wildtype cells.[276,277]

Furthermore, Hayakawa *et al.* connected the expression of the Y box transcription factor YB-1 to a higher resistance of *E. coli* towards oxidative stress.[278] In addition to possible speculative repair mechanisms, bacteria have developed mechanisms against oxidative stress, resulting in a tolerance to ROS up to a certain level.[242] Such mechanisms include the aforementioned superoxide dismutase, converting $O_2^{\cdot-}$ to H_2O_2, which can then be degraded by the alkyl hydrogen peroxide reductase (Ahp) or the catalases KatG and KatE.[242,279,280] In addition, the cytochrome c peroxidase (Ccp) can transfer electrons from the respiratory chain to H_2O_2, which can be useful under anaerobic conditions.[281,282]

1.4.1 Paraquat

The herbicide paraquat is redox active and susceptible to reduction to a radical stabilised by the bipyridine structure of paraquat. The cofactors NADPH and NADH can serve as electron sources in the reductive reaction catalysed by NAD(P)H oxidases or cytochrome P450.[283–285]

The paraquat radical can undergo a so-called redox cycling with oxygen generating the superoxide radical, which can then be dismutated to hydrogen peroxide and further ROS as described above (Figure 11). Several studies imply that the redox cycling and the resulting production of ROS play a key role in paraquat toxicity. Paraquat accumulates particularly in lung tissue and induces diffuse alveolitis, followed by an extensive pulmonary fibrosis causing severe hypoxia.[286,287] The exposure to paraquat can cause severe neuronal damage and induce neurodegenerative disorders as Parkinson's disease. Yang *et al.* reported a protective role of a long non-coding RNA in paraquat-induced neurotoxicity and suggested it as a potential target for the treatment of paraquat-induced neurodegenerative disorders.[288,289] Moreover, alterations in circular RNAs by m^6A methylation have been linked to paraquat-induced oxidative stress. As circular RNAs have been associated with Parkinson's disease, this link might point to the underlying mechanism of paraquat-induced neurotoxicity.[290]

Additional to the ROS production, paraquat exposure leads to NADPH depletion as a result of the reduction, unbalancing the $NADPH/NADP^+$ ratio and the associated $NADH/NAD^+$ ratio, which is regulated intracellularly by NAD kinases and NADPH phosphatases. NADPH and NADH are the reducing agents in a variety of enzymatic reactions, with NADPH serving as reducing agent mainly in anabolic reactions and NADH in catabolic reactions, which underlies their importance for the organism.[291,292] Interestingly, a metabolic pathway has been reported in *Pseudomonas fluorescens* that generates NADPH from NADH to fight against oxidative stress.[293]

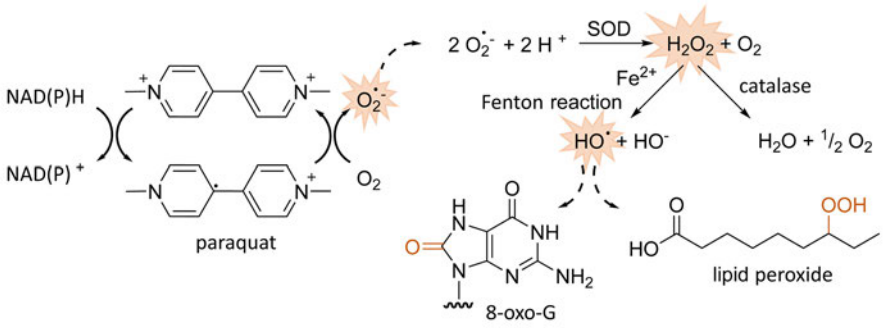

Figure 11: Oxidative damage induced by paraquat. Reduction of paraquat by redox equivalents NADH or NADPH and subsequent re-oxidation by oxygen producing the superoxide anion ($O_2^{\cdot-}$) which is further dismutated into hydrogen peroxide (H_2O_2) and oxygen by the superoxide dismutase (SOD). The Fenton reaction generates hydroxyl radicals ($HO^{\cdot}$) causing oxidative damage as the oxidation of nucleic acids, exemplarily 8-oxo-guanosine (8-oxo-G) is shown, and generation of lipid peroxides. Figure adapted from Gray *et al.* and Barbusinski.[285,294]

Supplementation of bacterial cultures with paraquat can be a useful experimental tool to analyse biological processes under changed redox conditions. Interestingly, Kitzler *et al.* observed differences between *E. coli* strains in the retention of paraquat: while the *E. coli* B strain retains paraquat for many hours, the K-12 strain allows paraquat to diffuse rapidly out of the cell, resulting in the latter strain being more resistant to paraquat treatment.[295]

2 Motivation and Objectives

The field of RNA modifications has become a rapidly developing research area, as precise analytical techniques lead to the elucidation of new modified nucleoside structures, the number and chemical diversity of which are still increasing. They are of significant importance in all biological processes involving RNA, particularly in their central role in mRNA translation, and have been implicated in several diseases, making the understanding of their biological roles of considerable medical concern. Recently, mRNA modifications have been in the spotlight as mRNA vaccines emerged as a successful tool in the fight against the SARS-CoV-2 pandemic, with the modified nucleosides leading to enhanced stability and translation efficacy as well as a low immunogenicity of the mRNA.[151,152] tRNA is the most densely and chemically diverse modified RNA species, with the modified nucleosides ensuring correct positioning of the tRNA at the ribosomal binding site, thus playing an important role in mRNA decoding fidelity.[32,296] The aim of this work was to investigate the tRNA modifications dihydrouridine and queuosine in order to further elucidate their biological roles, with a particular focus on their role during translation. Since tRNAs isolated from polysomes have not yet been extensively studied, a method for the preparation of polysomes was supposed to be adapted to allow the isolation and subsequent analysis of tRNAs that are actively involved in translation.

One part of this thesis was ought to focus on dihydrouridine, which is NADPH-dependently introduced by one of the three dihydrouridine synthases. The NADPH-dependency was thought to link the redox equivalents, and thus the redox status of the cell, to dihydrouridylation, raising the hypothesis that the redox status of the cell might be reflected in the D levels of the cell. This work aimed to investigate this, as well as the influence of each of the three Dus enzymes in this context. Intrigued by previous reports about dihydrouridine's importance for tRNA structure, it was hypothesised that D might be crucial for the correct positioning of tRNAs in the ribosome during mRNA translation, and thus might play a role in this process, which was supposed to be investigated using the polysome preparation method developed for this purpose. As it has been suggested that the redox status affects the modification status of the cell, including dihydrouridylation, this might also affect the translational process, hence also the influence of redox stress was ought to be investigated. LC-MS/MS analysis was available to quantify the dihydrouridine levels, albeit without providing information on the modified positions. AlkAniline sequencing was therefore ought to be tested as a potential tool in this context.

The introduction of modified derivatives, whether natural or synthetic ones, into RNA is a method of increasing interest. The queuosine precursor $preQ_1$ is suitable for introducing semi-synthetic analogues into RNA as the TGT enzyme exchanging a guanine with $preQ_1$ in bacteria or the base queuine in eukaryotes, has been shown to tolerate diverse structural analogues

of preQ$_1$ *in vitro*. However, in most cases, the biological impact of the analogues after their introduction into the tRNA was not considered.[129,130,132,297,298] The aim of this work was to develop an *in vivo* incorporation of clickable analogues of preQ$_1$ in order to subsequently track the incorporated tRNAs and facilitate their affinity purification. As four tRNAs are known to carry the natural queuosine modification, it was hypothesised that the semi-synthetic analogues might be incorporated in the same tRNAs, thus retaining the natural TGT substrates. Such incorporation would plausibly also affect the biological functions of these tRNAs, which was to be investigated with a particular focus on the impact on translation, as queuosine has been reported to affect the translation. In previous studies, queuosine was also reported to be involved in a modification circuit in *S. pombe*, raising the question of the derivative's potential role in this regard. Click chemistry, sequencing approaches and LC-MS/MS analysis were available to study the biological consequences of such a derivatisation in order to further assess the suitability of such methods for medical applications.

3 List of Publications

3.1 Publication included in this thesis

Bessler, L.*, Kaur, N.*, Vogt, L.*, Flemmich, L., Siebenaller, C., Winz, M., Tuorto, F., Micura, R., Ehrenhofer-Murray, A., Helm, M. Functional integration of a semi-synthetic azido-queuosine derivative into translation and a tRNA modification circuit. *Nucleic Acids Research* **50**, 10785–10800; 10.1093/nar/gkac822 (2022).

* These authors contributed equally to this work.

Author contributions: L. Vogt, [redacted] performed the majority of the experimental work. L. Vogt investigated the growth behaviour of respective knockout strains and the phenotypic consequences of supplementing the analogue *in vivo* in *E. coli*. [redacted] established the feeding protocol and the copper click reaction with subsequent detection via gel electrophoresis. L. Vogt performed the *E. coli* polysome preparations and subsequent tRNA purification. [redacted] helped with gradient formation and fractionation. HeLa cultures and eukaryotic polysome preparations were performed by [redacted], subsequent tRNA purification was done by L. Vogt. LC-MS/MS analysis was performed by [redacted] with help of L. Vogt. [redacted] performed all experiments in *S. pombe*, as well as the *E. coli in vitro* experiments, including the subsequent analysis. [redacted] provided the $preQ_1$-compounds. [redacted] conceived and supervised the project. L. Vogt, [redacted] wrote the manuscript with input from the other authors.

3.2 Publications not included in this thesis

Galvanin, A., Vogt, L., Grober, A., Freund, I., Ayadi, L., Bourguignon-Igel, V., Bessler, L., Jacob, D., Eigenbrod, T., Marchand, V., Dalpke, A., Helm, M., Motorin, Y. Bacterial tRNA 2'-O-methylation is dynamically regulated under stress conditions and modulates innate immune response. *Nucleic Acids Research* **48**, 12833–12844; 10.1093/nar/gkaa1123 (2020).

Contribution as co-author: L. Vogt performed the polysome preparations of *E. coli* wildtype and TrmH knockout strains.

Koshla, O., Vogt, L., Rydkin, O., Sehin, Y., Ostash, I., Helm, M., Ostash, B. Landscape of Post-Transcriptional tRNA Modifications in Streptomyces albidoflavus J1074 as Portrayed by Mass Spectrometry and Genomic Data Mining. *Journal of Bacteriology* **205**, e0029422; 10.1128/jb.00294-22 (2023).

Contribution as co-author: L. Vogt performed the LC-MS analysis.

Bessler, L., Vogt, L., Lander, M., Dal Magro, C., Keller, P., Kühlborn, J., Kampf, C., Opatz, T., Helm, M. A New Bacterial Adenosine-Derived Nucleoside as an Example of RNA Modification Damage. *Angewandte Chemie (International Edition)* **62**, e202217128; 10.1002/anie.202217128 (2023).

Contribution as co-author: L. Vogt performed the polysome preparations.

Sudol, C., Kilz, L., Marchand, V., Thuillier, Q., Guérineau, V., Goyenvalle, C., Faivre, B., Toubdji, S., Lombard, M., Jean-Jean, O., de Crécy-Lagard, V., Helm, M., Motorin, Y., Brégeon, D., Hamdane, D. Functional redundancy in tRNA dihydrouridylation. *Nucleic Acids Research*; 10.1093/nar/gkae325 (2024).

Contribution as co-author: L. Kilz performed the LC-MS analysis.

4 Results and Discussion

4.1 Dihydrouridylation of *E. coli* tRNA under redox stress

Dihydrouridylation of tRNA is dependent on the cellular availability of NADPH, as mechanistically the prosthetic flavin group of the dihydrouridine synthase is reduced by NADPH prior to hydride transfer of the reduced flavin to uridine. This leads to a hypothesised link between dihydrouridylation and the redox status of the cell, which was aimed to be investigated in this work. Therefore, the redox-dependency of tRNA dihydrouridylation in *E. coli* was examined by supplementing bacterial cultures with paraquat to induce changes in the NADPH/$NADP^+$ ratio and subsequently analysing the dihydrouridine levels to provide insight into the effect on dihydrouridylation. Since three dihydrouridine synthases share the dihydrouridylation in *E. coli*, single knockout strains of each of these enzymes were used to analyse the effect of each enzyme in the context of redox stress.

4.1.1 Dihydrouridine levels in *E. coli* wildtype and Dus knockout strains

Prior to the induction of redox stress by the treatment with paraquat, the D levels in *E. coli* wildtype and knockout strains were investigated under non-treated conditions to determine native levels of dihydrouridylation by the different enzymes. For this purpose, tRNA was isolated from wildtype and triple knockout (*ΔdusA,B,C*) cultures, digested to nucleoside level and subjected to LC-MS/MS analysis. It is noteworthy that when separated on a reversed-phase C18 HPLC column, D elutes earlier than U, as depicted in the merged chromatograms in Figure 12A. As a result of fragmentation at the *N*-glycosidic bond, D shows the mass transition of *m/z* = 247 → 115, sharing the fragmentation corresponding to the loss of a ribose moiety (-132 Da) with most nucleoside structures. Using this mass transition, D was detected in tRNA isolated from a wildtype *E. coli* culture (bluish green solid line), in contrast to tRNA isolated from a triple knockout strain in which the genes for all three dihydrouridine synthases were deleted. In the latter case, a signal corresponding to the mass transition of D was barely detectable (bluish green dashed line). Accordingly, the detected D signal in the wildtype tRNA was introduced by the three Dus enzymes, or at least by one of them. To analyse this further, single knockout strains of the three Dus enzymes were scrutinised regarding their D levels. The abundance of the signal corresponding to the mass transition of D was normalised to the UV signal of adenosine to correct potential inaccuracies in the amount of tRNA injected and were then related to the normalised D signal of wildtype tRNA, which was set to 100%. The knockout of DusA resulted in a 50% reduction of D levels compared to the wildtype, while the knockouts of DusB and DusC revealed a decrease in the D level of 30% and 27%, respectively (Figure 12B).

These findings indicate that DusA contributes most to dihydrouridylation, reducing the half of the D modifications detected in the wildtype tRNA. This is in line with literature, reporting that DusA introduces half of the dihydrouridines while DusB and DusC modify the other half.[72]

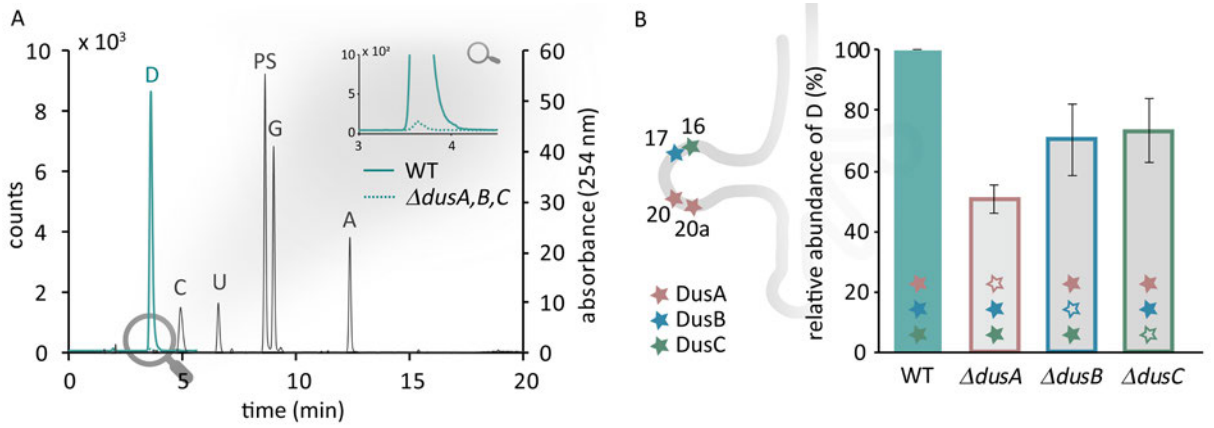

Figure 12: LC-MS/MS analysis of dihydrouridine modification levels in *E. coli* wildtype and knockout strains. A Extracted ion chromatogram (EIC) of the mass transition *m/z* = 247 → 115 corresponding to D (bluish green) merged with the UV chromatogram at 254 nm (grey) showing the detection of the main nucleosides cytidine (C), uridine (U), guanosine (G) and adenosine (A). The D signal in tRNA isolated from a wildtype *E. coli* culture is depicted as solid line while the EIC from tRNA isolated from a triple knockout culture (*ΔdusA,B,C*) is shown as dashed line. The deaminase inhibitor pentostatin (PS) was added during sample preparation and was also detected by UV spectroscopy. **B** LC-MS/MS analysis of D modification levels in tRNA isolated from the wildtype culture (bluish green) and single knockout strains of the dihydrouridine synthases DusA (*ΔdusA*, framed in rose), DusB (*ΔdusB*, framed in blue) and DusC (*ΔdusC*, framed in green). D positions in the tRNA D loop and corresponding modifying Dus enzymes are schematically shown on the left. Active enzymes are indicated with filled stars, while the knocked-out enzymes are shown as empty stars. Experiments were performed in biological duplicates and results are shown as average, the standard deviations are depicted as error bars.

4.1.2 Effect of paraquat treatment on bacterial growth and D modification levels

The bipyridine salt paraquat is readily reduced to a mesomerically stabilised radical, which induces the production of reactive oxygen species and is highly toxic.[285–287] Therefore, before investigating the effect of PQ on tRNA D levels, the toxic effect on bacterial cultures had to be determined. For this purpose, wildtype *E. coli* cultures were supplemented with increasing concentrations of PQ (0.1 mM, 0.3 mM, 0.5 mM and 1 mM) and the growth behaviour was investigated by measuring the optical density (Figure 13A). While the non-treated culture (black solid line) showed a classical exponential growth curve, the treatment with 0.1 mM PQ (grey dashed line) resulted in a decelerated growth. Cultures treated with the concentrations 0.3 mM, 0.5 mM and 1 mM PQ were severely affected and no differences in growth were observed between these concentrations. Based on this, the lowest and second lowest concentrations were selected for subsequent experiments to study both phenotypes for their dihydrouridine levels.

In addition to the wildtype, the effect of PQ on D levels in the DusA knockout strain was examined since DusA was shown to introduce more D modifications compared to DusB and

DusC (Figure 12B). After growing the cultures supplemented with either 0 mM, 0.1 mM or 0.3 mM PQ, the tRNA was isolated and analysed by LC-MS/MS (Figure 13B). Again, the detected signals with the mass transition of *m/z* = 247 → 115 were normalised to the respective UV signal of adenosine and then related to the normalised D signal in tRNA isolated from the non-treated wildtype culture, which was set to 100%. Treatment with PQ resulted in a decrease in D level by 23% in wildtype tRNA in the presence of 0.1 mM PQ and a decrease by 28% when the culture was treated with 0.3 mM (bluish green). Inactivation of DusA (framed in rose) resulted in a 47% reduction in D modifications compared to the wildtype control sample, confirming the previous results shown in Figure 12. The paraquat supplementation resulted in a further decrease of D levels, indicating that DusB and/or DusC, as the remaining active enzymes in the *ΔdusA* strain, are affected by redox changes introduced by PQ.

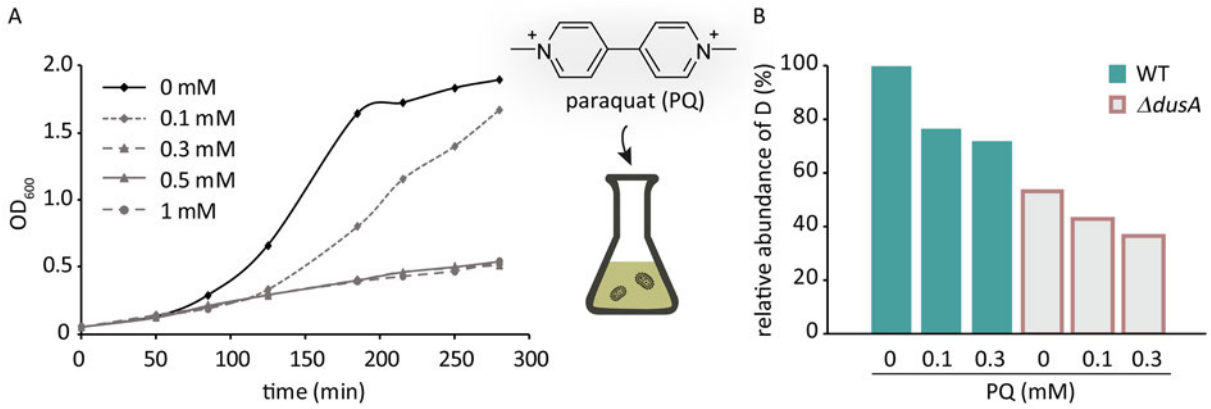

Figure 13: Effect of paraquat treatment on bacterial growth and D modification levels in *E. coli* wildtype and DusA knockout cultures after paraquat treatment. A Growth behaviour of *E. coli* wildtype cultures after supplementation with different concentrations (0 mM, 0.1 mM, 0.3 mM, 0.5 mM and 1 mM) of paraquat (PQ). **B** LC-MS/MS analysis of D modification levels in tRNA isolated from wildtype (bluish green) and DusA knockout cultures (*ΔdusA*, framed in rose) treated with 0 mM, 0.1 mM or 0.3 mM PQ. After normalisation to the respective UV signal of adenosine, the D signals were related to the signal detected in tRNA isolated from the untreated wildtype (set to 100%).

These results lead to the conclusion that PQ affects the dihydrouridylation in tRNA, as evidenced by a decrease in D levels in LC-MS/MS analysis. However, analysis at nucleoside level does not provide information on the dihydrouridylated positions, as is the case in sequencing-based approaches. AlkAniline sequencing has been reported to detect D modifications, although method validation for D detection has not yet been conducted.[218,220] For further insight into the dihydrouridylated tRNA positions and aiming for further method validation, the described data set was also analysed by AAS performed by [redacted].

Analysis of tRNA isolated from the wildtype strain by AAS revealed signals at the known D positions in the tRNA D loop 16, 17, 20 and 20a, indicating that all Dus enzymes were involved in the reduction of U to D in the wildtype. Apart from some noise, tRNA isolated from the DusA

knockout culture showed only signals at tRNA positions 16 and 17 (Figure 14). As DusB and DusC are the active enzymes in this strain, this was expected and confirms the position specificity of DusA and in turn validates the position-specific detection of AAS. In the triple knockout strain some noise was detectable but the signals remained below a stop ratio score of 0.04 which confirms as well the knockout of all three Dus enzymes in this knockout strain.

Interestingly, most of the D signals detected at positions 20 and 20a in the wildtype did not show a decrease as a result of the paraquat treatment, while the D signals at positions 16 and 17 showed a reduction upon PQ supplementation to the culture. This leads to the suggestion that the previously described decrease of D levels in the wildtype after PQ treatment (Figure 13B) was mainly caused by less D modifications at positions 16 and 17 and thus that the DusA enzyme might be less vulnerable towards PQ treatment. Notably, while all signals detected at position 16 decreased clearly with paraquat exposure, only about 56% of D signals detected at position 17 were reduced, indicating that there might be also a differential sensitivity of DusB and DusC.

In conclusion, the AAS results provided further evidence of a paraquat dependent decrease of D levels and confirmed the position specific detection by analysing the DusA knockout strain, thus validating the AAS for the detection of D modifications in *E. coli* tRNA.

Figure 14: Analysis of dihydrouridylation sites in *E. coli* tRNA by AlkAniline sequencing. AAS results of total tRNA isolated from *E. coli* wildtype cultures as well as DusA knockout (*ΔdusA*) and triple knockout (*ΔdusA,B,C*) cultures that were treated

with 0 mM, 0.1 mM or 0.3 mM PQ. The various tRNAs and the corresponding D positions are shown on the left with the following code: organism_tRNA species_anticodon – position of D / modifying enzyme, while the numbering of tRNAs and modifying enzymes are indicated on the right. AAS results are presented as stop ratio score (ranging from 0 to 1).

4.1.3 Elucidation of the oxygen dependency

Since paraquat was reported to possibly undergo redox cycling with oxygen, combined with fluctuations in D levels that were observed in some experiments, the necessity of controlled and reproducible oxygen availability during bacterial growth was evident. To enable this and to examine the paraquat induced effect on dihydrouridylation in an oxygen-dependent manner, the experimental setup was changed to cultivation in a bioreactor as shown schematically in Figure 15A, which allows not only the cultivation under controlled aerobic conditions but also the cultivation under anaerobic conditions. The cultures were grown in a glass bioreactor positioned in a water bath at 37 °C and equipped with a magnetic stirrer. A constant stream of air was provided to grow the bacterial cultures under reproducible aerobic conditions, while a constant gas flow of nitrogen enabled the cultivation under anaerobic conditions. The attachment of an oxygen electrode as well as a pH electrode allowed for continuous monitoring of the oxygen saturation and the pH of the culture medium (Figure A1). The monitoring was completed by a manual measurement of the optical density at various time points.

The experiments described in this subchapter were performed by [redacted] as part of her master's thesis under my supervision.

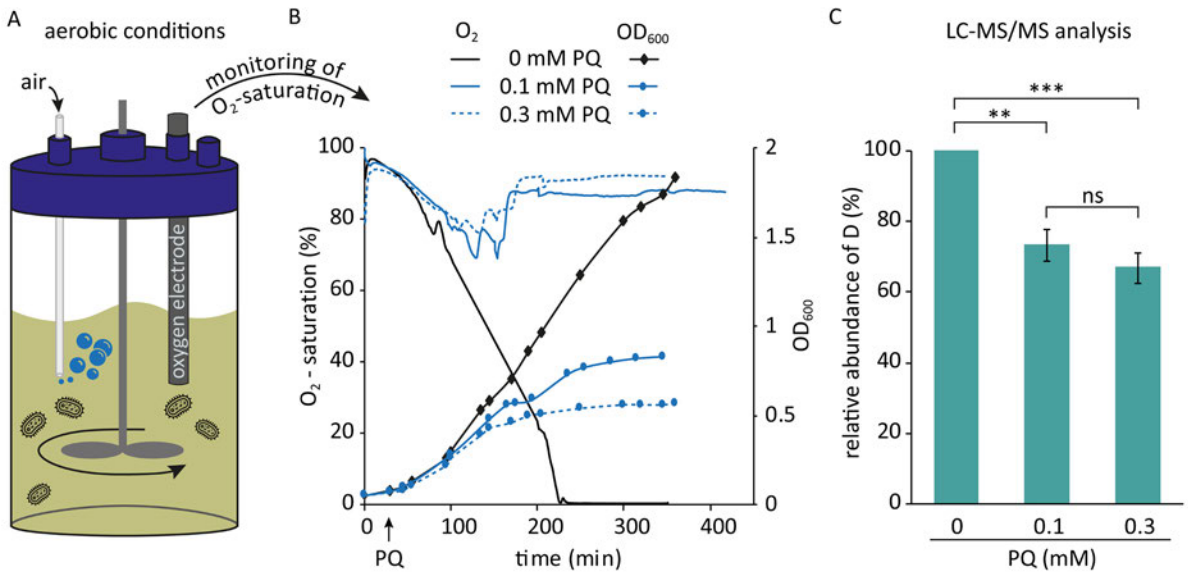

Figure 15: Analysis of tRNA dihydrouridylation under defined aerobic conditions. A Schematic illustration of the bioreactor used for cultivation under defined conditions. A continuous stream of air ensured a constant oxygen supply, the resulting oxygen saturation of the medium was monitored by attaching an oxygen electrode to the bioreactor. **B** Monitoring of the oxygen saturation and the bacterial growth of untreated (black) and treated (0.1 mM and 0.3 mM PQ, blue) cultures. The

time point of PQ addition is indicated with an arrow. **C** LC-MS/MS analysis of dihydrouridine levels in total tRNA isolated from treated and untreated *E. coli* wildtype cultures. The signals detected with the mass transition *m/z* = 247 → 115 corresponding to D were normalised to the UV signal of adenosine in the respective sample and related to the normalised D signal of tRNA isolated from the non-treated culture. The results are shown as average of biological triplicates, the standard deviations are indicated as error bars. Significance was evaluated using a two-tailed Student's t-test (ns: not significant, **: $p < 0.01$, ***: $p < 0.001$).

The continuous stream of air ensured a reproducible oxygen supply to the culture medium during bacterial growth thus avoiding slight changes of oxygen availability between biological replicates. To analyse the previously observed paraquat dependent decrease of dihydrouridylation under these defined aerobic conditions (Figure 15A), wildtype *E. coli* cultures were supplemented with 0 mM, 0.1 mM or 0.3 mM paraquat. The oxygen saturation curves are displayed together with the bacterial growth curve of the respective culture in Figure 15B. The oxygen saturation of the untreated culture (black solid line) decreased simultaneously with the increase in optical density (black line, rhombuses), demonstrating the increasing consumption of oxygen by the growing number of bacteria cells. In contrast to that, the oxygen saturation of the treated cultures (blue lines) decreased in the beginning of culturing but started to increase again when the culture reached an optical density of around 0.4 – 0.5. In line with the previously recorded growth curves (Figure 13), the bacterial growth in the bioreactor was dose-dependently affected by the supplementation of paraquat (blue lines, points). The slow growth of the bacteria in the treated cultures after reaching an optical density of around 0.4 – 0.5 may explain the observed increase in oxygen saturation.

The total tRNA was subsequently isolated and analysed for D levels using LC-MS/MS. Again, the D signal in tRNA isolated from the non-treated culture was set to 100% and the results are shown as average of biological triplicates (Figure 15C). Under controlled oxygen supply, the D levels in isolated total tRNA decreased significantly upon paraquat treatment, as observed before (Figure 13B). The supplementation with 0.1 mM PQ resulted in dihydrouridylation of 73% compared to the untreated culture, while the 0.3 mM PQ treated cultures showed an averaged dihydrouridylation level of 67%. Thus, the previously observed decrease of D levels upon paraquat treatment was confirmed under defined aerobic growth conditions.

A similar experimental setup was used to analyse the paraquat dependent dihydrouridylation under anaerobic conditions, with the continuous air stream being replaced by a continuous stream of nitrogen. As expected, when the cultures were grown anaerobically (Figure 16), the oxygen saturation rapidly decreased to 0% in all three cultures, independently of the paraquat supplementation. Interestingly, even without any left oxygen, the bacteria were able to grow, albeit very slowly compared to the cultures grown aerobically (Figure 15B). No difference in growth behaviour was observed between the treated and non-treated cultures. Of note, the aerobic paraquat dependent deceleration of the bacterial growth was observed above an optical density of 0.4, a level that was never reached under anaerobic conditions. Thus,

anaerobic growth might also be affected by PQ supplementation if the bacteria would generally grow better under these conditions.

Analysis of D levels revealed only slight differences between tRNA isolated from non-treated and treated cultures, which were not statistically significant (Figure 16C).

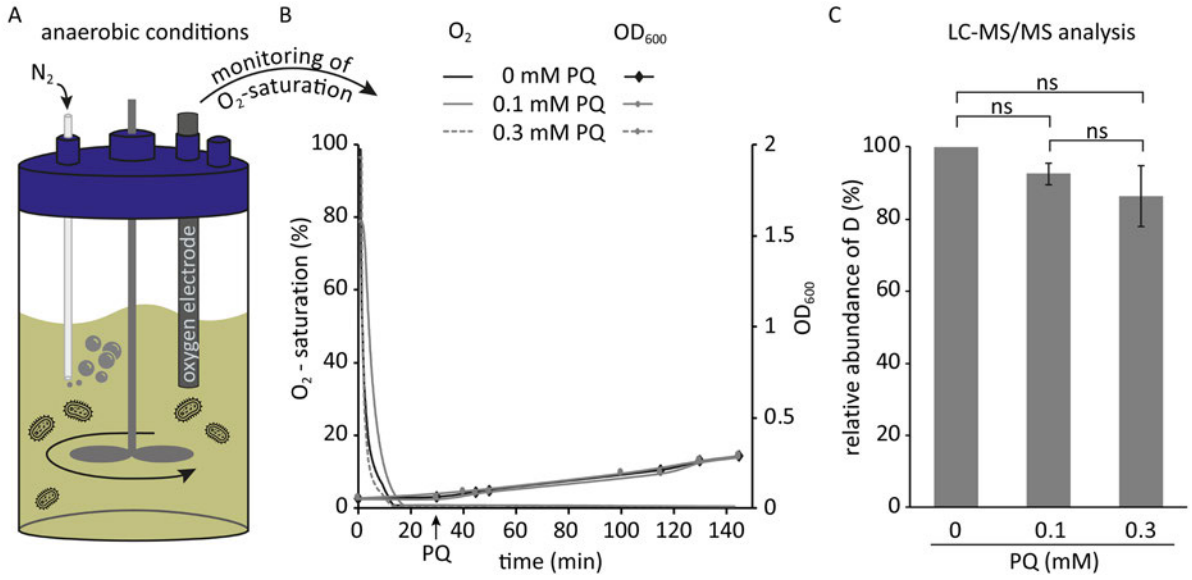

Figure 16: Analysis of tRNA dihydrouridylation under anaerobic conditions. A Schematic illustration of the bioreactor used for the cultivation under anaerobic conditions. The latter was enabled by a continuous stream of nitrogen that was passed through the culture medium. An attached oxygen electrode allowed to monitor the oxygen saturation of the medium during bacterial growth. **B** Monitoring of the oxygen saturation and the bacterial growth of untreated (black) and treated (0.1 mM and 0.3 mM PQ, grey) cultures. The time point of PQ addition is indicated with an arrow. **C** LC-MS/MS analysis of dihydrouridine levels in total tRNA isolated from treated and untreated *E. coli* wildtype cultures. The signals detected with the mass transition *m/z* = 247 → 115 corresponding to D were normalised to the UV signal of adenosine in the respective sample and related to the normalised D signal of tRNA isolated from the non-treated culture. The results are shown as average of biological triplicates, the standard deviations are indicated as error bars. Significance was evaluated using a two-tailed Student's t-test (ns: not significant).

The decrease in dihydrouridylation was exclusively observed in the presence of oxygen, meaning in samples from bacteria grown under uncontrolled standard conditions (Figure 13) and defined aerobic conditions (Figure 15C). These findings indicate that oxygen plays an important role in this experimental setup, presumably in form of the redox cycling with paraquat, leading to a regeneration of the paraquat radical and thus to a higher consumption of NADPH equivalents. The concomitant reduction in cellular NADPH availability results in less reduced flavins bound to the Dus enzymes and hence less U to D reduction. These results emphasise the relevance of considering oxygen as an important parameter in the analysis of dihydrouridylation, therefore the described controlled aerobic conditions were used for further experiments.

4.1.4 Investigation of dihydrouridine's role in translation under redox stress

Since dihydrouridine is thought to play a role in tRNA structure and tRNA conformation was reported to be important for correct tRNA binding to the ribosome during mRNA translation,[87,235] a potential role of D in the translational process was investigated. This was addressed by using polysome preparations to examine the levels of D on tRNAs bound to actively translating ribosomes as these can be considered to functionally interact with translational factors. Additionally, it was analysed whether the D levels on polysomes are further affected by redox changes, again introduced by paraquat as the previous results had demonstrated a PQ-dependent effect on the D levels. Since no significant difference was observed between the treatment with 0.1 mM or 0.3 mM PQ under defined aerobic conditions (Figure 15C), the higher concentration of 0.3 mM PQ was used for polysome preparations.

To isolate the polysomal complexes, whole cell lysate was loaded on top of a sucrose gradient which was centrifuged at high speed, resulting in an assembly of particles along the sucrose gradient according to their size. While light molecules, such as the free cytosolic tRNA pool, were located in the lower concentrated part of the gradient, the large polysome complexes accumulated in the higher concentrated part. Using absorbance at 260 nm, the sucrose gradient was fractionated into a free RNA fraction (F0), a fraction F1 containing the ribosomal subunits, a monosome fraction (F2) and a polysome fraction (F3) (Figure 17A). Interestingly, the absorbance of the majority of the polysome fractions showed an apparent reduction upon paraquat treatment when normalised to the free RNA fraction. Although one might speculate on this basis that paraquat affects not only the bacterial growth but also the translational machinery (Figure A2 - Figure A6), in the context of the present work this was only a rather incidental observation that requires further clarification in the future.

As the composition of RNAs differs substantially between the free RNA and the polysome fraction, analysis of D levels in total RNA isolated from these fractions would not give conclusive results. Therefore, only the tRNA was subsequently purified by denaturing polyacrylamide gel electrophoresis (PAGE) (Figure 17B) and analysed in biological triplicates by LC-MS/MS to determine tRNA dihydrouridylation. The signals detected with the mass transition corresponding to D were again normalised to adenosine and related to the signal detected for free cytosolic (F0) tRNA isolated from the untreated wildtype culture (WT 0 mM PQ F0) (Figure 17C).

Comparing the single Dus knockout strains with the wildtype, the dihydrouridylation levels in cytosolic tRNAs (F0) were reduced, as described in section 4.1.1 for the non-polysome preparations. Supplementation with paraquat affected dihydrouridylation of cytosolic tRNAs in both wildtype cultures and single Dus knockout cultures. While D levels decreased by 33% in the wildtype, which is comparable to the reduction observed previously (Figure 15C), the D

levels in free tRNAs in the DusA knockout strain were even more affected, resulting in a 67% decrease (compared to *ΔdusA* 0 mM PQ). In contrast, dihydrouridylation was less affected by PQ supplementation in the DusB and DusC knockout strains. Here, the D modification levels showed a decrease of only 20% and 22%, respectively, when compared to the corresponding untreated knockout cultures. The triple knockout, in which all three Dus enzymes are deleted, was cultivated under untreated and treated conditions and was used as negative control. Only low D levels (below 2%) were detected here (Figure A7).

Given that DusB and DusC are the active enzymes in the DusA knockout strain, the results indicate that these enzymes are severely affected by paraquat supplementation, whereas DusA, which is active in *ΔdusB* and *ΔdusC*, appears to be less sensitive. These results are consistent with the previous results obtained from AlkAniline sequencing (Figure 14), showing a stronger reduction upon PQ treatment at tRNA positions 16 (DusC) and 17 (DusB) as opposed to positions 20 and 20a (both DusA).

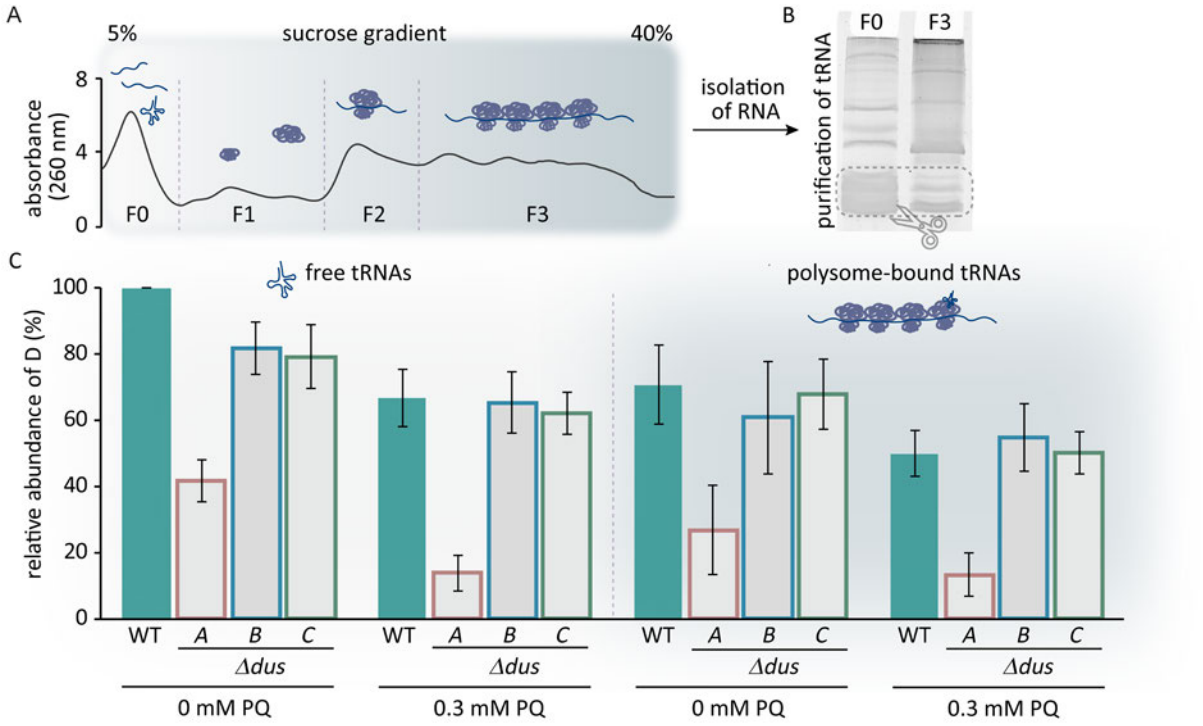

Figure 17: Analysis of D modification levels on polysome-bound tRNAs. A Absorbance curve (260 nm) during fractionation of RNA-protein complexes distributed along a sucrose gradient ranging from 5% to 40%. Fractions were collected by using the absorbance curve (F0: free RNAs, F1: ribosomal subunits, F2: monosomes, F3: polysome complexes) and total RNA was isolated from these fractions. **B** Subsequent tRNA purification from the isolated total RNA by extraction from a 10% denaturing polyacrylamide gel electrophoresis (PAGE) and subsequent GelRed staining which was visualised using a Typhoon (excitation wavelength 532 nm). **C** LC-MS/MS analysis of D modification levels in free tRNAs (F0) and polysome-bound tRNAs (F3) isolated from treated and untreated wildtype and single Dus knockout strains (*ΔdusA*, *ΔdusB* and *ΔdusC*). After normalisation of the signals detected with the mass transition *m/z* = 247 → 115 (corresponding to D) to the UV signal of adenosine in the respective sample, the normalised signals were related to the normalised D signal detected in the free tRNA fraction isolated from the untreated wildtype culture (WT 0 mM PQ F0). Results are shown as average of biological triplicates, the standard deviations are indicated as error bars.

Compared to D levels in the free tRNA fraction, dihydrouridylation in polysome-bound tRNAs was significantly reduced in the untreated wildtype culture, while D levels in the Dus knockout cultures did not show a significant difference. When the effect of paraquat supplementation was analysed, D levels on polysome-bound tRNAs were not significantly altered, neither in the wildtype nor in the knockout cultures, indicating that paraquat does not affect the dihydrouridylation on polysomes.

In conclusion, these results did not reveal an indication that D modifications play a specific role in the translational process, although dihydrouridylated tRNAs were detected on actively translating polysomes, which is not unexpected as D is one of the most abundant modifications in tRNAs.[21]

In addition to the LC-MS/MS analysis, the free tRNAs and polysome-bound tRNAs isolated from the various treated cultures were also analysed by AlkAniline sequencing in order to study them in a position-specific manner. The AAS analysis was performed by [redacted].

As previously shown by the analysis of the DusA and triple Dus knockouts (Figure 14), mainly no or less signals were obtained at tRNA positions expected to be modified by the knocked-out enzyme. In contrast to the previous analysis, signals of medium intensities were also detected, interestingly predominantly in the polysome fraction (F3) (Figure 18, Figure A8 and Figure A9). However, although higher signals were detected in the analysed knockouts, the position specificities of the three Dus enzymes are still evident.

Overall, tRNA positions modified by DusA (20 and 20a) show high dihydrouridylation even under paraquat treatment in wildtype as well as in DusB and DusC knockout cultures in which the DusA remains active. In contrast, positions modified by DusB and DusC (16 and 17) showed predominantly reduced D signals. These results are consistent with the previous findings (described in 4.1.2) and confirm a differential sensitivity of the three Dus enzymes to paraquat, with DusA being the least sensitive, whereas DusB and DusC are severely impaired.

Regarding the polysome-bound tRNAs, some tRNAs showed increased signal intensities of D compared to the free tRNA fraction, while others decreased or remained unchanged, thus no consistent trend can be identified. However, a striking observation was that higher signal intensities were detected for the initiator $tRNA^{fMet}$ isolated from the polysome fraction, particularly conspicuous in DusA and triple Dus knockout preparations, but also noticeable in the other strains (Figure 18, tRNA no. 16). This opens up for speculations that dihydrouridylation might be important for ribosome binding of the initiator tRNA. Another noteworthy finding is that in two of the three replicates, signals at position 16 were more


F0: free tRNAs
F3: polysome-bound tRNAs
WT
ΔdusA
ΔdusB
ΔdusC
ΔdusA,B,C
0
0.3
PQ (mM)
F0 F3
no.
ec_tRNAArg_ACG-D20a/DusA
ec_tRNAArg_TCT-D20a/DusA
ec_tRNAAsn_GTT-D20/DusA
ec_tRNAAsp_GTC-D20/DusA
ec_tRNAAsp_GTC-D20a/DusA
ec_tRNACys_GCA-D20/DusA
ec_tRNACys_GCA-D20a/DusA
ec_tRNAGln_CTG_TTG-D20/DusA
ec_tRNAGly_CCC-D20/DusA
ec_tRNAGly_GCC-D20/DusA
ec_tRNAHis_GTG-D20/DusA
ec_tRNAIle_CAT-D20/DusA
ec_tRNAIle_CAT-D20a/DusA
ec_tRNAIle_GAT-D20/DusA
ec_tRNAIle_GAT-D20a/DusA
ec_tRNAiMet_CAT-D20/DusA
ec_tRNALeu_CAA-D20/DusA
ec_tRNALeu_CAG-D20/DusA
ec_tRNALeu_GAG-D20/DusA
ec_tRNALeu_TAA-D20/DusA
ec_tRNALeu_TAG-D20/DusA
ec_tRNAMet_CAT-D20/DusA
ec_tRNAMet_CAT-D20a/DusA
ec_tRNAPhe_GAA-D20/DusA
ec_tRNAPro_CGG-D20/DusA
ec_tRNAPro_GGG-D20/DusA
ec_tRNAPro_TGG-D20/DusA
ec_tRNASer_CGA-D20a/DusA
ec_tRNASer_GCT-D20a/DusA
ec_tRNASer_GGA-D20/DusA
ec_tRNASer_TGA-D20/DusA
ec_tRNASer_TGA-D20a/DusA
ec_tRNAThr_CGT1-D20/DusA
ec_tRNAThr_GGT-D20/DusA
ec_tRNAThr_TGT-D20/DusA
ec_tRNATrp_CCA-D20/DusA
ec_tRNAVal_GAC-D20/DusA
ec_tRNAVal_GAC-D20a/DusA
ec_tRNAAla_GGC_TGC-D17/DusB
ec_tRNAArg_ACG-D17/DusB
ec_tRNAGly_GCC-D17/DusB
ec_tRNAHis_GTG-D17/DusB
ec_tRNAIle_GAT-D17/DusB
ec_tRNALeu_CAG-D17/DusB
ec_tRNALeu_GAG-D17/DusB
ec_tRNALeu_TAG-D17/DusB
ec_tRNALys_TTT-D17/DusB
ec_tRNAMet_CAT-D17/DusB
ec_tRNAPro_TGG-D17/DusB
ec_tRNAThr_CGT1-D17/DusB
ec_tRNAThr_GGT-D17/DusB
ec_tRNATrp_CCA-D17/DusB
ec_tRNAVal_GAC-D17/DusB
ec_tRNAVal_TAC-D17/DusB
ec_tRNAAsn_GTT-D16/DusC
ec_tRNAAsp_GTC-D16/DusC
ec_tRNAGly_GCC-D16/DusC
ec_tRNAHis_GTG-D16/DusC
ec_tRNALeu_CAA-D16/DusC
ec_tRNALeu_CAG-D16/DusC
ec_tRNALeu_GAG-D16/DusC
ec_tRNALeu_TAA-D16/DusC
ec_tRNALeu_TAG-D16/DusC
ec_tRNALys_TTT-D16/DusC
ec_tRNAMet_CAT-D16/DusC
ec_tRNAPhe_GAA-D16/DusC
ec_tRNAThr_CGT1-D16/DusC
ec_tRNAThr_GGT-D16/DusC
ec_tRNAThr_TGT-D16/DusC
ec_tRNATrp_CCA-D16/DusC
ec_tRNAVal_GAC-D16/DusC
1
2
3
4
5
6
7
8
9
10
11
12
13
14
15
16
17
18
19
20
21
22
23
24
25
26
27
28
29
30
31
32
33
34
35
36
37
38
39
40
41
42
43
44
45
46
47
48
49
50
51
52
53
54
55
56
57
58
59
60
61
62
63
64
65
66
67
68
69
70
71
DusA
DusB
DusC
Colour Key and Histogram
Count
250
200
150
100
50
0
0
0.4
0.8
Value

Figure 18: Analysis of polysome-bound tRNAs by AlkAniline sequencing. Stop ratio score (ranging from 0 to 1) of signals detected in cytosolic (F0) and polysome-bound (F3) tRNA fractions isolated from non-treated and treated (0.3 mM PQ) *E. coli* wildtype and Dus knockout cultures. The various tRNAs and the corresponding D positions are shown on the left with the following code: organism_tRNA species_anticodon – position of D / modifying enzyme, while the numbering of tRNAs and modifying enzymes are indicated on the right (similar numbering in Figure 19). Results of one of three biological replicates are shown, results of two further replicates are included in the Appendix (Figure A8 and Figure A9).

intense in polysome-bound tRNAs isolated from the DusA knockout cultures. This might point to a certain importance of DusC dihydrouridylation for tRNAs during translation in the absence of DusA and concomitant D modifications in positions 20 and 20a of the tRNA. However, given the unreliable reproducibility of these results further experiments are required to draw definite conclusions on this.

The previously suggested differential sensitivity of the Dus enzymes to paraquat (Figure 13, Figure 14 and Figure 17) was further substantiated by the AlkAniline sequencing results. In order to analyse the changes in D signal intensities associated with paraquat in more detail, the AAS signal of cytosolic tRNA isolated from the untreated wildtype culture was set to 100% for each tRNA position and the corresponding treated signals were related. The positions modified by DusA, DusB or DusC are collected separately in a graph, with the bars representing the related treated signals (as an average of biological triplicates), while the corresponding untreated signals, set to 100%, are shown as dashed lines (Figure 19).

Analysing the signals at positions 20 and 20a that are modified by DusA (Figure 19A), 31 out of 38 dihydrouridylated tRNAs were not affected or showed higher signal intensities upon the supplementation with paraquat, demonstrating that DusA is still active under these conditions, which confirms the previous assumption that DusA persistently modifies the tRNA. On the other hand, tRNA positions 16 and 17 were strongly affected, with DusC being even more impaired. While all DusC-dependent D signals at position 16 were significantly decreased after PQ treatment, three D signals at position 17 were not affected and one was even increased after paraquat exposure (Figure 19B+C). These results are in agreement with the previous ones, leading to a decreasing sensitivity to paraquat from DusC over DusB to DusA.

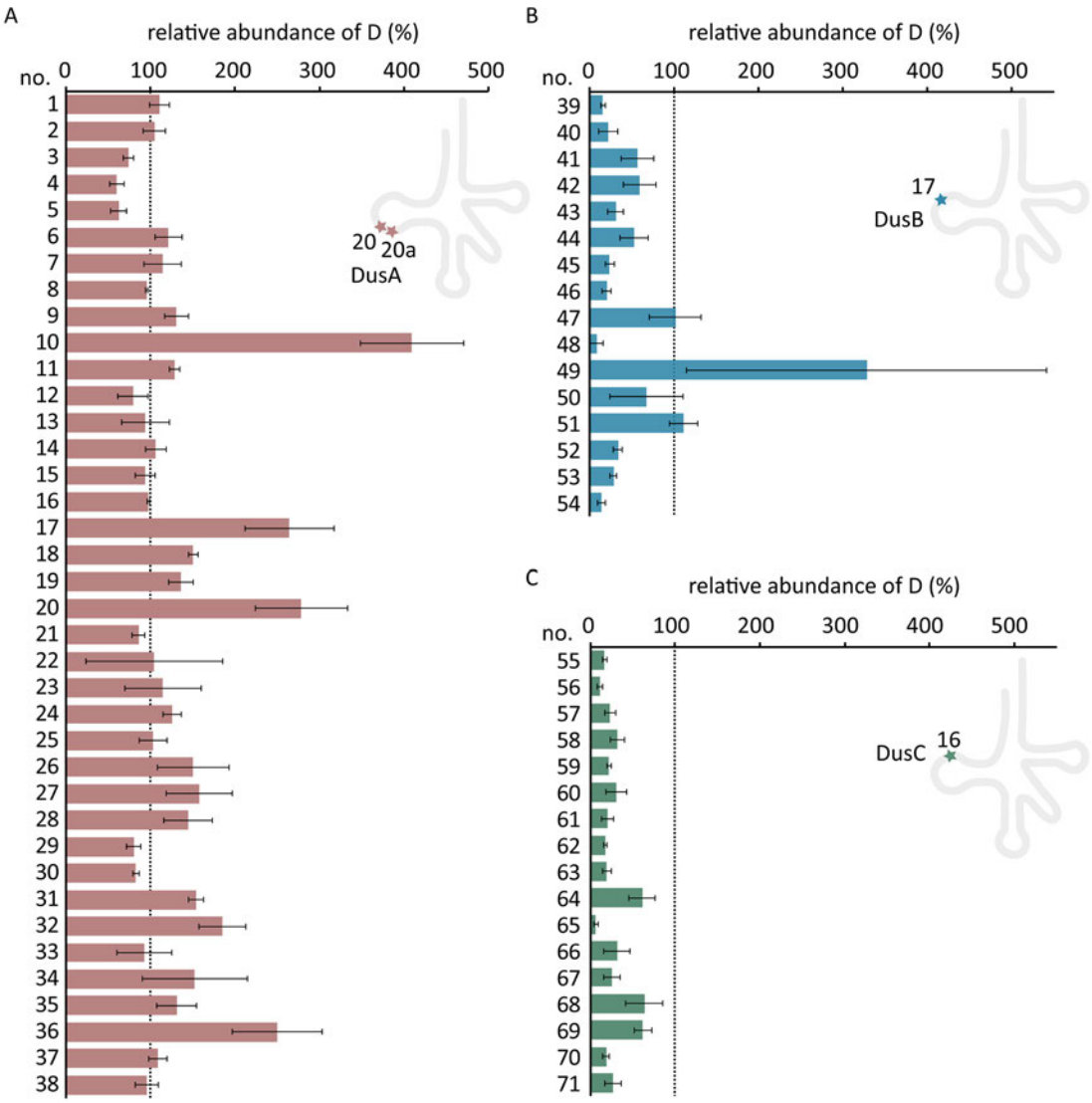

Figure 19: Position-specific changes of dihydrouridine signals in cytosolic tRNAs (F0) upon paraquat treatment. A AlkAniline sequencing results of cytosolic tRNA fraction (F0) isolated from the treated (0.3 mM PQ) wildtype culture at positions 20 and 20a (modified by DusA). Stop ratio score values of samples isolated from treated cultures (WT 0.3 mM PQ F0) were related to the signal of the corresponding tRNA isolated from the untreated culture (WT 0 mM PQ F0), which was set to 100% as indicated as black dashed line. Results are shown as average of biological triplicates, standard deviations are indicated as error bars. The tRNA numbering corresponds to the tRNA numbering in Figure 18, Figure A8 and Figure A9. **B** AlkAniline sequencing results of cytosolic tRNA fraction (F0) isolated from the treated (0.3 mM PQ) wildtype culture at position 17 (modified by DusB). Calculations were performed as described in A. **C** AlkAniline sequencing results of cytosolic tRNA fraction (F0) isolated from the treated (0.3 mM PQ) wildtype culture at position 16 (modified by DusC). Calculations were performed as described in A.

4.1.5 Kinetic activities of Dus enzymes *in vitro*

Since the previous *in vivo* experiments revealed that the Dus enzymes were differentially affected by paraquat, the redox reactivities of recombinant *E. coli* Dus enzymes were characterised *in vitro* to investigate the molecular basis for the differential sensitivities towards paraquat. The *in vitro* assays described in this subchapter were performed by [redacted].

The three recombinantly expressed Dus enzymes were tested for their NADPH oxidase activity by monitoring the NADPH consumption spectrophotometrically (Figure 20A), demonstrating that DusA is the most efficient enzyme, oxidising NADPH with an efficiency constant (k_{cat}/K_m) of $2.8 \cdot 10^{-2}$ $\mu M^{-1} \cdot s^{-1}$, calculated with a catalytic constant of $k_{cat} \approx 0.48 \pm 0.072$ s^{-1} and a Michaelis-Menten constant of $K_m \approx 17 \pm 3$ µM, while DusB and DusC are less active. The activity of DusB was low, but still measurable with an efficiency constant of $1.15 \cdot 10^{-4}$ $\mu M^{-1} \cdot s^{-1}$ ($k_{cat} \approx 0.011 \pm 0.003$ s^{-1}, $K_m \approx 95 \pm 35$ µM), in contrast to DusC, where no activity was detectable, probably because of an extremely slow oxidation reaction.

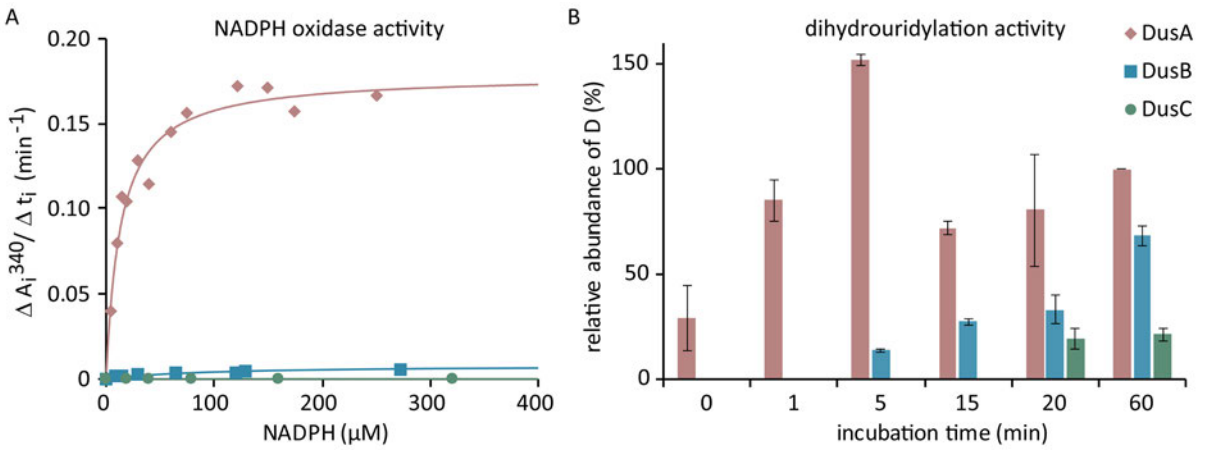

Figure 20: *In vitro* kinetics of *E. coli* dihydrouridine synthases. A Spectrophotometric monitoring of NADPH oxidase activity of DusA (rose rhombuses), DusB (blue squares) and DusC (green dots) *in vitro*, displayed as change in absorbance at 340 nm per time. **B** Dihydrouridylation activity determined as D modification level after different incubation times (0, 1, 5, 15, 20 and 60 min) of the enzymes with non-dihydrouridylated tRNA (isolated from *ΔdusA,B,C*). Signals detected with the mass transition *m/z* = 247 → 115 corresponding to D were normalised to the UV signal of adenosine and compared to the normalised D signal after 60 min incubation with DusA (set to 100%). Dihydrouridylation (shown as average of biological duplicates) catalysed by DusA is shown in rose, DusB catalysed dihydrouridines are shown in blue and DusC ones in green. Error bars depict the standard deviation.

In order to investigate the dihydrouridylation capacity of the three Dus enzymes, they were incubated with non-dihydrouridylated tRNA that was isolated from the triple knockout *ΔdusA,B,C* for different incubation times and the tRNA D levels were subsequently determined by LC-MS/MS analysis (Figure 20B). Dihydrouridines were detected immediately after the

addition of recombinant DusA, with 85% of the dihydrouridines observed after only one minute of incubation, relative to the signal after an hour of incubation, confirming the high activity of DusA. DusB was able to reduce U to D to a detectable level *in vitro* after an incubation time of 5 minutes, whereas an incubation time of at least 20 minutes was required to detect D modifications introduced by the recombinant DusC, implying a lower activity of DusC compared to DusB.

The observed increasing activities from DusC over DusB to DusA correspond to the observed decreasing order of sensitivity towards paraquat from DusC over DusB to DusA, with DusA being the most robust enzyme, indicating a correlation between the detected differential redox sensitivity and the differential enzyme activities. Presumably, the availability of NADPH is reduced upon the addition of paraquat, which has more severe consequences for the less active enzymes DusB and DusC as they have a lower substrate affinity and are unable to reduce uridines to the same extent as under normal conditions. In contrast to that, DusA, which has a high substrate affinity, is still able to catalyse reductions to D, although less NADPH is available.

4.2 Replacement of Q with a clickable azido-preQ$_1$ analogue to study its biological role

The high variety of tRNA modifications is ranging from simple methylations or reductions, such as uridine to dihydrouridine, to complex structures, so-called hypermodifications, like the queuosine modification. Queuosine, located in the anticodon-loop, is assumed to play a crucial role in tRNA-mRNA interactions in the ribosome during translation.[122–124] While prokaryotes are able to synthesize Q *de novo*, eukaryotes have to salvage the precursor base queuine from their nutrition. However, the incorporation mechanisms of the precursors preQ$_1$ respectively q are similar, in both the exchange reaction is catalysed by a transglycosylase enzyme. *In vitro* studies of recombinant TGT enzymes have shown to tolerate synthetic analogues of the natural preQ$_1$, opening the queuosine field for the incorporation of non-natural derivatives.[129,130] Using a synthetic substrate of the TGT, Varghese *et al.* observed a therapeutic effect in a mouse model of multiple sclerosis, demonstrating the potential of this method in a medical context.[128]

To realise the work presented in the following, our working group collaborated with the group of [redacted] at the [redacted], who synthesised the different preQ$_1$ analogues, with the group of [redacted] at the [redacted], who contributed their competence in working with bacterial and eukaryotic TGT *in vitro* as well as *S. pombe* as a eukaryotic model organism, and [redacted] from the [redacted], who investigated the translational role of Q in human cells.

Three preQ$_1$ derivatives containing an azide group (L1: 3-azidopropyl-preQ$_1$, L2: 4-azidobutyl-preQ$_1$ and L3: 2-(2-azidoethoxy)ethyl-preQ$_1$, synthesised by [redacted], [redacted]) were incorporated into *E. coli and S. pombe* tRNA *in vitro* instead of the natural preQ$_1$ by the transglycosylation reaction, resulting in Q-L1, Q-L2 and Q-L3 (experiments were performed by [redacted], [redacted]). The azide entity facilitated cupper click chemistry upon its incorporation into the tRNA, thereby enabling for fluorescent labelling which in turn allowed to proof the incorporation after tRNA isolation. Using this approach, the analogue preQ$_1$-L1 was shown to be successfully incorporated *in vivo* in *E. coli*, *S. pombe* and in human cells (contributions of [redacted] from [redacted], [redacted] and [redacted]). Assuming that Q plays a crucial role in the translational process, it was further investigated whether queuosine and the synthetic analogue are present on tRNAs that are actively involved in translation. Polysome complexes were isolated from *E. coli* polysome preparations by separation along a sucrose gradient and the analysis of tRNAs bound to these complexes by LC-MS/MS revealed the presence of both the natural queuosine modification as well as the semi-synthetic modification Q-L1 (experimental work was performed by myself). The abundance of natural queuosine on polysomes was higher than its presence in the

cytosolic tRNA pool, emphasizing the crucial role in the translational process. However, the semi-synthetic Q-L1 was detected in a similar range on polysomes and in the cytosolic tRNA pool, indicating that the synthetic analogue was functionally incorporated but unable to fully replace the role of the natural queuosine during translation. The azide group in Q-L1 not only enabled click chemistry but also facilitated the conjugation of biotin for further affinity purification. The combination of the latter with RNA sequencing, performed by [redacted], revealed that the TGT retained its natural tRNA targets for the incorporation of the synthetic analogue in *S. pombe*. The queuosine modification was reported to stimulate the formation of m^5C in *S. pombe* $tRNA^{Asp}$ at position 38.[134,135] Interestingly, the incorporated Q-L1 imitated this stimulation, as shown by bisulfite sequencing (contribution of [redacted]), confirming the fully functional integration of this derivate *in vivo*.

This functional replacement is a minimally invasive tool to study the role of Q in biological processes and opens up the possibility to incorporate further non-natural nucleobases within the cellular (t)RNA *in vivo*.

Published online 28 September 2022

Nucleic Acids Research, 2022, Vol. 50, No. 18 ***10785–10800***
https://doi.org/10.1093/nar/gkac822

Functional integration of a semi-synthetic azido-queuosine derivative into translation and a tRNA modification circuit

Larissa Bessler[1,†], Navpreet Kaur[2,†], Lea-Marie Vogt[1,†], Laurin Flemmich[3], Carmen Siebenaller[4], Marie-Luise Winz[1], Francesca Tuorto[5], Ronald Micura[3], Ann E. Ehrenhofer-Murray[2,*] and Mark Helm[1,*]

[1]Institute of Pharmaceutical and Biomedical Sciences, Johannes Gutenberg-University Mainz, 55128 Mainz, Germany, [2]Institute of Biology, Humboldt-Universität zu Berlin, 10117 Berlin, Germany, [3]Department of Organic Chemistry, University of Innsbruck, 6020 Innsbruck, Austria, [4]Department of Chemistry – Biochemistry, Johannes Gutenberg-University Mainz, 55128 Mainz, Germany and [5]Division of Biochemistry, Mannheim Institute for Innate Immunoscience (MI3), Medical Faculty Mannheim, Heidelberg University, Mannheim, Germany

Received June 15, 2022; Revised September 09, 2022; Editorial Decision September 09, 2022; Accepted September 27, 2022

ABSTRACT

Substitution of the queuine nucleobase precursor preQ$_1$ by an azide-containing derivative (azido-propyl-preQ$_1$) led to incorporation of this clickable chemical entity into tRNA *via* transglycosylation *in vitro* as well as *in vivo* in *Escherichia coli*, *Schizosaccharomyces pombe* and human cells. The resulting semi-synthetic RNA modification, here termed Q-L1, was present in tRNAs on actively translating ribosomes, indicating functional integration into aminoacylation and recruitment to the ribosome. The azide moiety of Q-L1 facilitates analytics *via* click conjugation of a fluorescent dye, or of biotin for affinity purification. Combining the latter with RNAseq showed that TGT maintained its native tRNA substrate specificity in S. *pombe* cells. The semi-synthetic tRNA modification Q-L1 was also functional in tRNA maturation, in effectively replacing the natural queuosine in its stimulation of further modification of tRNA^{Asp} with 5-methylcytosine at position 38 by the tRNA methyltransferase Dnmt2 in *S. pombe*. This is the first demonstrated *in vivo* integration of a synthetic moiety into an RNA modification circuit, where one RNA modification stimulates another. In summary, the scarcity of queuosinylation sites in cellular RNA, makes our synthetic q/Q system a 'minimally invasive' system for placement of a non-natural, clickable nucleobase within the total cellular RNA.

INTRODUCTION

Post-transcriptional modification of tRNAs is a ubiquitous yet idiosyncratic feature with versatile chemical structures contributing to stability and folding, as well as fidelity of decoding and translational control (1–3). The largest variety of chemical structures in RNA is found in the anticodon loop which directly interacts with the mRNA during decoding in the translating ribosome. The chemical variety of the more than 170 modifications known to date is dominated by tRNA anticodon modifications occurring at positions 34 and 37, ranging from simple methylations to highly complex structures of which queuosine (Q) is a particular case (4,5). In both, prokaryotes and eukaryotes, this hypermodified 7-deazaguanosine is exclusively found in the anticodon wobble position 34 of tRNAs containing a $G_{34}U_{35}N_{36}$ motif and therefore specific for a selected group of four tRNAs, namely tRNA^{Asn}, tRNA^{Asp}, tRNA^{His} and tRNA^{Tyr} (6,7). In an intricate multi-step process involving various enzymes and co-factors, *Escherichia coli* and other prokaryotes are capable of first synthesising the modified precursor base 7-aminomethyl-7-deazaguanine (preQ$_1$) *de novo*. GTP is converted to preQ$_1$ *via* five enzymatic steps successively catalysed by the GTP cyclohydrolase I (GCH I), QueD, QueE, QueC and QueF (8–11). As a rare type of post transcriptional modification, the noncanonical nucleobase structure is then introduced into tRNA in an exchange reaction. During this transglycosylation step, the bacterial tRNA guanine transglycosylase (bTGT) replaces

*To whom correspondence should be addressed. Tel: +49 6131 39 25731; Fax: +49 6131 39 20373; Email: mhelm@uni-mainz.de
Correspondence may also be addressed to Ann E. Ehrenhofer-Murray. Tel: +49 30 2093 49630; Fax: +49 30 2093 49641; Email: ann.ehrenhofer-murray@hu-berlin.de
†The authors wish it to be known that, in their opinion, the first three authors should be regarded as Joint First Authors.

a guanosine in the anticodon wobble position of cognate tRNAs with the precursor base $preQ_1$ (12,13) which is then further enzymatically modified by QueA and QueG to yield the final queuosine structure (14,15). In contrast to prokaryotes, eukaryotes salvage the nucleoside queuosine and the corresponding nucleobase queuine (q) from environmental sources including the gut microbiota (reviewed in (5)). Queuosine is hydrolyzed by a queuosine nucleoside glycosylase to release q (16). The incorporation of the salvaged q into tRNA is catalysed by eukaryotic TGT (eTGT), which is a heterodimeric enzyme (17–19) composed of a catalytic queuine tRNA-ribosyltransferase subunit 1 (QTRT1) and a noncatalytic queuine tRNA-ribosyltransferase subunit 2 (QTRT2) (20).

Despite its suggestive positioning at position 34 of the tRNA anticodon, molecular details of the physiological relevance of Q remain scarce. It is generally accepted that Q impacts the decoding process on the translating ribosome, with cumulative evidence pointing to pivotal interactions at the A-site. The specific occurrence of Q in GUN anticodons is consistent with a general concept by Grosjean and Westhof (21), wherein modifications at position 34 compensate for the lower stability of codon-anticodon interactions including 2 or more base pairs with less than three hydrogen bonds. This concept receives support from computational modelling, which characterised a stabilising effect of Q on the overall tRNA-mRNA complex involving additional hydrogen bonds (22). *In vivo* and *in cellulo* studies did not reveal any strong phenotypes under Q deficiency or in strains lacking TGT. However, the presence of Q improved viability under stress conditions and affected translation accuracy in *E. coli* (23,24). *In vivo* studies in eukaryotes likewise reported an impact on the decoding process, enabling decoding of synonymous codons by wobble base pairing (22,25,26), and affecting translation speed and accuracy (27,28). Queuosine's multifaceted involvement in the cellular machinery was reported to be associated with cancer (29–32), neuronal disorders (33–35) as well as bacterial and parasitic infection (36,37). Consequently, the perception of therapeutic potential associated with its biogenesis has consistently increased, in keeping with a general trend in epitranscriptomics

So far, the only demonstrated molecular interaction affected by Q outside the ribosome is a so-called modification circuit with 5-methylcytidine (m^5C) in position 38 of *Schizosaccharomyces pombe* $tRNA^{Asp}$, stimulating its formation by the Dnmt2 homologue Pmt1 (38,39). Structural analysis suggested that the presence of Q34 leads to optimal positioning of the interacting substrates in the active site of Dnmt2, enhancing the catalytic efficiency of the methyltransferase (40).

Arguably, approaches to a deeper understanding of the molecular action of Q in living cells would need to involve manipulations of details of the structure of Q, e.g. *via* an incorporation of q-derivatives through transglycosylation. Apart from their natural substrates, both bTGT and eTGT have been shown to tolerate a certain variety of synthetic analogues harbouring large functional groups *in vitro* (41,42). Leveraging the short hairpin recognition motif of the bTGT installed on different RNA transcripts, Devaraj and co-workers developed a method called RNA-TAG (transglycosylation at guanosine), allowing to site-specifically incorporate analogues *in vitro*, which contained large fluorophores or affinity labels for pull-down experiments. This method was also applied to visualize mRNA transcripts containing the recognition motif in a fixed cell environment in a direct one-step-reaction (42) and extended to the development of a light-activated mRNA translation system (43). Furthermore, RNA-TAG was used on modified mRNAs in a two-step-approach, incorporating a $preQ_1$-derivative bearing a bioorthogonal tetrazine moiety in the first step, and thus enabling further derivatization by IEDDA click chemistry in a second step (44). However, labelling with click-competent compounds *in vivo* or *in cellulo* has not yet been achieved in the queuosine field. Indeed, there is strongly suggestive, albeit indirect evidence of successful *in vivo* incorporation of a non-natural q-analogue as published by Kelly and co-workers in the context of an animal model of multiple sclerosis (34). In addition to concerns about cell permeability of a q-derivative, important aspects to determine for *in vivo* labelling studies would include the physiological impact of an artificial chemical structure in a functioning tRNA, which would primarily be expected on the level of translation.

In this study, we metabolically label tRNA with a $preQ_1$ derivative functionalized with an azide group, allowing for further derivatization by click reaction and thus facilitating the proof of successful incorporation as well as the isolation of accordingly tagged RNAs. The latter was combined with RNAseq, in order to re-investigate the RNA substrates of the TGT, which turned out to be specific for the previously reported tRNAs Asn, Asp, His and Tyr. While in previous studies the transglycosylation step was performed in a fixed cell environment, we herein focus on the incorporation of the analogues by the natively expressed TGT *in vivo* and the physiological consequences in the natural environment. Polysome preparations revealed an enrichment of Q-containing tRNAs in the polysomal fraction, indicating a targeted selection for modified tRNA to be integrated in the translational process. Moreover, our data demonstrate that the semi-synthetic tRNA modification replaces Q34 and is functionally integrated into the translational process, as well as in the modification circuit with m^5C38 in $tRNA^{Asp}$ in *S. pombe*.

MATERIALS AND METHODS

S. pombe strains used in this study are given in Supplementary Table S1, Plasmids used in this study are given in Supplementary Table S2, oligonucleotides used in this study are given in Supplementary Table S3. The names and versions of all software used are provided in Supplementary Table S4.

Synthesis of $preQ_1$-L1, $preQ_1$-L2 and $preQ_1$-L3

The $preQ_1$-ligands were synthesized as previously described (45).

Recombinant expression and purification of bTGT

The pASK-IBA13plus vector expressing the *Zymomonas mobilis* TGT (bTGT) with a N-terminal Strep-tag II was kindly provided by Prof. Dr Klaus Reuter (Philipps-University, Marburg). Expression and purification were carried out as previously described with minor changes (46). Briefly, the TGT was expressed in *E. coli* BL21-CodonPlus (DE3)-RIPL cells, grown in 2× YT medium and protein production was induced using anhydrotetracycline to a final concentration of 0.2 mg/l. After growing the cells for 14 h at 15°C, cells were harvested and the cell pellets were stored at –80°C until further processing. To purify the bacterial TGT, cells were thawed in lysis buffer (100 mM Tris pH 7.8, 150 mM NaCl, 1 mM EDTA pH 8.0, 2 mM PMSF, 1 μg/ml leupeptin, 1 μg/ml aprotinin, 1 μg/ml pepstatin and 25 U of DNase I and RNase I, respectively). After sonication (60% amplitude, 6 min, 0.5 s on, 2 s off; Sonifier 250 D, Branson), soluble proteins were isolated by centrifugation at 20 000 g for 1 h, 4°C. Affinity chromatography was then used to purify the Strep II-tagged TGT. For this purpose, the lysate was incubated with Strep-Tactin® Superflow Plus resin (Qiagen) for 3 h at 4°C, 15 rpm. After washing with washing buffer (100 mM Tris pH 7.8, 150 mM NaCl, 1 mM EDTA pH 8.0), the protein complex was eluted in 100 mM Tris pH 7.8, 150 mM NaCl, 1 mM EDTA pH 8.0 and 2.5 mM desthiobiotin. Further purification was achieved by Superdex S200 (GE Healthcare) size exclusion chromatography (10 mM Tris pH 7.8, 150 mM NaCl, 1 mM EDTA pH 8.0). The purified bTGT was stored at –80°C in 10 mM Tris pH 7.8, 150 mM NaCl, 1 mM EDTA pH 8.0 with 50% glycerol.

E. coli strains and growth conditions

The *E. coli* Keio parent strain (BW25113) and the knockout strains for QueD, QueC, QueE, QueF and TGT were obtained from the *E. coli* Keio knockout collection (GE Healthcare (Dharmacon™), England) and grown in standard M9 medium (6.8 g/l Na_2HPO_4, 3 g/l KH_2PO_4, 0.5 g NaCl, 1 g/l NH_4Cl, 2 mM $MgSO_4$, 0.1 mM $CaCl_2$, 0.4% glucose) at 37°C and 190 rpm. Growth medium of knockout strains was additionally supplemented with kanamycin (25 μg/ml). Synthetic preQ$_1$-derivatives were added to final concentrations of 0.1, 1, 5 or 10 μM to the culture, respectively.

Isolation of total tRNA from *E. coli*

To isolate total tRNA, *E. coli* cells were grown to an OD_{600} of 1 in 50 ml cultures and harvested by centrifugation (10 min, 10 000 g, 4°C). The RNA was extracted by using the RNA isolation reagent TRI Reagent© (Sigma-Aldrich, Germany) following the manufacturer's instructions and dissolved in MQ-water.

Polysome preparations from *E. coli*

For polysome preparations the *E. coli* cells were grown in M9 medium in 150 ml culture volume until they reached an OD of 0.6, chloramphenicol was added to final concentration of 100 μg/ml and after further incubation of 3 min the cells were harvested by centrifugation (10 min, 10 000 g, 4°C). For cell lysis, cell pellets were resuspended in buffer (100 mM NH_4Cl, 10 mM $MgCl_2$, 20 mM Tris, pH 7.5), lysozyme was added and freeze-thaw cycles in liquid nitrogen were performed. Subsequent to this 10% deoxycholate was added to complete lysis, remaining cell wall debris were separated by centrifugation (12 000 g, 10 min, 4°C). Sucrose gradients from 5 to 40% were generated using a Biocomp gradient station model 108 (settings: time 1.24 min, angle 81.5°, speed 21 rpm) and lysate was loaded on top of the gradient. After ultracentrifugation (Beckman Ultracentrifuge Optima LE-80K, SW40 Ti rotor from Beckman Coulter) at 150 000 g and 4°C for 2.5 h, gradients were fractionated by measuring the absorbance at 280 nm (Biocomp Gradient Station model 108 in combination with Gilson Fraction Collector FC203B). Total RNA was isolated from the respective fractions using TRI reagent© (Sigma-Aldrich).

Purification of total tRNA from collected fractions by gel elution

Total RNA extracted from polysomal fraction was separated on a 10% denaturing PAGE gel, stained with GelRed (Biotium) and the bands were visualized on Typhoon 9400 at an excitation wavelength of 532 nm. According to the resulting image, bands of interest were excised from the gel and mashed with a scalpel. The mashed gel pieces were frozen for 1 h and 300 μl of 0.5 M ammonium acetate were added. Subsequently, the samples were shaken at 25°C and 750 rpm overnight. The gel suspension was filtered through NanoSep® centrifugal filters and the filtrate was precipitated with three volumes of 100% ethanol.

S. pombe strains, plasmids and growth conditions

The *S. pombe* strains and plasmids used in this study are shown in Supplementary Table S1. Cells were cultured in YES (5 g/l yeast extract, 30 g/l glucose, 250 mg/l adenine, 250 mg/l histidine, 250 mg/l leucine, 250 mg/l uracil, 250 mg/l lysine) which did not contain queuosine or queuine. Synthetic queuine (kindly provided by Hans-Dieter Gerber and Gerhard Klebe (Universität Marburg) (47)) and preQ$_1$ derivatives were added to 0.1 μM to the culture.

Isolation of total RNA and small RNAs from *S. pombe*

To isolate total RNA, *S. pombe* cells were grown to an optical density at 600 nm (OD_{600}) of 1 in 50 ml cultures. 50 OD of cells were harvested and 1 ml of phenol, glass beads were added. After vigorous shaking for 5 min, samples were centrifuged at 20 000 g for 5 min to clear the cell debris. Equal volume of phenol/chloroform/isoamylalcohol was added to the aqueous phase and centrifuged at 20 000 g for 5 min. After mixing the upper phase with an equal volume of chloroform followed by centrifugation at 20 000 g for 5 min, the RNA was precipitated at –80°C for 1 h using 0.7 volume of isopropyl alcohol. Following precipitation, total RNA was washed with 70% ethanol and eluted in DEPC-treated water.

Isolation of small RNAs was performed using the PureLink™ miRNA Isolation Kit (Invitrogen) according to the manufacturer's instructions. Yeast cells were grown to an OD_{600} of 1 in 5 ml cultures. After harvesting 1 OD of cells, RNAs were isolated using 1 ml TriFast reagent (Peqlab), 0.2 ml chloroform and glass beads. After vigorous shaking for 2 min, samples were centrifuged at 16 000 g, 4°C for 15 min. After adding 215 µl ethanol to the aqueous phase, the samples were transferred to a spin cartridge followed by centrifugation at 12 000 g for 1 min. 700 µl ethanol was added to the flow-through and the sample was transferred to a new spin cartridge. Following centrifugation at 12 000 g for 1 min, the cartridge was washed and small RNAs were dissolved in DEPC-treated water. Northern blot–acryloyl aminophenylboronic acid (APB) gels were performed as previously described (28).

Removal of ribosomal RNA

Depletion of ribosomal RNA was performed as previously described (48). Oligonucleotides specific for 5.8S and 5S rRNA were ordered with a 5'-biotin tag from Metabion (see Supplementary Table S3). The oligonucleotides were diluted to 100 µM each in nuclease-free water and equal volumes of the 100 µM stock were combined to generate the rRNA depletion mix.

For hybridization, 8 µg of small RNAs were incubated with 9.92 µl of the 100 µM rRNA depletion mix in reaction buffer (10 µl of formamide, 2.5 µl of 20× SSC (3 M NaCl, 0.3 M sodium citrate, pH 7.0) and 5 µl of 0.005 M EDTA, pHnbsp;8). Reactions were carried out in a total volume of 50 µl with the following thermocycling: 80°C for 5 min, ramp down to 25°C at intervals of 5°C per minute. Following hybridization, 2 µl of RNase-OUT (Invitrogen) and 50 µl of 1× SCC containing 20% formamide were added. Removal of rRNA/oligonucleotide hybrids was performed using Dynabeads™ MyOne™ Streptavidin C1 (ThermoFisher) according to the manufacturer's instructions. 500 µl streptavidin coated magnetic beads were washed as instructed for immunoprecipitation of RNA and added to the hybridization reaction. After incubation for 15 min at room temperature with mild agitation and bead separation on a magnetic rack, the supernatant was once more incubated with 500 µl of washed beads for 15 min at room temperature under mild agitation followed by bead separation. Subsequently, the supernatant containing the 5S/5.8S rRNA-depleted RNA was precipitated with 1/10 volume of ammonium acetate and three volumes of 100% ethanol.

RNA substrates for *in vitro* modification

The *S. pombe* $tRNA^{Asp}$ substrate was prepared as previously described (49). Briefly, the pJET1 vector carrying the $tRNA^{Asp}$ sequence was linearized with NcoI, and 2.5 µg of the linear vector was used for *in vitro* transcription using the TranscriptAid T7 High Yield Transcription Kit (Thermo Fisher Scientific) according to the manufacturer's instructions. Following an 8 h incubation at 37°C with nucleotides and the T7 RNA polymerase and subsequent DNase I treatment, the respective tRNA was purified from the reaction using phenol/chloroform extraction followed by gel filtration with Sephadex G50 (GE Healthcare).

Recombinant expression and purification of hTGT

The pCDF-Duet1 vector co-expressing the human TGT (hTGT) heterodimer QTRT1 and QTRT2 with a cleavable N-terminal 6xHis tag to QTRT1 was kindly provided by Prof. Dr. Ralf Ficner (GZMB, Göttingen). Expression and purification were carried out as previously described with minor changes (20). Briefly, the heterodimer QTRT1/QTRT2 was co-expressed in *E. coli* (DE3) Rosetta cells, and protein production was induced using autoinduction. After growing the cells for 50 h at 18°C, cells were harvested and the cell pellets were stored at –80°C until further processing. To purify the human TGT, cells were thawed in lysis buffer (50 mM HEPES pH 7.5, 100 mM NaCl, 10 mM imidazole, 2 mM PMSF, 1 µg/ml leupeptin, 1 µg/ml aprotinin, 1 µg/ml pepstatin and 25 U of DNase I and RNase I, respectively). After sonification (60% amplitude, 6 min, 0.5 s on, 2 s off; Sonifier 250 D, Branson), soluble proteins were isolated by centrifugation at 20 000 g for 1 h. Affinity chromatography was then used to purify the 6xHis tagged QTRT1/QTRT2 complex. For this purpose, the lysate was incubated with Talon® Superflow™ resin (Cytiva) for 3 h at 4°C, 15 rpm. After washing with washing buffer (50 mM HEPES pH 7.5, 100 mM NaCl, 10 mM imidazole and 1 M LiCl), the protein complex was eluted in 50 mM HEPES pH 7.5, 100 mM NaCl and 500 mM imidazole. Further purification was achieved by Superdex S200 (GE Healthcare) size exclusion chromatography (20 mM HEPES pH 7.5, 100 mM NaCl). The purified hTGT was stored at –80°C in 20 mM HEPES pH 7.5, 100 mM NaCl with 50% glycerol.

In vitro labelling of tRNA with $preQ_1$ derivatives

For *in vitro* labelling of tRNA with the $preQ_1$ derivatives, 10 µM of *in vitro* transcribed tRNAs or alternatively 10 µg of total RNA from *S. pombe* was incubated with 200 nM hTGT (QTRT1:QTRT2) and 5 µM queuine in reaction buffer (50 mM Tris–HCl pH 7.5, 20 mM NaCl, 5 mM $MgCl_2$ and 2 mM dithiothreitol) for 5 h at 37°C. The RNA was purified using phenol/chloroform extraction and precipitated with 1/10 volume of ammonium acetate and three volumes of 100% ethanol.

HeLa cells growth conditions and *in vivo* labelling with $preQ_1$-L1

HeLa cell lines were obtained from ATCC and authenticated by multiplex human cell line authentication test (Multiplexon). Cells were grown in Dulbecco's modified Eagle's medium (DMEM) (Thermo Fisher Scientific). The cultures were supplemented with 10% heat-inactivated FBS, 2 mM L-glutamine and a commercial cocktail of antibiotics (Thermo Fisher Scientific). For minus-Q conditions, ultraculture serum-free medium (Lonza) was supplemented with 2 mM L-glutamine and 100 units/ml Penicillin/Streptomycin. $preQ_1$-L1 derivative was added at a concentration of 0.1 µM for 72 h to the culture.

HeLa cell polysome profiling

10^7 cells were treated with 100 μg/ml cycloheximide for 5 min at RT to stabilize existing polysomes before washing with ice-cold PBS and harvesting by scraping in 400 μl polysome lysis buffer (20 mM Tris–HCl, pH 7.4, 5 mM $MgCl_2$, 150 mM NaCl, 1 mM DTT, 1% Triton X-100, 100 μg/ml cycloheximide, 1 × Complete Protease Inhibitors (Roche)). Lysates were rotated end-over-end for 10 min at 4°C and cleared by at 10 000 rpm for 10 min at 4°C. 40 μl of supernatant lysate was saved as input before loading the lysates to linear 17.5 to 50% sucrose gradients in 20 mM Tris–HCl (pH 7.4), 5 mM $MgCl_2$, 150 mM NaCl. Centrifugation was carried out at 35 000 rpm for 2.5 h at 4°C in a Beckmann SW60 rotor. Gradients were eluted with an ISCO UA-6 gradient fractionator, and polysome profiles were recorded by continuously monitoring the absorbance at 254 nm using PeakTrak software. During gradient elution, fractions of ∼300 μl were collected every 14 s. For RNA isolation, 300 μl urea buffer (10 mM Tris, pH 7.5, 350 mM NaCl, 10 mM EDTA, 1% SDS, and 7 M urea) and 300 μl phenol:chloroform:isoamylalcohol (25:24:1) were added to each fraction. After phase separation, RNA was isolated from the aqueous phase and precipitated using isopropanol and GlycoBlue (Thermo Fisher Scientific).

CuAAC click reaction

Chemical clicking was performed as previously described (50). Briefly, up to 10 μg of RNA was incubated in reaction buffer containing 50% (v/v) DMSO, 5 mM Tris ((1-hydroxy-propyl-1*H*-1,2,3-triazol-4-yl)methyl) amine (THPTA), 5 mM sodium ascorbate, 0.5 mM $CuSO_4$ and 50 μM ligand alkyne under light-protection for 2 h at 25°C. The ligand alkynes used were AlexaFluor 594 alkyne (Thermo Fisher Scientific) or biotin alkyne (PEG4 carboxamide-Propargyl biotin; Thermo Fisher Scientific). RNA was precipitated with 1/10 volume of ammonium acetate and three volumes of 100% ethanol.

Detection of queuine and preQ$_1$ modification of RNAs

Labelled RNA that had been CuAAC-clicked with AlexaFluor 594 alkyne was analyzed by denaturing PAGE. Up to 10 μg of labelled RNA was separated in 10% polyacrylamide gels (acrylamide/ bisacrylamide (19:1), urea 8 M in 1× TBE buffer). Detection was carried out on the Typhoon 9500 (GE Healthcare) using 532 nm for excitation. As a loading control, gels were stained with Sybr Gold nucleic acid gel stain (Thermo Fisher Scientific) or GelRed (Biotium) for 10 min followed by detection using 495 or 532 nm, respectively, for excitation.

To detect the queuine modification, 300 ng of total RNA or small RNAs from *S. pombe* WT and *qtr2Δ* strains were separated in a 10% polyacrylamide gel (acrylamide/ bisacrylamide (19:1), urea 8 M) supplemented with 5 mg/ml 3-(acrylamido)-phenylboronic acid as described previously (51). The separation was performed at room temperature in 1× TBE. The electrophoresed gels were transferred to a Biodyne B Nylon membrane (0.45 μM). Selected RNAs were detected using a 5′-biotin-labeled probe at a final concentration of 0.3 μM and the Chemiluminescence Nucleic Acid Detection Module Kit (Thermo Fisher Scientific) according to the manufacturer's instructions. The first blocking step was carried out using the DIG Easy Hyb buffer (Roche), and hybridization was performed overnight at 45°C.

Detection of Q and Q-L1 by LC–MS/MS analysis

Up to 5 μg of total tRNA was digested to nucleoside level using 0.6 U nuclease P1 from *P. citrinum* (Sigma-Aldrich), 0.2 U snake venom phosphodiesterase from *C. adamanteus* (Worthington), 2 U FastAP (Thermo Fisher Scientific), 10 U benzonase (Sigma-Aldrich), 200 ng Pentostatin (Sigma-Aldrich) and 500 ng Tetrahydrouridine (Merck-Millipore) in 25 mM ammonium acetate (pH 7.5; Sigma-Aldrich) overnight at 37°C. 1 μg of total tRNA was analyzed *via* LC–MS using an Agilent 1260 series LC with a Synergi Fusion column (4 μM particle size, 80 Å pore size, 250 × 2.0 mM; Phenomenex) and an Agilent 6460 Triple Quadrupole mass spectrometer equipped with an electrospray ion source (ESI). The elution started with 100% solvent A (5 mM ammonium acetate buffer, pH 5.3) with a flow rate of 0.35 ml/min at 35°C, followed by a linear gradient to 8% solvent B (LC–MS grade acetonitrile; Honeywell) at 10 min and 40% solvent B after 20 min. Initial conditions were regenerated with 100% solvent A for 10 min. The UV signal at 254 nm was recorded *via* a multiple wavelength detector (MWD) detector at 254 nm to monitor the main nucleosides. The following ESI parameters were defined for the measurement: gas temperature 350°C, gas flow 8 l/min, nebulizer pressure 50 psi, sheath gas temperature 350°C, sheath gas flow 12 l/min, capillary voltage 3000 V, nozzle voltage 0 V. The MS was operated in the positive ion mode using Agilent MassHunter software in the dynamic MRM (multiple reaction monitoring) mode.

Identification of preQ$_1$-L1-modified RNAs by HTS

Metabolically labelled and biotin-clicked RNA was purified from total RNA or isolated small RNAs using Dynabeads™ MyOne™ Streptavidin C1 (Thermo Fisher Scientific) according to the manufacturer's instructions. Streptavidin coated magnetic beads were washed as instructed for immunoprecipitation of RNA. 20 μg of biotin-labelled RNA was incubated with the beads for 1 h at room temperature with light agitation. After washing the beads, they were resuspended in nuclease-free water, and bound RNA was dissolved from the beads by incubating the samples at 95°C for 10 min. Library preparation of immunoprecipitated RNAs for deep sequencing was done using the NEBNext Small RNA Library Prep Set for Illumina (Multiplex Compatible; New England Biolabs). 300 ng of RNA per library as starting material was used, and ligation was performed with undiluted adaptors. Adaptor-ligated cDNA was amplified with 15 cycles of PCR reaction using barcoded primers and purified using the Monarch PCR & DNA Cleanup Kit (5 μg) (New England Biolabs). Libraries were eluted in nuclease-free water, multiplexed in equimolar ratios and sequenced on one lane of the Illumina MiSeq platform using paired-end 150 bp sequencing.

RT-qPCR quantification of $tRNA^{Asp}$, snoR38 and snoR69

For quantification of $preQ_1$-L1-labelled $tRNA^{Asp}$, snoR38 and snoR69 from metabolically labelled and immunoprecipitated (IPed) RNAs, quantitative RT-PCR was performed using a stem-loop primer (see Supplementary Table S3). cDNA was synthesized using IPed RNAs from *S. pombe* WT and *qtr2Δ* and a sequence specific stem-loop primer. First strand synthesis was carried out using the SuperScript™ III First-Strand Synthesis System (Invitrogen) according to the manufacturer's protocol. Synthesized cDNA was subsequently used for qPCR using the PerfeCTa SYBR Green SuperMix (QuantaBio). 4 µl of cDNA was used in a reaction mix containing 12.5 µl Master Mix (Quanta, 2×) and 250 nm primers. Reactions were carried out in a total volume of 25 µl with the following thermocycling: 95°C for 2 min, followed by 40 cycles of 95°C for 10 s, 58°C for 15 s and 72°C for 20 s.

RNA bisulfite sequencing

Bisulfite sequencing of $tRNA^{Asp}$ was performed as previously described (38). Briefly, bisulfite-treated tRNAs were reverse transcribed using $tRNA^{Asp}$ 3'-specific stem-loop primer followed by amplification with primers binding only to the deaminated sequence at their 5' end. Primer sequences are listed in Supplementary Table S3. Library preparation of the PCR products was performed with the NEXTflex^R qRNA-Seq™ Kit v2—Set C (Bioo Scientific) according to the manufacturer's instructions and sequenced on a MiSeq platform using paired-end 150 bp sequencing. Reads were processed using in-house R scripting and the Bioconductor package ShortRead (52). Following the processing, including trimming of PCR primers, selection of high-quality reads and sorting of the reads based on the sequence in the degenerate region of the RT-primer, the reads were analyzed for bisulfite conversion using BISMA (53).

HTS data processing

The sequencing data was adapter-trimmed using Skewer version 0.2.2 (54) and aligned to *S. pombe* non-coding RNAs (main and mitochondrial) excluding rRNA sequences from Pombase (https://www.pombase.org/) using Salmon version 14.0 (55) and HISAT2 version 2.1.1 (56), as a splice-site sensitive alignment program. The conversion of sam to bam files was performed using SAMtools (57). Aligned sequences were analyzed using custom R scripts and the Bioconductor package DESeq2 (58). Parameters were set to analyze only regions with a minimum of 10 reads and the adjusted *P*-value was set to <0.1. Additionally, independent hypothesis weighting was conducted using the Bioconductor package IHW (59,60) with an adjusted *P*-value of <0.1. Furthermore, peak calling was performed using the Bioconductor package exomePeak2 (61). Plots were generated using the integrative genomics viewer version 2.11.1 (IGV) (62).

RESULTS

In vitro incorporation of synthetic $preQ_1$ analogues in prokaryotes

To assess the substrate properties of synthetic $preQ_1$-ligands, their incorporation into tRNA by bacterial TGT (bTGT) was tested *in vitro* (Figure 1). For this purpose, $preQ_1$-ligands 1–3 ($preQ_1$-L1-3, Figure 1A), each harbouring an azide group, were incubated with $tRNA^{Asp}$ in the presence of recombinant bTGT from *Z. mobilis*. Taking advantage of the terminal azide group, the successful *in vitro* incorporation of $preQ_1$-ligands was visualized by copper(I)-catalyzed azide alkyne cycloaddition (CuAAC) click reaction of $tRNA^{Asp}$ with the fluorescent AlexaFluor 594-alkyne in the presence of $CuSO_4$, sodium ascorbate and THPTA (tris-((1-benzyl-1*H*-1,2,3-triazol-4-yl)methyl)amine) (Figure 1B and Supplementary Figure S1). As shown by fluorescence scan, all of the tested $preQ_1$-ligands were incorporated to the same extent (Figure 1C), indicating that the side chains attached to the $preQ_1$ structure do not hinder the recognition and turnover by bTGT. This indicates a tolerance of the bTGT active site for large ligands, similar to what was previously described for eTGT *in vitro* (42).

In vivo incorporation of synthetic $preQ_1$ analogues in prokaryotes

After the successful *in vitro* application of synthetic $preQ_1$-ligands with bTGT, we proceeded to metabolic labelling of RNAs *in vivo* in *E. coli*. First experiments were performed with the smallest $preQ_1$ ligand in the series, i.e. $preQ_1$-L1. In a feeding experiment, where an *E. coli* wild-type (WT) strain was grown in medium supplemented with $preQ_1$-L1, total tRNA was isolated and enzymatically digested to the nucleoside level for separation on an RP-C18 HPLC column and subsequent analysis of the Q levels by MS/MS. Of note, queuosine exhibits a fragmentation pattern differing from the standard nucleosides. Instead of the exclusive fragmentation at the *N*-glycosidic bond, cleavage of the ribose in combination with cleavage of the amino linker with a mass shift m/z 410 to m/z 163 was determined as the most abundant product ion (Supplementary Figure S2a) eluting at a retention time of 12.2 min in the WT sample. Using a fragmentation pattern for the incorporated synthetic nucleoside (Q-L1) that was inferred from that of native queuosine, additional signals for the expected transitions were detected at 16.9 min (Figure 2). Since the product ion m/z 163 was the most prevalent species, it was chosen as diagnostic ion in subsequent LC–MS/MS experiments. Monitoring this product ion produced a strong signal for queuosine and only a weak signal for Q-L1 (Supplementary Figure S3c). We concluded that $preQ_1$-L1 was indeed incorporated, but also that it was a weak competitor against the endogenous bacterial $preQ_1$. Consequently, we reasoned that abrogating $preQ_1$ biosynthesis would facilitate the incorporation of the supplied $preQ_1$-ligands. Considering the various steps of Q *de novo* synthesis in *E. coli* (Figure 2A), four different gene deletions, namely *ΔqueD*, *ΔqueE*, *ΔqueC* and *ΔqueF*, were tested for generation of $preQ_1$ by monitoring the presence of

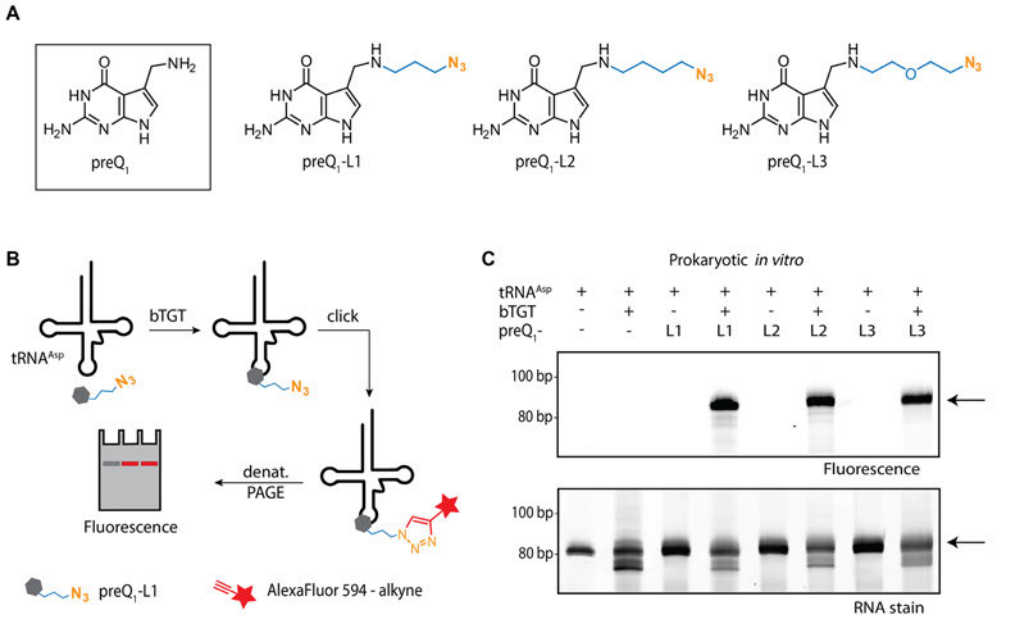

Figure 1. *In vitro* incorporation of preQ$_1$ analogues in tRNA^{Asp}. (**A**) Natural preQ$_1$ and synthetic preQ$_1$-ligands 1 (L1, 3-azidopropyl-preQ$_1$), 2 (L2, 4-azidobutyl-preQ$_1$) and 3 (L3, 2-(2-azidoethoxy)ethyl-preQ$_1$) containing side chains of different length and constitution (blue) but identical terminal azide groups (orange) designated for click chemistry. (**B**) Scheme of the *in vitro* experiment: incubation of tRNA^{Asp} with preQ$_1$ ligands (exemplarily shown for preQ$_1$-L1) in the presence of bacterial TGT (bTGT) and subsequent click reaction with AlexaFluor 594-alkyne (red), allowing the detection of tRNA with incorporated preQ$_1$ ligand *via* fluorescence scan. (**C**) Analysis of the tRNA^{Asp} click product after bTGT-catalysed incorporation of preQ$_1$-ligands L1–L3 by denaturing PAGE and following visualization by fluorescence scan for AlexaFluor 594 (excitation: 532 nm, emission: 610 nm). A loading control was obtained by RNA staining with GelRed. In both scans, tRNA^{Asp} is indicated by an arrow. Untreated tRNA^{Asp} and tRNA^{Asp} incubated with bTGT or preQ$_1$-ligands L1–L3, respectively, served as controls.

Q at position 34 of tRNAs. The deletion strains showed no significant growth defects compared to the wild type (Figure 2C). To validate the absence of Q *de novo* biosynthesis, tRNA was isolated and analyzed by LC–MS as before; none of the deletion strains generated measurable levels of Q (Supplementary Figure S2b–e). Since all deletions were on a par regarding growth and absence of Q in the isolated total tRNA, *ΔqueD* was chosen for further experiments, given that the absence of QueD prevents *de novo* synthesis of Q in its earliest stages and avoids synthesis of any precursor form (e.g. preQ$_0$ in *ΔqueF*) that was reported to be incorporated by the TGT and might thus compete with preQ$_1$-L1 (Supplementary Figure S3c) (13).

To determine a suitable feeding concentration, the *ΔqueD* cells were supplemented with increasing amounts of preQ$_1$-L1 (Figure 2B), which did not impair the bacterial growth compared to the control without preQ$_1$-L1 feeding (Supplementary Figure S3b). Total tRNA isolated from thus treated *ΔqueD* cells was labelled *via* CuAAC click chemistry and subsequently analysed by denaturing urea PAGE. The fluorescence scan revealed clearly visible fluorescent bands after feeding with preQ$_1$-L1 in a dose-dependent manner, providing evidence for the enzymatic incorporation of the analogue into *E. coli* tRNA *in vivo* (Figure 2D). The signal intensity was quantified using ImageJ software and plotted against the feeding concentration of preQ$_1$-L1 (Figure 2E). To validate these observations, total tRNA isolated from the *ΔqueD* strain treated with preQ$_1$-L1 was further analysed *via* LC–MS/MS. The MS-based analysis of total tRNA isolated from the *ΔqueD* fed with increasing concentrations of preQ$_1$-L1 (0.1–10 μM) confirmed the results obtained from denaturing urea PAGE analysis and related quantification of the fluorescence signal (Figure 2E). Both plots indicate a beginning saturation around 10 μM. Based on the above, a ligand concentration of 5 μM for further feeding experiments was identified as a viable compromise between ligand material consumption and labelling efficiency. Supplementation of a *Δtgt* strain with the optimized concentration of 5 μM preQ$_1$-L1 resulted in no signal for Q-L1 in LC–MS/MS measurements, thus confirming that the incorporation was catalysed by bTGT (Supplementary Figure S3c).

Since preQ$_1$-L1 was successfully incorporated into RNA in bacteria, the *in vivo* experiments were expanded to preQ$_1$-L2 and preQ$_1$-L3. However, in contrast to the previously

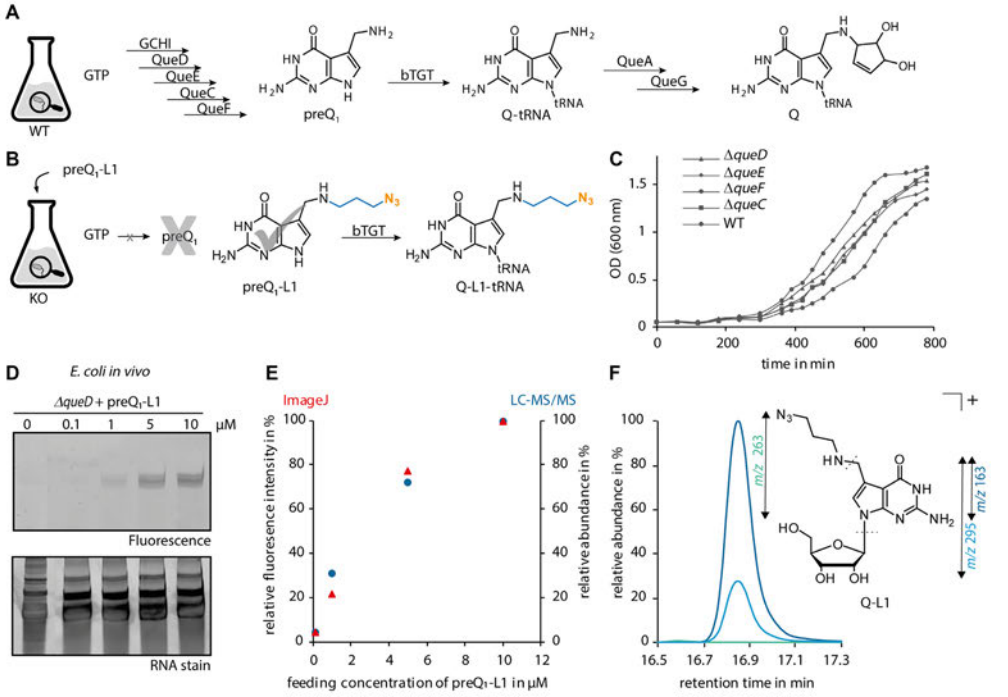

Figure 2. *De novo* biosynthesis of Q and induced incorporation of preQ$_1$-L1 in bacteria. (**A**) Biosynthesis of Q in position 34 of tRNAs (Q34-tRNA) *via* insertion of preQ$_1$ into tRNA, which is catalysed by the bacterial tRNA guanine transglycosylase (bTGT). (**B**) Treatment of *E. coli* mutant cells unable to synthesize preQ$_1$ with preQ$_1$-L1 and concomitant bTGT-catalysed incorporation of this analogue into tRNA. (**C**) Growth of the *E. coli* wild-type (WT) strain compared to the growth of several strains with deletions in genes encoding enzymes for Q *de novo* synthesis. (**D**) Analysis of total tRNA from *ΔqueD* cells grown with the indicated concentrations of preQ$_1$-L1 after click reaction by denaturing PAGE and subsequent scanning for fluorescence of AlexaFluor 594 (excitation: 532 nm, emission: 610 nm). (**E**) Merged diagram displaying the quantification of the dose-dependent fluorescence signal obtained from (D) by ImageJ software (Wayne Rasband, NIH) (shown as red triangles) and relative quantification of Q-L1 levels by LC–MS/MS (blue dots). Peak areas of Q-L1 (*m/z* 163) were normalized to the UV signal of adenosine and set in relation to the peak area of the highest feeding concentration (10 μM). (**F**) Extracted ion chromatograms displaying the fragmentation pattern of the incorporated synthetic nucleoside Q-L1 (*m/z* 395) in LC–MS/MS experiments, normalized to the highest peak area (*m/z* 163). Product ions are assigned in the structure of Q-L1.

described *in vitro* experiments, neither feeding preQ$_1$-L2 nor preQ$_1$-L3 at the optimized concentration of 5 μM or at higher concentrations (10 μM for preQ$_1$-L2 and 20 μM preQ$_1$-L3) led to a clear fluorescence signal in the clicked total tRNA samples (Supplementary Figure S3a), indicating that the incorporation efficiency of preQ$_1$-L2 and preQ$_1$-L3 into tRNA *in vivo* was drastically lower compared to preQ$_1$-L1. Since the *in vitro* results indicate indifference of the TGT enzyme towards the alkyl-modified preQ$_1$-ligands, the low incorporation *in vivo* suggests lower bioavailability of preQ$_1$-L2 and preQ$_1$-L3 for the bacteria.

In vivo interactions of synthetic preQ$_1$ analogues in prokaryotes

To investigate possible changes in the ensemble of molecular interactions undergone by Q-L1-carrying tRNA under physiological conditions, we turned to the analysis of polysomes. Given that these consist of actively translating ribosomes, their components, including tRNA, can be considered functional in interactions with essential molecular factors involved in translation. We thus aimed at determining the ratio of Q-L1-carrying tRNAs from polysomes versus that in the remainder of tRNAs.

For this purpose, cell lysates from *E. coli* WT and *ΔqueD* cells supplemented with 10 μM preQ$_1$-L1 were applied to a sucrose gradient (5–40%), enabling the separation of different fractions according to their size after ultracentrifugation. As schematically shown in Figure 3A, free RNAs including tRNAs and some mRNAs were located in fraction F0 at the top of the gradient (5% sucrose), while polysomes accumulated in fraction F3 at a sucrose concentration of ∼40%. This separation was monitored by UV absorbance at 260 nm, and the different fractions were collected. Subsequent to fractionation, total RNA was extracted from these fractions and applied to denaturing PAGE for purification of tRNA *via* gel elution. Digested tRNA samples were subjected to LC–MS/MS

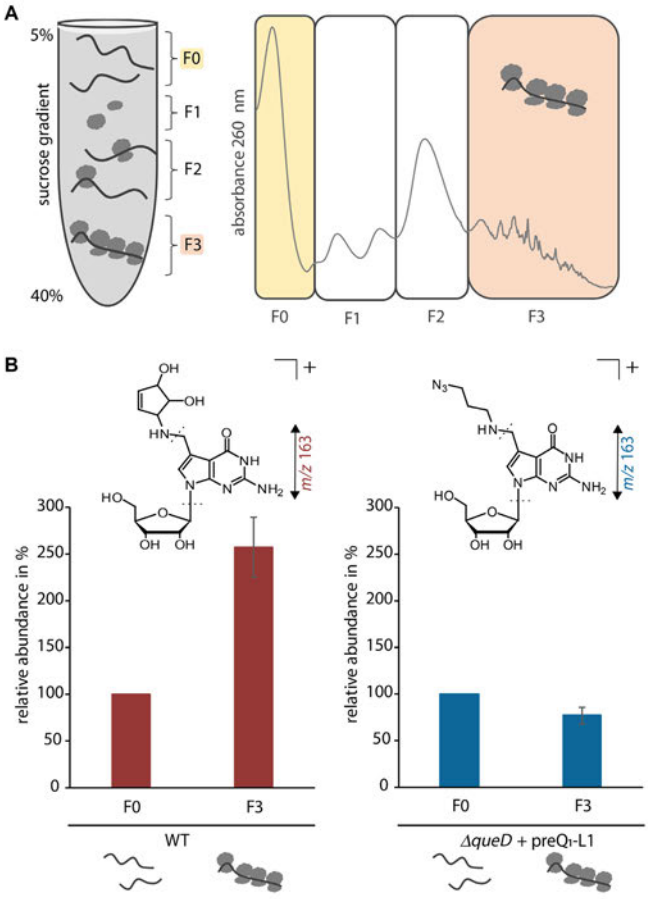

Figure 3. *E. coli* polysome preparation and analysis of isolated tRNA obtained from these samples by LC–MS/MS. (**A**) Schematic distribution of fractions F0-F3 from a cell lysate after sucrose gradient (5–40 %) fractionation and ultracentrifugation and representative UV trace at 260 nm (representing RNA) across the sucrose gradient. (**B**) Relative quantification of Q (*m/z* 410 → 163, red) and Q-L1 (*m/z* 395 → 163, blue) in tRNA purified from fractions F0 and F3 of WT and *ΔqueD* cells supplemented with 10 μM preQ$_1$-L1 *via* LC–MS/MS. Peak areas were normalized to the UV signal of adenosine and related pairwise to the respective F0 fraction which was set to 100%. The average of normalized and related fractions F0 and F3 of three independent biological replicates are shown.

analysis, and the respective abundances of Q and Q-L1 were compared between the free RNA fraction F0 and the polysomal fraction F3 (Figure 3B). Interestingly, in WT cells, endogenous Q was more abundant in tRNAs isolated from the polysomal fraction compared to fraction F0. This suggests that queuosinylated tRNAs are selectively enriched in polysomes that are actively engaged in translation.

In contrast, the Q-L1 level in polysomal tRNA (F3 fraction) from preQ$_1$-L1 fed *ΔqueD* cells reached a similar amount compared to its level in the respective F0 fraction. This may reflect either a deficit in the aforementioned selection, or a cumulation of minor detrimental effects at the different steps of translation. However, the data clearly illustrate that Q-L1-containing tRNAs actively engage in protein biosynthesis and are able to sustain it at a high enough level to not cause any perceivable growth phenotype.

In vitro incorporation of synthetic preQ$_1$ analogues in eukaryotes

In a next step, the investigations were extended from bacteria to eukaryotes. Of note, eukaryotes do not possess the enzymes to synthesize queuosine *de novo,* but salvage it from external sources for incorporation into tRNA (16). *S. pombe* is a particularly well-suited single cell eukaryotic

model organism, because salient features of queuosine have already been elaborated in this yeast, and queuosine levels can easily be manipulated by supplementation of the growth medium with queuine (38).

We next tested the ability of eTGT to incorporate the preQ$_1$-ligands into RNA *in vitro*. As substrates for this reaction, total RNA was isolated from *S. pombe* wild-type cells or *qtr2Δ* cells cultured in the presence of queuine. In WT cells, this results in Q-modification of the tRNAs, whereas *qtr2Δ* cells lack the essential Qtr2 subunit of *S. pombe* eTGT, therefore maintaining a guanosine in position 34 of the respective tRNAs. Total RNA preparations of these strains were incubated with the preQ$_1$ ligands in presence of hTGT, and subsequently labelled by click reaction. The incorporation of all three ligands into tRNA from both *S. pombe* strains was measured by fluorescence scan (Figure 4A and Supplementary Figure S4b). In comparison to the fluorescence signals of the tRNA from WT cells, the respective signals of the *qtr2Δ* tRNAs showed significantly higher intensities. This indicates that more tRNAs unmodified at position G34 are available for *in vitro* modification with preQ$_1$-L1 in the *qtr2Δ* sample. In contrast, in WT cells only guanosines that were not replaced by Q despite the presence of a functional enzyme remained for the *in vitro* reaction. Unlike observed for the bTGT, the hTGT incorporated the preQ$_1$-ligands to differing degrees, indicating a higher ability to distinguish between these analogues in accordance with previously published results by Kelly and co-workers (41). Additionally, incubation of *in vitro* transcribed tRNAs Asp, His, Tyr and Asn with human TGT and preQ$_1$-L1 showed successful incorporation of the analogue into all of the four tRNAs (Supplementary Figure S4a).

In vivo incorporation of synthetic preQ$_1$ analogues in eukaryotes

Subsequent to the successful *in vitro* experiment, the *in vivo* incorporation of the synthetic preQ$_1$ analogues was examined in *S. pombe*. To this end, *S. pombe* WT and *qtr2Δ* cells (as a control), were cultured in the presence of preQ$_1$-ligands in medium that otherwise lacked Q or q, and RNA was isolated and analysed as before. After click reaction, a fluorescence signal was detected in the RNA isolated from the WT cells treated with preQ$_1$-L1, but not *qtr2Δ* (Figure 4B), showing that the presence of Q-L1 in tRNA *in vivo* depended on functional TGT. As in bacteria, preQ$_1$-L1 did not negatively affect cell growth (Supplementary Figure S4c), and no labelling was observed with preQ$_1$-L2 and -L3, again indicating that their derivatives are not bioavailable for incorporation into tRNAs *in vivo*.

Collectively, the above experiments indicate that preQ$_1$-L1 can readily be employed as a proxy for Q from the perspective of synthetic biology. To further develop this compound for the investigation of the epitranscriptome, we made use of the click chemistry feature of preQ$_1$-L1 to identify RNAs into which it was incorporated *in vivo* by eTGT.

For this purpose, total RNA isolated from *S. pombe* wild-type or *qtr2Δ* cells that were cultured in the presence of preQ$_1$-L1 was bio-conjugated *in vitro* with alkyne-functionalized biotin. Subsequent to affinity purification using streptavidin-coated magnetic beads, the biotin-labelled RNA was subjected to reverse transcription and high-throughput sequencing (Figure 5A, termed Q-RIP-Seq). The analysis showed that the known cytosolic Q-tRNAs tRNA^{Asn}, tRNA^{Asp}, tRNA^{His} and tRNA^{Tyr} were significantly enriched from WT, but not *qtr2Δ* cells ($n = 3$, $P_{adj} < 0.1$, Figure 5B, C and Supplementary Figure S5). Other enriched signals from snoR38 and snoR69 were scrutinised as potential substrates of TGT-mediated incorporation of preQ$_1$-L1. However, neither APB Northern blotting nor quantification by q-RT-PCR substantiated this hypothesis (Supplementary Figure S6). Interestingly, mitochondrial tRNA^{Asn}, when analysed for q content by APB-northern blot, was queuosinylated to about 50% (Supplementary Figure S5b). The fact that no mitochondrial tRNA sequences were found in Q-RIP-Seq could mean that they are too low in abundance. An alternative explanation would be that preQ$_1$-L1 is not incorporated into mitochondrial tRNA. The above findings indicate that the four known Q-tRNAs are the only cytosolic RNAs that are Q-modified in *S. pombe*, which is congruent with crosslinking-based studies in human cells (41). These results establish that any major metabolic influence resulting from feeding preQ$_1$-L1 would be mediated through the four classical tRNA substrates of TGT. It should, however, be noted that an early study reported preQ1-modification *in vitro* of larger RNA species in *E. coli* (63).

In vivo interactions of synthetic preQ$_1$ analogues in eukaryotes

Having established that preQ$_1$-L1 is actively incorporated into native tRNAs, we next investigated a particularly interesting effect of queuosine, namely a so-called tRNA modification circuit, where the formation of one modification is enhanced by the presence of another modification (64). The particular circuit involving queuosine was first identified in *S. pombe*. We had shown earlier by RNA bisulfite sequencing that the formation of m^{5}C38 in tRNA^{Asp} by the Dnmt2 tRNA methyltransferase is strongly enhanced by the presence of queuosine at position 34 (Figure 6A) (38,49).

We therefore asked whether Q-L1 can serve as a biologically active surrogate for queuosine in this circuit. Figure 6B shows the m^{5}C38 levels of tRNA^{Asp} in response to increasing concentrations of preQ$_1$-L1 in medium otherwise free of queuosine derivatives. A clear dose-dependent increase of the C38 methylation level was observed, indicating that the incorporated preQ$_1$-L1 is functionally integrated into this modification circuit, efficiently replacing queuosine in its capability of triggering Dnmt2 activity in *S. pombe*. Considering the direct functional connection of Q/Q-L1 and m^{5}C38, the increase of the C38 methylation level from 15% in non-treated culture up to 60% in cultures supplemented with 100 nm preQ$_1$-L1 points to its incorporation in significant amounts in *S. pombe*. However, it is important to mention that the effect of preQ$_1$-L1 incorporation on tRNA^{Asp} methylation is less efficient compared to the known effect of Q under

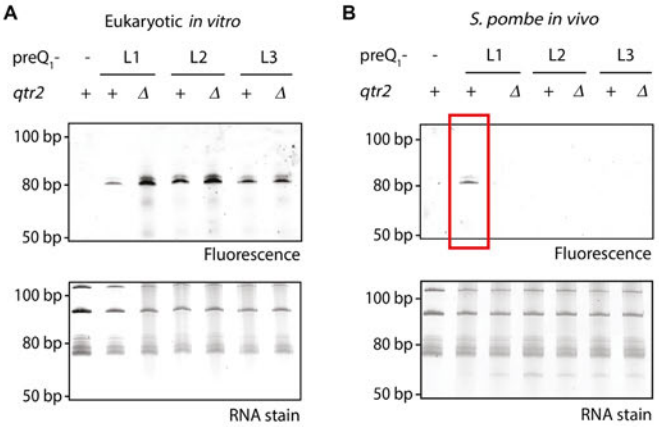

Figure 4. *In vitro* and *in vivo* incorporation of preQ$_1$-ligands in *S. pombe* tRNA. (**A**) Analysis of the total RNA click product after human tRNA guanine transglycosylase (hTGT)-catalysed incorporation of preQ$_1$-ligands L1–L3 into RNA from *S. pombe* by denaturing PAGE and visualization by fluorescence scan for AlexaFluor 594 (excitation: 532 nm, emission: 610 nm). Total RNA was extracted from *S. pombe* WT cells containing functional TGT (+) and *qtr2Δ* cells that lack functional TGT (*Δ*), which were both cultured in the presence of queuine. The incubation of total RNA from WT cells without preQ$_1$-ligand (-) served as a negative control. A loading control was obtained by RNA staining with SybrGold. (**B**) Analysis of total tRNA from *S. pombe* WT (+) and *qtr2Δ* (*Δ*) cells that were cultured in the presence of 0.1 μM of the respective preQ$_1$-ligand after click reaction by denaturing PAGE and subsequent visualization as described above. Total RNA from *S. pombe* WT cells supplemented with 0.1 μM queuine (–) instead of preQ$_1$-ligands was used as a negative control.

normal conditions, as we previously reported (38). The incorporation efficiency in *E. coli* can only be gauged even more indirectly, namely by comparison of fluorescent signals after click (Supplementary Figure S4d).

Lastly, we were also able to demonstrate successful incorporation of preQ$_1$-L1 in HeLa human cells deprived of q (Supplementary Figure S7a). In analogy to the earlier presented analysis of *E. coli* polysomes, we also investigated the levels of Q-L1 in tRNA purified from F0 and F3 of accordingly treated HeLa cultures. Similar to our observations in *E. coli*, the amount of Q-L1 detected in the polysomal tRNA (F3 fraction) from preQ$_1$-L1 fed HeLa cells was comparable to its level in the respective F0 fraction, indicating that Q-L1-containing tRNAs actively engage in protein biosynthesis *in cellulo* (Supplementary Figure S7b). This result indicates relevance of our investigations with respect to biomedical considerations, e.g. potential therapeutic interventions.

DISCUSSION

Interest in concepts for the incorporation of modified and/or non-natural derivatives of metabolites into nucleic acids has been steadily increasing, boosted in part by a surge in RNA modification research, and, more recently, in mRNA-based vaccines. Post-synthetic derivatization of RNA *in vitro*, e.g. by methyltransferases has been exploited for labelling in conjunction with click chemistry (65–69). In the queuosine field, a number of q-derived compounds, including clickable tetrazine derivatives, have been incorporated into native RNA preparation *in vitro* using recombinant TGT, and applied to fluorescent labelling, affinity purification, and interactome research (42–44,70,71). In a previous study, Brooks *et al.* reported that azide congeners of preQ$_1$ lacking the methylene amine were not incorporated by the TGT which they traced to the necessity of this structural element for a successful binding to the enzyme forming hydrogen bonds between aminoacid residues Leu231 and Met260 of the enzyme (72,73). Although, as mentioned, strong indirect evidence (34) suggested that incorporation of nonnatural q derivatives should be feasible in principle, no *in vivo* labelling of Q-tRNAs with clickable q-derivatives has been demonstrated so far.

Overall, concepts and applications in the RNA field currently move from *in vitro* (74) to metabolic feeding approaches *in cellulo* and *in vivo*. Here, the use of noncanonical nucleoside structures has opened up new experimental avenues in the community. As an example, in RNA modification research feeding of methionine analogues featuring e.g. propargyl residues, has enabled their incorporation into RNA *in lieu* of methyl groups. Subsequent derivatization by click chemistry was exploited for determination of modification sites (75,76,66).

An important progress featured in our work is that we demonstrate low toxicity of the labelling compound and provide corresponding data at the molecular level. Elsewhere in the field, little attention is paid to the physiological impact of surrogate feeding. In most cases, a moderate survival rate in cell culture is sufficient to conduct e.g. -omics type analyses after incorporation (75–77). However, in the next steps of its development, the field might conceivably move to applications in model organisms. Here, by the latest, one will need

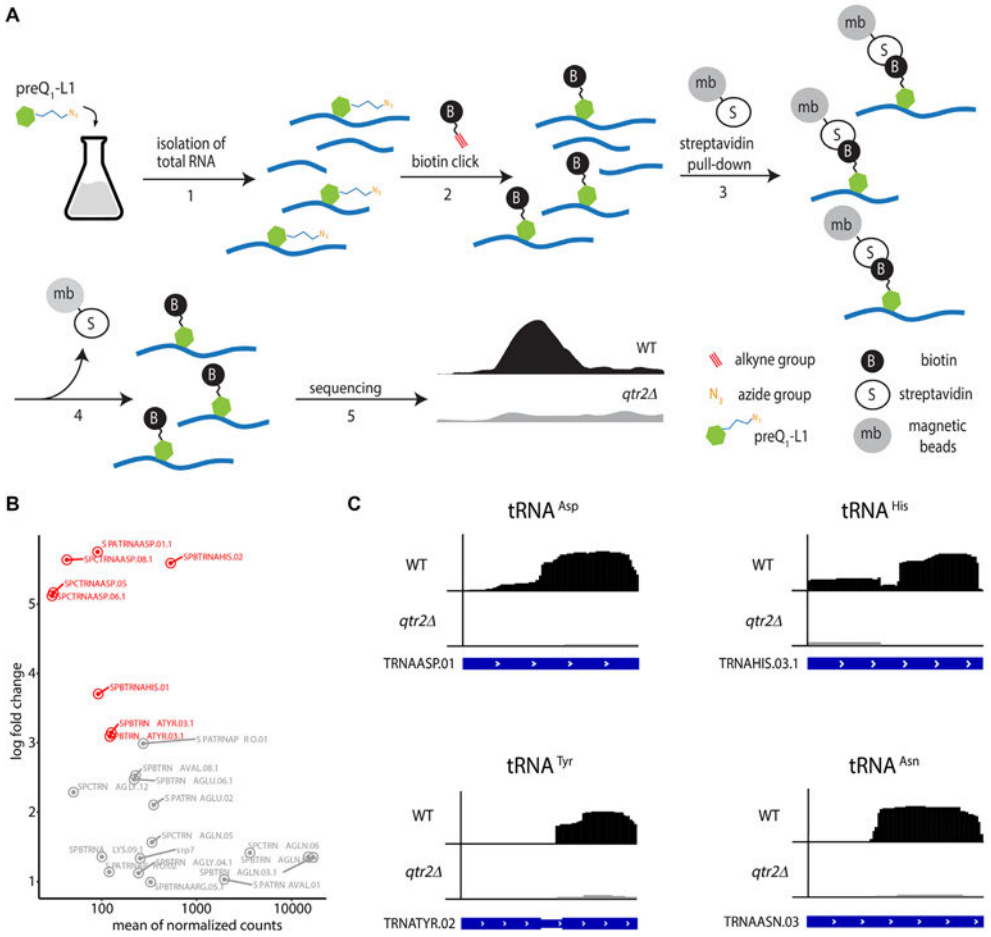

Figure 5. *In vivo* identification of Q-modified RNAs in *S. pombe* based on metabolic labelling with preQ$_1$-L1 and high-throughput sequencing (Q-RIP-Seq). (**A**) Concept of metabolic labelling and immunoprecipitation of Q-modified RNAs. *S. pombe* was cultured in the presence of 0.1 μM preQ$_1$-L1, leading to incorporation into otherwise Q-modified RNAs. Total RNA was extracted (1) and bio-conjugated *in vitro* with alkyne-functionalized biotin (2). Biotin-labelled RNAs were subsequently affinity-purified using streptavidin-coated magnetic beads (3), reverse-transcribed and subjected to high-throughput sequencing (5). As a control, metabolic labelling was performed in an *S. pombe* strain lacking TGT (*qtr2Δ*). (**B**) Log2 fold change of normalized read counts of RNAs from WT compared to *qtr2Δ* determined by exomePeak2. Red: tRNA^{Asp}, tRNA^{His} and tRNA^{Tyr}; (three independent replicates). (**C**) Q-RIP-Seq of tRNA^{Asp}, tRNA^{His}, tRNA^{Tyr} and tRNA^{Asn} after metabolic labelling with preQ$_1$-L1 in *S. pombe* WT and *qtr2Δ* cells. Coverage of the tRNA sequences from modified (WT, black) and unmodified (*qtr2Δ*, grey) samples is shown. The transcript architecture is shown below with thin and thick parts representing introns and mature tRNA sequences. Replicate 1 of three independent experiments is shown. Plots were generated using IGV.

to adopt concepts from medicinal chemistry, such as cell permeability, and toxicity. In this respect, the work presented here pioneers the combination of metabolic feeding of clickable surrogates with investigations into their physiological molecular impact after cellular uptake and their usage for the enrichment and identification of RNA species that were labelled *in vivo* by endogenous TGT. Apart from the observation of growth inhibition of q derivatives in eukaryotic cell culture, which are somewhat suggestive (78), there is strong indirect evidence for the actual incorporation of a q-derivative by TGT *in vivo* in mouse (34), however without direct analysis of the tRNA. Significantly, said case features a background of medicinal chemistry, and the compound used is structurally related to our preQ1-L series used here. It does, however, feature a lipophilic phenylpropyl sidechain which is likely causative

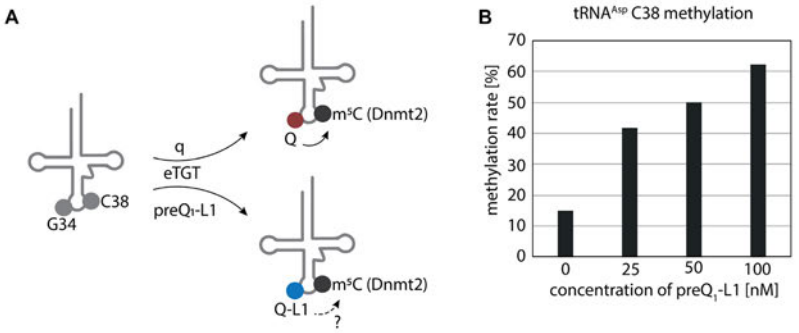

Figure 6. Incorporation of preQ$_1$-L1 in tRNA^{Asp} in *S. pombe* stimulates C38 methylation by Dnmt2. (**A**) Incorporation of q or preQ$_1$-L1 by eukaryotic tRNA guanine transglycosylase (eTGT) affects Dnmt2 activity in *S. pombe* (Pmt1). (**B**) Determination of tRNA^{Asp} methylation levels at C38 in total RNA from *S. pombe* WT supplemented with the indicated concentrations of preQ$_1$-L1 by RNA bisulfite sequencing combined with high throughput sequencing.

of, or enhancing the compound's cell permeability and biodistribution.

In the present work, we have developed the azido-propyl-derivative preQ$_1$-L1 as a bioactive surrogate for preQ$_1$ *in vivo*. preQ$_1$-L1 is taken up into unicellular prokaryotes as well as into eukaryotes, and incorporated into the known tRNA substrates of TGT. The resulting nucleoside is semi-synthetic in that its sugar moiety is native, while its nucleobase is synthetic. Its azide moiety can be employed to metabolically label and isolate Q-modified RNAs by affinity purification after conjugation by click chemistry. We used this feature to confirm similar data from human cells, obtained after UV-crosslinking (41). Taken together, this means that the single most important molecular interaction for a physiological impact of q (or preQ$_1$-L1) is mediated through position 34 in the anticodons of the four known TGT substrate tRNAs.

Known molecular interactions issuing from this nucleobase are mostly restricted to tRNA aminoacylation and mRNA decoding, which we have interrogated by investigating the amount of Q-L1 carrying tRNAs on polysomes. While Q-L1 was less abundant there than was native Q, it was clearly present, featuring an equal distribution between actively translating tRNAs and the cytoplasmic pool in both bacterial and human cell preparations.

One other known effect of Q was also faithfully emulated by Q-L1, namely the stimulation of m^{5}C38 formation by Dnmt2 in the anticodon stem of tRNA^{Asp}, representing a so-called modification loop. Technically speaking, we report the first-ever manipulation of a modification loop by atomic mutagenesis *in vivo*.

In spite of numerous described Q-dependent implications in various diseases, starting from cancer (29–32) to neurological and neuropsychiatric disorders, such as multiple sclerosis, schizophrenia and Parkinson (79,80,33,34), a defined mechanism explaining the role of Q in these pathologies is still missing (28). Recently, we discovered a direct connection between Q, accuracy and the speed of codon-biased translation (27,28), which promotes protein folding and prevents the accumulation of misfolded proteins. The fact that Q-L1 is functionally involved in the translational process in a 'minimally invasive' system, opens the possibility to study the roles of Q34 modifications in protein translation in normal and pathogenic human cell lines, directly combining click chemistry or LC–MS/MS with polysome profiling.

In summary, the combination of very few queuosinylation sites and the effective functional replacement of Q by Q-L1 on the molecular level, makes the q/Q system uniquely suited for a 'minimally invasive' placement of a non-natural nucleobase within the total cellular RNA.

DATA AVAILABILITY

HTS data for Q-RIP-Seq experiments are available in the NCBI GEO database, record GSE210404. All data needed to evaluate the conclusions in the paper are present in the paper and/or Supplementary Data. Additional data related to this paper may be requested from the authors.

SUPPLEMENTARY DATA

Supplementary Data are available at NAR Online.

ACKNOWLEDGEMENTS

Eva Neuner (Innsbruck) is thanked for discussions.
Author contributions: A.E.E.-M. and M.H. conceived and supervised the project. L.B., N.K. and L.V. performed the majority of the experimental work. These authors contributed equally and are listed in alphabetical order. L.F. and R.M. provided preQ$_1$-L1-3. F.T. performed HeLa culture and polysome preparations. C.S. and M.W. helped with *E. coli* polysome preparations. All authors discussed the results. L.B., M.H. and L.V. wrote the manuscript with input from all the other authors.

FUNDING

Deutsche Forschungsgemeinschaft (DFG, German Research Foundation) [TRR-319 TP C03, SPP1784, HE

3397/13-2, HE 3397/14-2 to M.H., TRR-319 TP A06 to F.T., TRR-319 TP B05 to M.-L.W.]; [DFG SPP1784 to A.E.E.-M.]; R.M. was supported by the Austrian Science Fund FWF [P31691 and F8011-B]. Funding for open access charge: Johannes Gutenberg University.

Conflict of interest statement. M.H. is a consultant for Moderna Inc. The other authors declare that they have no competing interests.

REFERENCES

1. El Yacoubi,B., Bailly,M. and de Crécy-Lagard,V. (2012) Biosynthesis and function of posttranscriptional modifications of transfer RNAs. *Annu. Rev. Genet.*, **46**, 69–95.
2. Lorenz,C., Lünse,C.E. and Mörl,M. (2017) tRNA modifications: impact on structure and thermal adaptation. *Biomolecules*, **7**, 35.
3. Motorin,Y. and Helm,M. (2010) tRNA stabilization by modified nucleotides. *Biochemistry*, **49**, 4934–4944.
4. Boccaletto,P., Stefaniak,F., Ray,A., Cappannini,A., Mukherjee,S., Purta,E., Kurkowska,M., Shirvanizadeh,N., Destefanis,E., Groza,P. *et al.* (2022) MODOMICS: a database of RNA modification pathways. 2021 update. *Nucleic Acids Res.*, **50**, D231–D235.
5. Fergus,C., Barnes,D., Alqasem,M.A. and Kelly,V.P. (2015) The queuine micronutrient: charting a course from microbe to man. *Nutrients*, **7**, 2897–2929.
6. Harada,F. and Nishimura,S. (1972) Possible anticodon sequences of tRNA his tRNA asm and tRNA asp from escherichia coli b. Universal presence of nucleoside q in the first postion of the anticondons of these transfer ribonucleic acids. *Biochemistry*, **11**, 301–308.
7. Kasai,H., Oashi,Z., Harada,F., Nishimura,S., Oppenheimer,N.J., Crain,P.F., Liehr,J.G., Minden,D.L.von and McCloskey,J.A. (1975) Structure of the modified nucleoside q isolated from escherichia coli transfer ribonucleic acid. 7-(4,5-cis-Dihydroxy-1-cyclopenten-3-ylaminomethyl)-7-deazaguanosine. *Biochemistry*, **14**, 4198–4208.
8. Phillips,G., El Yacoubi,B., Lyons,B., Alvarez,S., Iwata-Reuyl,D. and Crécy-Lagard,V.de (2008) Biosynthesis of 7-deazaguanosine-modified tRNA nucleosides: a new role for GTP cyclohydrolase I. *J. Bacteriol.*, **190**, 7876–7884.
9. McCarty,R.M., Somogyi,A. and Bandarian,V. (2009) Escherichia coli QueD is a 6-carboxy-5,6,7,8-tetrahydropterin synthase. *Biochemistry*, **48**, 2301–2303.
10. McCarty,R.M., Somogyi,A., Lin,G., Jacobsen,N.E. and Bandarian,V. (2009) The deazapurine biosynthetic pathway revealed: in vitro enzymatic synthesis of preq(0) from guanosine 5'-triphosphate in four steps. *Biochemistry*, **48**, 3847–3852.
11. van Lanen,S.G., Reader,J.S., Swairjo,M.A., Crécy-Lagard,V.de, Lee,B. and Iwata-Reuyl,D. (2005) From cyclohydrolase to oxidoreductase: discovery of nitrile reductase activity in a common fold. *Proc. Nat. Acad. Sci. U.S.A.*, **102**, 4264–4269.
12. Okada,N. and Nishimura,S. (1979) Isolation and characterization of a guanine insertion enzyme, a specific tRNA transglycosylase, from escherichia coli. *J. Biol. Chem.*, **254**, 3061–3066.
13. Okada,N., Noguchi,S., Kasai,H., Shindo-Okada,N., Ohgi,T., Goto,T. and Nishimura,S. (1979) Novel mechanism of post-transcriptional modification of tRNA. Insertion of bases of q precursors into tRNA by a specific tRNA transglycosylase reaction. *J. Biol. Chem.*, **254**, 3067–3073.
14. Slany,R.K., Bösl,M. and Kersten,H. (1994) Transfer and isomerization of the ribose moiety of adomet during the biosynthesis of queuosine tRNAs, a new unique reaction catalyzed by the QueA protein from escherichia coli. *Biochimie*, **76**, 389–393.
15. Miles,Z.D., McCarty,R.M., Molnar,G. and Bandarian,V. (2011) Discovery of epoxyqueuosine (oQ) reductase reveals parallels between halorespiration and tRNA modification. *Proc. Nat. Acad. Sci. U.S.A.*, **108**, 7368–7372.
16. Patel,B.I., Heiss,M., Samel-Pommerencke,A., Carell,T. and Ehrenhofer-Murray,A.E. (2022) Queuosine salvage in fission yeast by Qng1-mediated hydrolysis to queuine. *Biochem. Biophys. Res. Commun.*, **624**, 146–150.
17. Farkas,W.R., Jacobson,K.B. and Katze,J.R. (1984) Substrate and inhibitor specificity of tRNA-guanine ribosyltransferase. *Biochim. Biophys. Acta*, **781**, 64–75.
18. Boland,C., Hayes,P., Santa-Maria,I., Nishimura,S. and Kelly,V.P. (2009) Queuosine formation in eukaryotic tRNA occurs via a mitochondria-localized heteromeric transglycosylase. *J. Biol. Chem.*, **284**, 18218–18227.
19. Chen,Y.-C., Kelly,V.P., Stachura,S.V. and Garcia,G.A. (2010) Characterization of the human tRNA-guanine transglycosylase: confirmation of the heterodimeric subunit structure. *RNA*, **16**, 958–968.
20. Johannsson,S., Neumann,P. and Ficner,R. (2018) Crystal structure of the human tRNA guanine transglycosylase catalytic subunit QTRT1. *Biomolecules*, **8**, 81.
21. Grosjean,H. and Westhof,E. (2016) An integrated, structure- and energy-based view of the genetic code. *Nucleic Acids Res.*, **44**, 8020–8040.
22. Morris,R.C., Brown,K.G. and Elliott,M.S. (1999) The effect of queuosine on tRNA structure and function. *J. Biomol. Struct. Dyn.*, **16**, 757–774.
23. Noguchi,S., Nishimura,Y., Hirota,Y. and Nishimura,S. (1982) Isolation and characterization of an escherichia coli mutant lacking tRNA-guanine transglycosylase. Function and biosynthesis of queuosine in tRNA. *J. Biol. Chem.*, **257**, 6544–6550.
24. Manickam,N., Joshi,K., Bhatt,M.J. and Farabaugh,P.J. (2016) Effects of tRNA modification on translational accuracy depend on intrinsic codon-anticodon strength. *Nucleic Acids Res.*, **44**, 1871–1881.
25. Meier,F., Suter,B., Grosjean,H., Keith,G. and Kubli,E. (1985) Queuosine modification of the wobble base in tRNAHis influences 'in vivo' decoding properties. *EMBO J.*, **4**, 823–827.
26. Zaborske,J.M., DuMont,V.L.B., Wallace,E.W.J., Pan,T., Aquadro,C.F. and Drummond,D.A. (2014) A nutrient-driven tRNA modification alters translational fidelity and genome-wide protein coding across an animal genus. *PLoS Biol.*, **12**, e1002015.
27. Müller,M., Legrand,C., Tuorto,F., Kelly,V.P., Atlasi,Y., Lyko,F. and Ehrenhofer-Murray,A.E. (2019) Queuine links translational control in eukaryotes to a micronutrient from bacteria. *Nucleic Acids Res.*, **47**, 3711–3727.
28. Tuorto,F., Legrand,C., Cirzi,C., Federico,G., Liebers,R., Müller,M., Ehrenhofer-Murray,A.E., Dittmar,G., Gröne,H.-J. and Lyko,F. (2018) Queuosine-modified tRNAs confer nutritional control of protein translation. *EMBO J.*, **37**, e99777.
29. Zhang,J., Lu,R., Zhang,Y., Matuszek,Ż., Zhang,W., Xia,Y., Pan,T. and Sun,J. (2020) tRNA queuosine modification enzyme modulates the growth and microbiome recruitment to breast tumors. *Cancers*, **12**, 628.
30. Sebastiani,M., Behrens,C., Dörr,S., Gerber,H.-D., Benazza,R., Hernandez-Alba,O., Cianférani,S., Klebe,G., Heine,A. and Reuter,K. (2022) Structural and biochemical investigation of the heterodimeric murine tRNA-Guanine transglycosylase. *ACS Chem. Biol.*, **17**, 2229–2247.
31. Chen,Y.L. and Wu,R.T. (1994) Altered queuine modification of transfer RNA involved in the differentiation of human K562 erythroleukemia cells in the presence of distinct differentiation inducers. *Cancer Res.*, **54**, 2192–2198.
32. Dirheimer,G., Baranowski,W. and Keith,G. (1995) Variations in tRNA modifications, particularly of their queuine content in higher eukaryotes. Its relation to malignancy grading. *Biochimie*, **77**, 99–103.
33. Richard,P., Kozlowski,L., Guillorit,H., Garnier,P., McKnight,N.C., Danchin,A. and Manière,X. (2021) Queuine, a bacterial-derived hypermodified nucleobase, shows protection in in vitro models of neurodegeneration. *PLoS One*, **16**, e0253216.
34. Varghese,S., Cotter,M., Chevot,F., Fergus,C., Cunningham,C., Mills,K.H., Connon,S.J., Southern,J.M. and Kelly,V.P. (2017) In vivo modification of tRNA with an artificial nucleobase leads to full disease remission in an animal model of multiple sclerosis. *Nucleic Acids Res.*, **45**, 2029–2039.
35. Rakovich,T., Boland,C., Bernstein,I., Chikwana,V.M., Iwata-Reuyl,D. and Kelly,V.P. (2011) Queuosine deficiency in eukaryotes compromises tyrosine production through increased tetrahydrobiopterin oxidation. *J. Biol. Chem.*, **286**, 19354–19363.
36. Kulkarni,S., Rubio,M.A.T., Hegedüsová,E., Ross,R.L., Limbach,P.A., Alfonzo,J.D. and Paris,Z. (2021) Preferential import of queuosine-modified tRNAs into trypanosoma brucei

mitochondrion is critical for organellar protein synthesis. *Nucleic Acids Res.*, **49**, 8247–8260.
37. Hurt,J.K., Olgen,S. and Garcia,G.A. (2007) Site-specific modification of shigella flexneri virF mRNA by tRNA-guanine transglycosylase in vitro. *Nucleic Acids Res.*, **35**, 4905–4913.
38. Müller,M., Hartmann,M., Schuster,I., Bender,S., Thüring,K.L., Helm,M., Katze,J.R., Nellen,W., Lyko,F. and Ehrenhofer-Murray,A.E. (2015) Dynamic modulation of Dnmt2-dependent tRNA methylation by the micronutrient queuine. *Nucleic Acids Res.*, **43**, 10952–10962.
39. Ehrenhofer-Murray,A.E. (2017) Cross-Talk between dnmt2-dependent tRNA methylation and queuosine modification. *Biomolecules*, **7**, 14.
40. Johannsson,S., Neumann,P., Wulf,A., Welp,L.M., Gerber,H.-D., Krull,M., Diederichsen,U., Urlaub,H. and Ficner,R. (2018) Structural insights into the stimulation of s. pombe dnmt2 catalytic efficiency by the tRNA nucleoside queuosine. *Sci. Rep.*, **8**, 8880.
41. Fergus,C., Al-Qasem,M., Cotter,M., McDonnell,C.M., Sorrentino,E., Chevot,F., Hokamp,K., Senge,M.O., Southern,J.M., Connon,S.J. *et al.* (2021) The human tRNA-guanine transglycosylase displays promiscuous nucleobase preference but strict tRNA specificity. *Nucleic Acids Res.*, **49**, 4877–4890.
42. Alexander,S.C., Busby,K.N., Cole,C.M., Zhou,C.Y. and Devaraj,N.K. (2015) Site-Specific covalent labeling of RNA by enzymatic transglycosylation. *J. Am. Chem. Soc.*, **137**, 12756–12759.
43. Zhang,D., Zhou,C.Y., Busby,K.N., Alexander,S.C. and Devaraj,N.K. (2018) Light-Activated control of translation by enzymatic covalent mRNA labeling. *Angew. Chem. Int. Ed. Engl.*, **57**, 2822–2826.
44. Ehret,F., Zhou,C.Y., Alexander,S.C., Zhang,D. and Devaraj,N.K. (2018) Site-Specific covalent conjugation of modified mRNA by tRNA guanine transglycosylase. *Mol. Pharmaceutics*, **15**, 737–742.
45. Neuner,E., Frener,M., Lusser,A. and Micura,R. (2018) Superior cellular activities of azido- over amino-functionalized ligands for engineered preQ1 riboswitches in E.coli. *RNA Biol.*, **15**, 1376–1383.
46. Jakobi,S., Nguyen,T.X.P., Debaene,F., Metz,A., Sanglier-Cianférani,S., Reuter,K. and Klebe,G. (2014) Hot-spot analysis to dissect the functional protein-protein interface of a tRNA-modifying enzyme. *Proteins*, **82**, 2713–2732.
47. Gerber,H.-D. and Klebe,G. (2012) Concise and efficient syntheses of preQ1 base, q base, and (ent)-Q base. *Org. Biomol. Chem.*, **10**, 8660–8668.
48. Kraus,A.J., Brink,B.G. and Siegel,T.N. (2019) Efficient and specific oligo-based depletion of rRNA. *Sci. Rep.*, **9**, 12281.
49. Becker,M., Müller,S., Nellen,W., Jurkowski,T.P., Jeltsch,A. and Ehrenhofer-Murray,A.E. (2012) Pmt1, a dnmt2 homolog in *Schizosaccharomyces pombe*, mediates tRNA methylation in response to nutrient signaling. *Nucleic Acids Res.*, **40**, 11648–11658.
50. Schmid,K., Adobes-Vidal,M. and Helm,M. (2017) Alkyne-Functionalized coumarin compound for analytic and preparative 4-thiouridine labeling. *Bioconjug. Chem.*, **28**, 1123–1134.
51. Yuan,Y., Hutinet,G., Valera,J.G., Hu,J., Hillebrand,R., Gustafson,A., Iwata-Reuyl,D., Dedon,P.C. and Crécy-Lagard,V.de (2018) Identification of the minimal bacterial 2'-deoxy-7-amido-7-deazaguanine synthesis machinery. *Mol. Microbiol.*, **110**, 469–483.
52. Morgan,M., Anders,S., Lawrence,M., Aboyoun,P., Pagès,H. and Gentleman,R. (2009) ShortRead: a bioconductor package for input, quality assessment and exploration of high-throughput sequence data. *Bioinformatics*, **25**, 2607–2608.
53. Rohde,C., Zhang,Y., Reinhardt,R. and Jeltsch,A. (2010) BISMA—fast and accurate bisulfite sequencing data analysis of individual clones from unique and repetitive sequences. *BMC Bioinf.*, **11**, 230.
54. Jiang,H., Lei,R., Ding,S.-W. and Zhu,S. (2014) Skewer: a fast and accurate adapter trimmer for next-generation sequencing paired-end reads. *BMC Bioinf.*, **15**, 182.
55. Patro,R., Duggal,G., Love,M.I., Irizarry,R.A. and Kingsford,C. (2017) Salmon provides fast and bias-aware quantification of transcript expression. *Nat. Methods*, **14**, 417–419.
56. Kim,D., Langmead,B. and Salzberg,S.L. (2015) HISAT: a fast spliced aligner with low memory requirements. *Nat. Methods*, **12**, 357–360.
57. Li,H., Handsaker,B., Wysoker,A., Fennell,T., Ruan,J., Homer,N., Marth,G., Abecasis,G. and Durbin,R. (2009) The sequence alignment/map format and SAMtools. *Bioinformatics*, **25**, 2078–2079.
58. Love,M.I., Huber,W. and Anders,S. (2014) Moderated estimation of fold change and dispersion for RNA-seq data with DESeq2. *Genome Biol.*, **15**, 550.
59. Ignatiadis,N., Klaus,B., Zaugg,J.B. and Huber,W. (2016) Data-driven hypothesis weighting increases detection power in genome-scale multiple testing. *Nat. Methods*, **13**, 577–580.
60. Ignatiadis,N. and Huber,W. (2021) Covariate powered cross-weighted multiple testing. *J. R. Stat. Soc. Series B*, **83**, 720–751.
61. Meng,J., Cui,X., Rao,M.K., Chen,Y. and Huang,Y. (2013) Exome-based analysis for RNA epigenome sequencing data. *Bioinformatics*, **29**, 1565–1567.
62. Robinson,J.T., Thorvaldsdóttir,H., Winckler,W., Guttman,M., Lander,E.S., Getz,G. and Mesirov,J.P. (2011) Integrative genomics viewer. *Nat. Biotechnol.*, **29**, 24–26.
63. Brooks,A.F., Vélez-Martínez,C.S., Showalter,H.D.H. and Garcia,G.A. (2012) Investigating the prevalence of queuine in escherichia coli RNA via incorporation of the tritium-labeled precursor, preQ(1). *Biochem. Biophys. Res. Commun.*, **425**, 83–88.
64. Motorin,Y. and Helm,M. (2022) RNA nucleotide methylation: 2021 update, wiley interdisciplinary reviews. *RNA*. **15**, 2021.
65. Motorin,Y., Burhenne,J., Teimer,R., Koynov,K., Willnow,S., Weinhold,E. and Helm,M. (2011) Expanding the chemical scope of RNA:methyltransferases to site-specific alkynylation of RNA for click labeling. *Nucleic Acids Res.*, **39**, 1943–1952.
66. Fischer,T.R., Meidner,L., Schwickert,M., Weber,M., Zimmermann,R.A., Kersten,C., Schirmeister,T. and Helm,M. (2022) Chemical biology and medicinal chemistry of RNA methyltransferases. *Nucleic Acids Res.*, **50**, 4216–4245.
67. Schulz,D., Holstein,J.M. and Rentmeister,A. (2013) A chemo-enzymatic approach for site-specific modification of the RNA cap. *Angew. Chem. Int. Ed. Engl.*, **52**, 7874–7878.
68. Muttach,F. and Rentmeister,A. (2016) A biocatalytic cascade for versatile one-pot modification of mRNA starting from methionine analogues. *Angew. Chem. Int. Ed. Engl.*, **55**, 1917–1920.
69. Ovcharenko,A., Weissenboeck,F.P. and Rentmeister,A. (2021) Tag-Free internal RNA labeling and photocaging based on mRNA methyltransferases. *Angew. Chem. (Int. Ed. Engl.)*, **60**, 4098–4103.
70. Busby,K.N., Fulzele,A., Zhang,D., Bennett,E.J. and Devaraj,N.K. (2020) Enzymatic RNA biotinylation for affinity purification and identification of RNA-Protein interactions. *ACS Chem. Biol.*, **15**, 2247–2258.
71. Zhou,C.Y., Alexander,S.C. and Devaraj,N.K. (2017) Fluorescent turn-on probes for wash-free mRNA imaging via covalent site-specific enzymatic labeling. *Chem. Sci.*, **8**, 7169–7173.
72. Brooks,A.F., Garcia,G.A. and Showalter,H.D. (2021) Synthesis of azide congeners of preQ 1 as potential substrates for tRNA guanine transglycosylase. *J Heterocyclic Chem*, **58**, 1192–1198.
73. Xie,W., Liu,X. and Huang,R.H. (2003) Chemical trapping and crystal structure of a catalytic tRNA guanine transglycosylase covalent intermediate. *Nat. Struct. Biol.*, **10**, 781–788.
74. Croce,S., Serdjukow,S., Carell,T. and Frischmuth,T. (2020) Chemoenzymatic preparation of functional click-labeled messenger RNA. *Chembiochem*, **21**, 1641–1646.
75. Hartstock,K., Nilges,B.S., Ovcharenko,A., Cornelissen,N.V., Püllen,N., Lawrence-Dörner,A.-M., Leidel,S.A. and Rentmeister,A. (2018) Enzymatic or in vivo installation of propargyl groups in combination with click chemistry for the enrichment and detection of methyltransferase target sites in RNA. *Angew. Chem. (Int. Ed. Engl.)*, **57**, 6342–6346.
76. Hartstock,K., Ovcharenko,A., Kueck,N.A., Spacek,P., Cornelissen,N.V., Hüwel,S., Dieterich,C. and Rentmeister,A. (2022) MePMe-seq: Antibody-free simultaneous m6A and m5C mapping in mRNA by metabolic propargyl labeling and sequencing. bioRxiv doi: https://doi.org/10.1101/2022.03.16.484494, 16 March 2022, preprint: not peer reviewed.
77. Shu,X., Cao,J., Cheng,M., Xiang,S., Gao,M., Li,T., Ying,X., Wang,F., Yue,Y., Lu,Z. *et al.* (2020) A metabolic labeling method detects m6A transcriptome-wide at single base resolution. *Nat. Chem. Biol.*, **16**, 887–895.
78. Akimoto,H., Nomura,H., Yoshida,M., Shindo-Okada,N., Hoshi,A. and Nishimura,S. (1986) Queuine analogues. Their synthesis and

inhibition of growth of mouse L5178Y cells in vitro. *J. Med. Chem.*, **29**, 1749–1753.
79. Bednářová,A., Hanna,M., Durham,I., VanCleave,T., England,A., Chaudhuri,A. and Krishnan,N. (2017) Lost in translation: defects in transfer RNA modifications and neurological disorders. *Front. Mol. Neurosci.*, **10**, 135.
80. Skolnick,S.D. and Greig,N.H. (2019) Microbes and monoamines: potential neuropsychiatric consequences of dysbiosis. *Trends Neurosci.*, **42**, 151–163.

Supplementary Data

Functional integration of a semi-synthetic azido-queuosine derivative into translation and a tRNA modification circuit

Larissa Bessler[1,†], Navpreet Kaur[2,†], Lea-Marie Vogt[1,†], Laurin Flemmich[3], Carmen Siebenaller[4], Marie-Luise Winz[1], Francesca Tuorto[5], Ronald Micura[3], Ann E. Ehrenhofer-Murray[2,*] and Mark Helm[1,*]

[1]Institute of Pharmaceutical and Biomedical Sciences, Johannes Gutenberg-University Mainz, 55128 Mainz, Germany
[2]Institute of Biology, Humboldt-Universität zu Berlin, 10117 Berlin, Germany
[3]Department of Organic Chemistry, University of Innsbruck, 6020 Innsbruck, Austria
[4]Department of Chemistry – Biochemistry, Johannes Gutenberg-University Mainz, 55128 Mainz, Germany.
[5]Division of Biochemistry, Mannheim Institute for Innate Immunoscience (MI3), Medical Faculty Mannheim, Heidelberg University, Mannheim, Germany

* To whom correspondence should be addressed. Tel: +49 (0) 6131 39 25731; Fax: +49 (0) 6131 39 20373; Email: mhelm@uni-mainz.de
Correspondence can also be addressed to Ann E. Ehrenhofer-Murray. Tel: +49 (0) 30 2093 49630; Fax: +49 (0) 30 2093 49641; Email: ann.ehrenhofer-murray@hu-berlin.de

† Joint Authors

Supplementary Table S1: *S. pombe* strains used in this study.

Designation	Genotype	Source
AEP1	*h⁻ leu1-32 ura4-D18 his3-D3*	YGRC
AEP288	*h⁻ leu1-32 ura4-D18 his3-D3 qtr2Δ::NatMX*	(1)

Supplementary Table S2: Plasmids used in this study.

Designation	Genotype	Source
pAE1688	pJET1-tRNA^{Asp} (*S.pombe*)	(2)
pAE2975	pASK-IBA13Plus - *Z. mobilis* TGTStrep-tag® II N-terminal	(3)
pAE2963	pCDF-Duet - hQTRT1-6xHis & hQTRT2	(4)

Supplementary Table S3: Oligonucleotides used in this study.

Designation	Sequence	Purpose
5S rRNA	5'-biotin-ACCCCGGATTCCCATGTTGTCTCCAACCATAGTAC-3'	rRNA depletion
5.8S rRNA	5'-biotin-CGTTCTTCATCGATGCGAGAGCCAAGAGATCCGTT-3'	rRNA depletion
tRNA Asp RT-Primer	5'-CTCaactggattggctnnnnngataaatccagttgagtggCTCTCCCT-3' [a]	RT
tRNA Asp bisulfite.fwd	5'- TTAGTATAGGGGTAGTATAT-3'	Bisulfite sequencing
stemloop.rev	5'- CGATCANNNNCTCAACTGGATTGGCT -3' [b]	Bisulfite sequencing
tRNAAsp_probe	5'-biotin-GGGCTGCAAGCGTGACAGG-3'	Northern
snoR38_probe	5'-biotin-CTCAACACTATGCTTTAGACAGGG-3'	Northern
snoR69_probe	5'-biotin-GCGTACTCGTCAATGTAAATAC-3'	Northern
RT-Primer_tRNAAsp	5'-AATCACTCAACTGGATTGGCT nnnnnGATAAATCCAGTTGAGTGGCTCTCCCTC-3' [a]	RT
RT-Primer_sno38	5'-AATCACTCAACTGGATTGGCT nnnnnGATAAATCCAGTTGAGTGGCAGATTTAC-3' [a]	RT
RT-Primer_snoR69	5'-AATCACTCAACTGGATTGGCT nnnnnGATAAATCCAGTTGAGTGGGTTCAGATA-3' [a]	RT
qPCR_tRNAAsp_fwd	5'-ATAGGGGTAGTACACAAGCCTGT-3'	qPCR
qPCR_sno38_fwd	5'-ACAGTTATCCCTGTCTAAAGCATAG-3'	qPCR
qPCR_snoR69_fwd	5'-CTTCGTTAAACCCAGCTCAC-3'	qPCR
qPCR_rev	5'-CGATCAATCACTCAACTGGATTGGCT-3'	qPCR

[a] Nucleotides marked as "n" are random nucleotides used as indices
[b] Nucleotides marked as "N" are the barcode region

Supplementary Table S4: Software used in this study.

Software	Version
R	3.6.3
Skewer	0.2.2
Salmon	14.0
HISAT2	2.2.1
SAMtools	1.12
DESeq2	1.26.0
ExomePeak2	2.16.0
IGV	2.11.1
M6A viewer	1.6.1

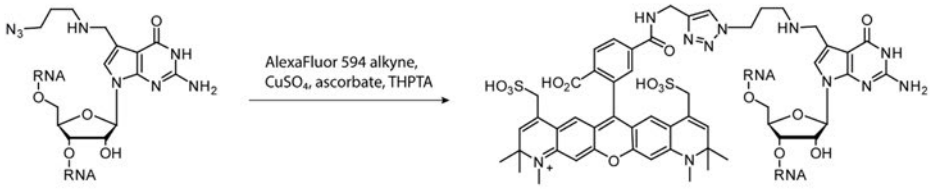

Supplementary Figure 1: Click derivatization of preQ$_1$-L1-containing RNA by a fluorescent alkyne. THPTA = Tris((1-hydroxy-propyl-1H-1,2,3-triazol-4-yl)methyl)amine.

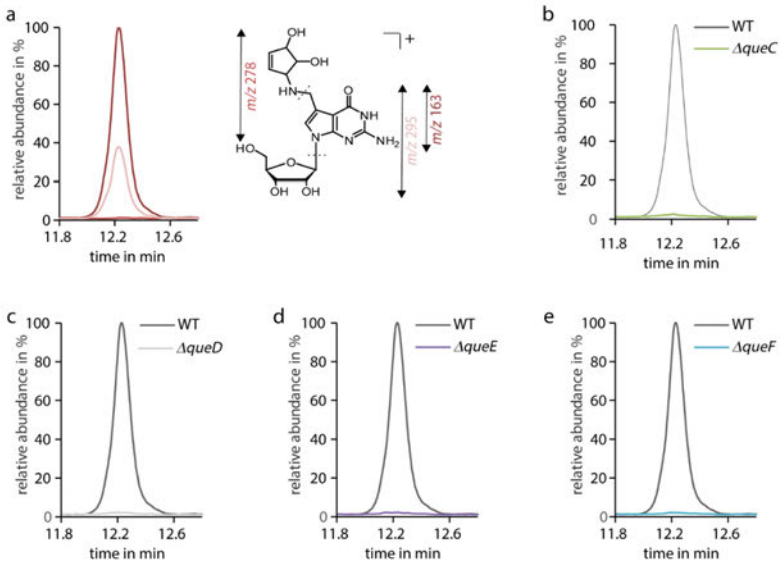

Supplementary Figure 2: LC-MS analysis of queuosine levels. a Extracted ion chromatograms displaying the fragmentation pattern of Q (*m/z* 410) in LC-MS/MS experiments, normalized to the highest peak area (*m/z* 163). Product ions are assigned in the structure of Q. **b** Relative LC-MS/MS quantification of Q levels in digested total tRNA from wild type and *ΔqueC* mutant cells, normalized to the UV signal of adenosine and set in relation to the peak area of Q in the WT cells. **c**, **d** and **e** show similar analysis of total tRNA from wild type and *ΔqueD, ΔqueE* and *ΔqueF*, respectively.

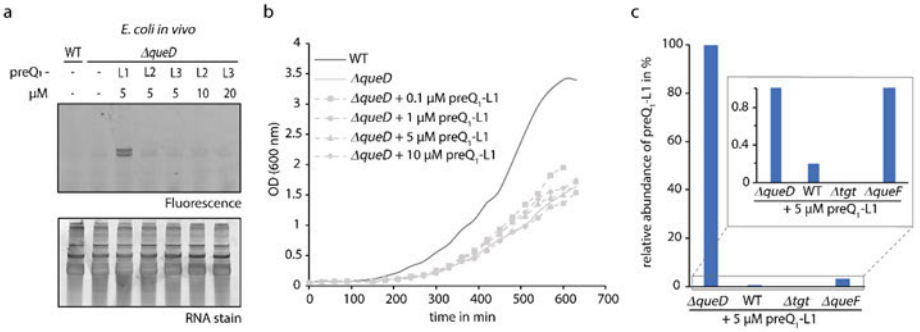

Supplementary Figure 3: Detection of incorporation of preQ$_1$-ligands L1-3 into total tRNA isolated from a *ΔqueD E. coli* strain via click derivatization. a Analysis of total tRNA from *ΔqueD* grown with the indicated concentrations of preQ$_1$-ligands L1-3 after click reaction by denaturing PAGE and subsequent scanning for fluorescence of AlexaFluor 594 (excitation: 532 nm, emission: 610 nm). **b** Growth of *E. coli* wild-type (WT) strain compared to the growth of the *ΔqueD* strain supplemented with indicated concentrations of preQ$_1$-L1. **c** Relative quantification of Q-L1 (*m/z* 395 → 163, blue) in total tRNA isolated from *E. coli* WT, *ΔqueD*, *Δtgt* and *ΔqueF* cells supplemented with 5 μM preQ$_1$-L1 via LC-MS/MS. Peak areas were normalized to the UV signal of adenosine and related the signal of Q-L1 in *ΔqueD* + 5 μM preQ$_1$-L1.

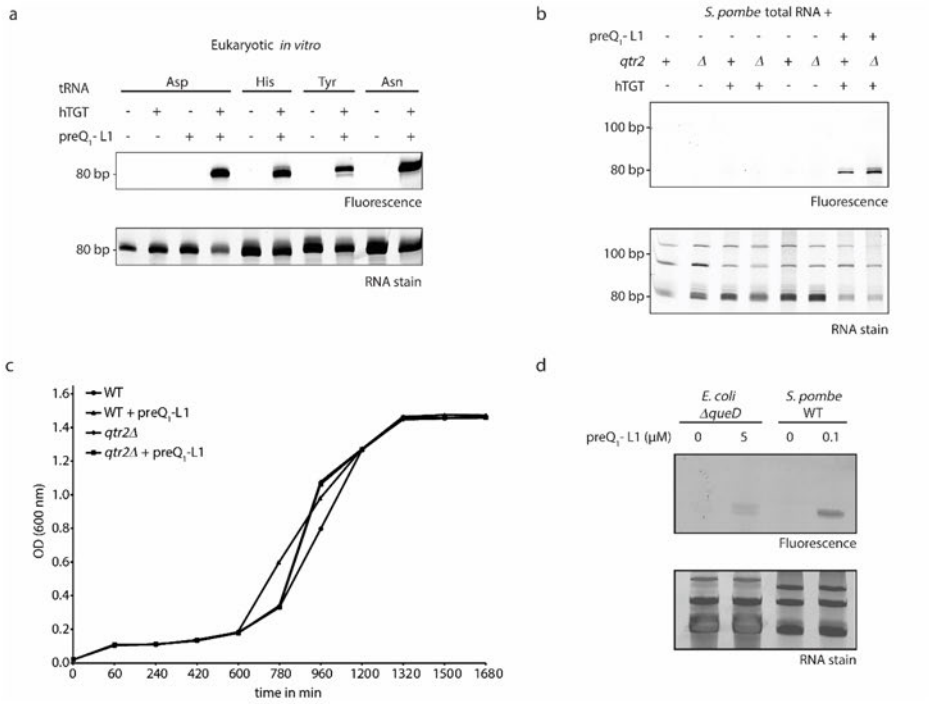

Supplementary Figure 4: Incorporation of preQ$_1$-L1 *in vitro* and *in vivo* in *S. pombe*. **a** Human tRNA guanine transglycosylase (hTGT) was incubated with respectively indicated *in vitro* transcribed *S. pombe* tRNA in presence of preQ$_1$-L1. After click reaction with AlexaFluor 594, the tRNAs were separated on a 10% polyacrylamide/ 8 M urea gel and visualized by scanning for fluorescence at 532 nm. Untreated tRNAs and tRNA^{Asp} incubated with hTGT or preQ$_1$-ligand L1, respectively, served as controls. A loading control was obtained by RNA staining with SybrGold. **b** Analysis of the total RNA click product after human tRNA guanine transglycosylase (hTGT)-catalysed incorporation of preQ$_1$-ligands L1 into RNA from *S. pombe* by denaturing PAGE and visualization by fluorescence scan for AlexaFluor 594 (excitation: 532 nm, emission: 610 nm). Total RNA was extracted from *S. pombe* WT cells containing functional TGT (+) and *qtr2Δ* cells that lack functional TGT (*Δ*), which were both cultured in the presence of queuine. The incubation of total RNA from WT and *qtr2Δ* cells without preQ$_1$-ligand or without hTGT, respectively, served as negative controls. A loading control was obtained by RNA staining with SybrGold. **c** Growth of *S. pombe* wild-type (WT) and *qtr2Δ* strains in the presence or absence of 0.1 µM preQ$_1$-L1. **d** Analysis of total tRNA from *E. coli ΔqueD* and *S. pombe* WT cells grown with the indicated concentrations of preQ$_1$-L1 after click reaction by denaturing PAGE and subsequent scanning for fluorescence of AlexaFluor 594. A loading control was obtained by RNA staining with GelRed.

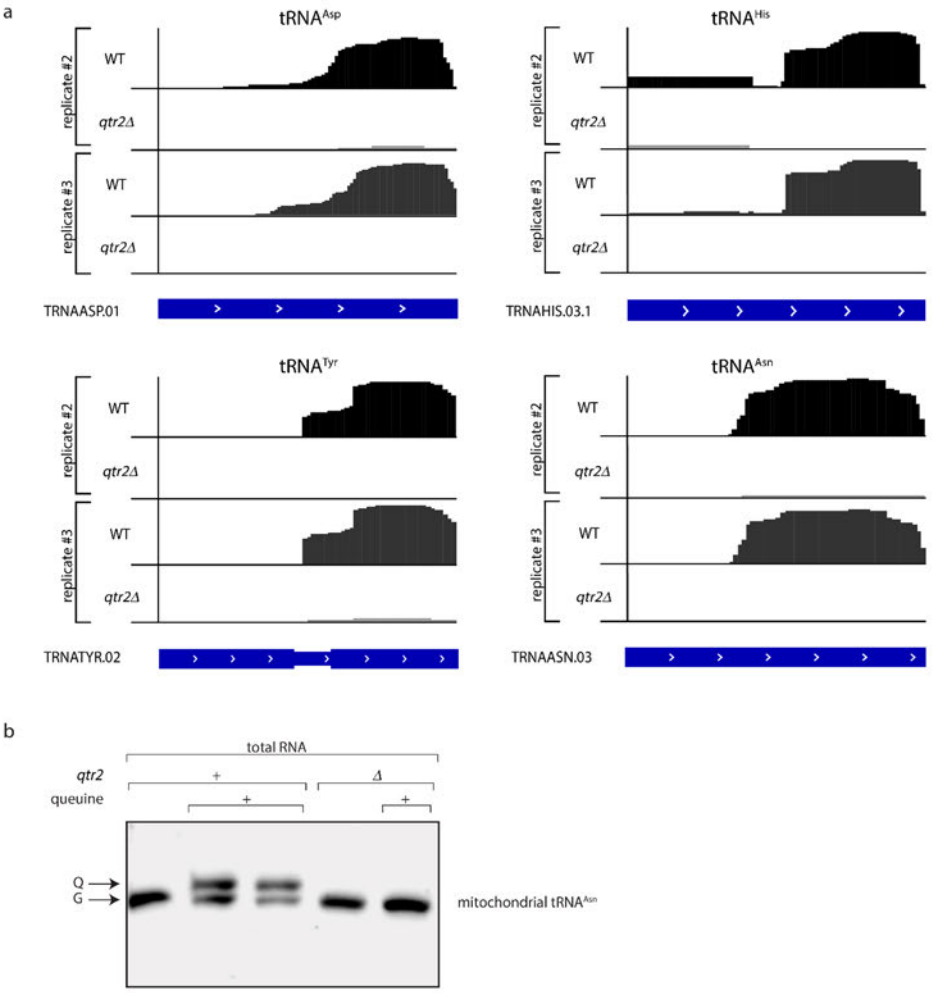

Supplementary Figure 5: *In vivo* detection of Q-modified tRNAs in *S. pombe* using metabolic labelling with preQ$_1$-L1 combined with high-throughput sequencing (Q-RIP-Seq). a Q-RIP-Seq of tRNA^{Asp}, tRNA^{His}, tRNA^{Tyr} and tRNA^{Asn} after metabolic labelling with preQ$_1$-L1 in *S. pombe* WT and *qtr2Δ* mutant cells and affinity purification. Coverage of the tRNA sequences from modified (WT, black) and unmodified (*qtr2Δ*, grey) samples is shown. The transcript architecture is shown below with thin and thick parts representing introns and mature tRNA sequences. Replicates #2 and #3 (c.f. Figure 5 for replicate #1) of three independent experiments are shown. Plots were generated using IGV. **b** Measurement of Q levels in mitochondrial tRNA^{Asn} using polyacrylamide gels covalently linked with N-acryloyl-3-aminophenylboronic acid (APB). Northern blotting with APB-gels was performed, and membranes were probed for mitochondrial tRNA^{Asn}. RNA samples from WT and *qtr2Δ* strains cultured with or without queuine are shown. The arrows indicate the migration distance of unmodified (G) and Q-modified (Q) tRNA, respectively.

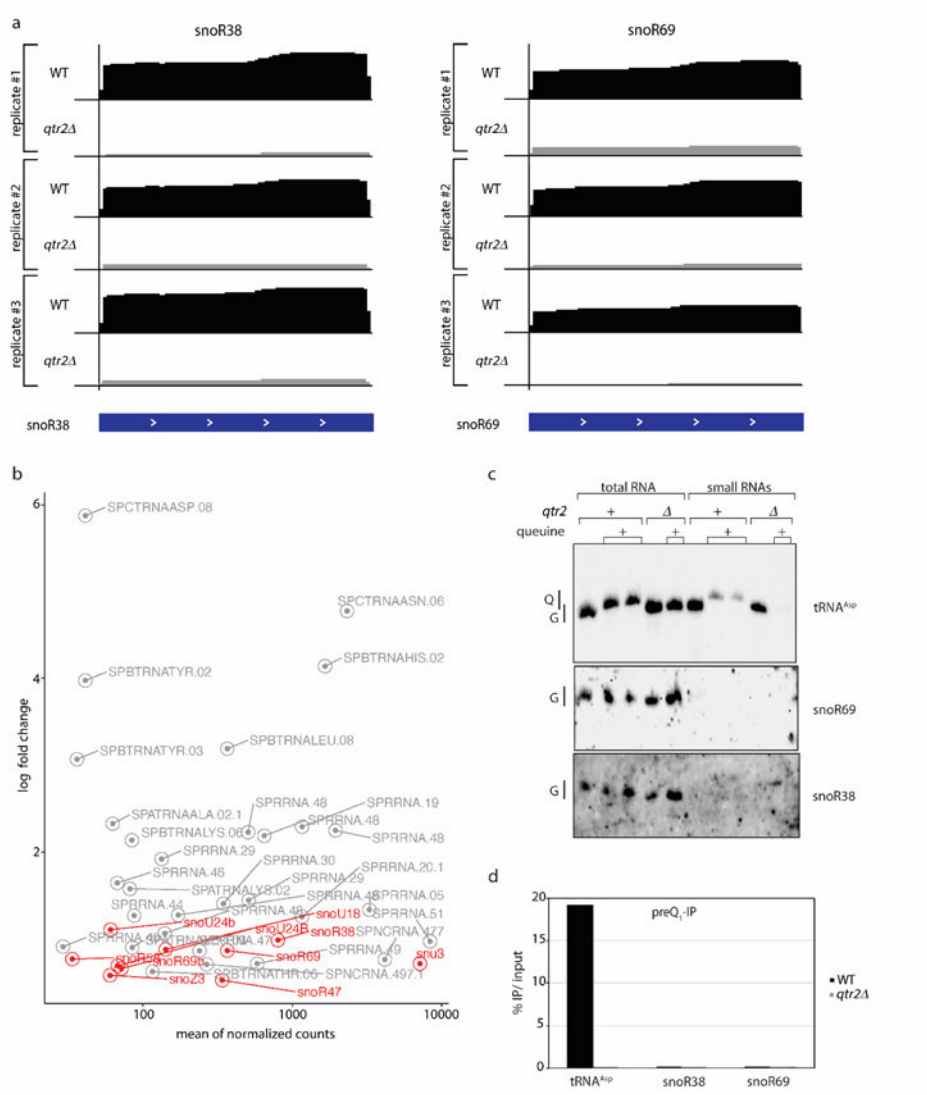

Supplementary Figure 6: Enrichment of snoRNA sequences of *S. pombe* in Q-RIP-Seq. RNAs that were metabolically labelled with azido-propyl-preQ$_1$ were bioconjugated with biotin-alkyne, enriched with streptavidin-coated magnetic beads and subjected to HTS as in Figure 5. **a** Coverage of the snoR38 and snoR69 sequences from WT ant *qtr2Δ S. pombe* RNAs are shown (three independent replicates). **b** Log2 fold change of normalized read counts of RNAs from WT compared to *qtr2Δ* determined by exomePeak2. Red: snoRNAs. **c** Measurement of Q levels in tRNA^{Asp}, snoR69 and snoR38 using polyacrylamide gels covalently linked with N-acryloyl-3-aminophenylboronic acid (APB). Northern blotting with APB-gels was performed, and membranes were probed with the indicated probes. RNA samples from WT and *qtr2Δ* strains cultured with or without queuine are shown. The label indicates the migration distance of unmodified (G) and Q-modified (Q) tRNA, respectively. **d** Measurement of

percentage of IP to input (%IP) for $tRNA^{Asp}$, snoR69 and snoR38 using qRT-PCR. RNAs from WT (black) and *qtr2Δ* (grey) were subjected to the Q-RIP method (IP) or only biotin-clicked (input).

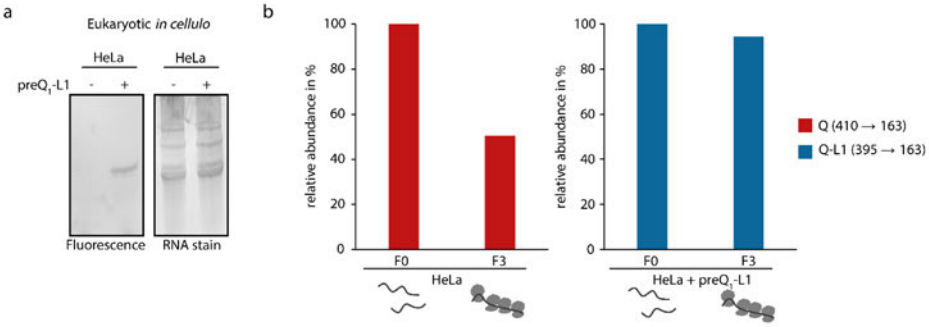

Supplementary Figure 7: *In cellulo* incorporation of $preQ_1$-L1 in HeLa cells and analysis of tRNA purified from HeLa cell polysome preparations. A single experiment is shown. **a** Analysis of total RNA from HeLa cells grown either in q-containing DMEM medium (-) or in q-free medium supplemented with 0.1 µM $preQ_1$-L1 (+) after click reaction by denaturing PAGE and subsequent scanning for fluorescence of AlexaFluor 594 (excitation: 532 nm, emission: 610 nm). b Relative quantification of Q (*m/z* 410 → 163, red) and Q-L1 (*m/z* 395 → 163, blue) in tRNA purified from fractions F0 and F3 of HeLa cells grown either in q-containing DMEM medium (HeLa) or in q-free medium supplemented with 0.1 µM $preQ_1$-L1 (HeLa + $preQ_1$-L1) via LC-MS/MS. Peak areas were normalized to the UV signal of adenosine and related to the respective F0 fraction.

Supplementary References

1. Müller, M., Hartmann, M., Schuster, I., Bender, S., Thüring, K.L., Helm, M., Katze, J.R., Nellen, W., Lyko, F. and Ehrenhofer-Murray, A.E. (2015) Dynamic modulation of Dnmt2-dependent tRNA methylation by the micronutrient queuine, *Nucleic acids research,* **43,** 10952–10962. First published on Sep 30, 2015.

2. Becker, M., Müller, S., Nellen, W., Jurkowski, T.P., Jeltsch, A. and Ehrenhofer-Murray, A.E. (2012) Pmt1, a Dnmt2 homolog in Schizosaccharomyces pombe, mediates tRNA methylation in response to nutrient signaling, *Nucleic acids research,* **40,** 11648–11658. First published on Oct 15, 2012.

3. Gerber, H.-D. and Klebe, G. (2012) Concise and efficient syntheses of preQ1 base, Q base, and (ent)-Q base, *Organic & biomolecular chemistry,* **10,** 8660–8668.

4. Johannsson, S., Neumann, P. and Ficner, R. (2018) Crystal Structure of the Human tRNA Guanine Transglycosylase Catalytic Subunit QTRT1, *Biomolecules,* **8.** First published on Aug 24, 2018.

5 Conclusion and Outlook

The first part of this work focused on the tRNA modification dihydrouridine, which is the result of an NADPH-dependent reduction of uridine. Based on this NADPH-dependency, the initial hypothesis was that cellular D levels might be dependent on the redox state of the cell. To test this, the effect of redox changes on the D modification level was analysed by manipulating the redox state through the addition of paraquat. This bipyridinium salt disrupts the cellular redox system, which is accompanied by an altered ratio of NAD(P)H to $NAD(P)^+$ and possibly an increased production of reactive oxygen species. The so-called redox cycle generates reactive oxygen species through oxygenation, which in turn oxidise the paraquat radical leading to its regeneration.[283–285] In line with this hypothesis, a significant reduction of D levels was observed under aerobic conditions as result of the paraquat treatment but this effect was not apparent under anaerobic conditions. Analysing single knockout strains, the Dus enzymes showed differential sensitivities towards paraquat, which was investigated by two complementary methods. While LC-MS/MS allowed a precise quantitative analysis of D levels, AlkAniline sequencing provided information on position-specific catalytic activities of the three Dus enzymes, thus allowing to match the D signals with their respective tRNA positions.

The impact of paraquat on D synthesis was most pronounced in tRNA isolated from the DusA knockout strain, where in turn DusB and DusC are the active enzymes, while strains having an active DusA were less affected. Analysing the positions modified by DusB and DusC more in detail, it was demonstrated that these two enzymes are also differentially affected with DusC being the most impaired by paraquat supplementation. *In vitro* kinetic studies with the three recombinant Dus enzymes showed an increase in enzyme activities from DusC over DusB to DusA, further substantiating the observed effects on dihydrouridylation *in vivo*. These differential activities might explain the differential sensitivities towards paraquat, whose addition leads to a reduction in NADPH availability in the cell, which is easily compensated by the active DusA enzyme with a high specificity for NADPH, whereas neither DusB nor DusC are able to overcome this.

The investigations were extended to polysome preparations, a method refined in this work to allow the analysis of tRNAs bound to polysomes and thus by definition actively involved in translation, and which has already provided insights into the role of other tRNA modifications during translation (not included in this thesis).[183,299] Here, the dihydrouridylation of tRNAs isolated from polysomes was compared with cytosolic tRNAs to examine the potential role of D during translation. Two interesting observations were made which provided first hints that D might be important for the binding of the initiator $tRNA^{fMet}$ and that DusC modified positions 17 might become increasingly important for tRNA binding to the ribosome in the absence of modifications at positions 20 and 20a. However, these hypotheses require further

investigation since no evidence for a specific role of D in the translational process was found, neither under untreated conditions nor under paraquat treatment.

To provide further evidence that the observed changes in dihydrouridylation *in vivo* can be directly attributed to changes in intracellular NADPH concentration, measurement of the cellular NADPH to NADP+ ratio upon PQ supplementation might be a useful tool in further studies. Furthermore, since a higher abundance of D has been reported in psychrophilic bacteria, suggesting an importance of D for correct tRNA folding at lower temperatures,[90] future studies growing the *E. coli* bacteria under these conditions might be interesting to further unravel the biological role of dihydrouridine.

The second part of this thesis focused on the queuosine modification, which has been successfully replaced by a derivative of the queuosine precursor $preQ_1$ in bacterial and eukaryotic tRNA *in vitro* and *in vivo.* The azide group present in the incorporated semi-synthetic analogue Q-L1 enabled copper click chemistry with fluorophores, facilitating the tracking of functionalised tRNAs. Additionally, the bio-conjugation of alkyne-biotin allowed for further purification using streptavidin beads, enabling the isolation of derivatised tRNAs. The four tRNAs that naturally carry the Q modification were functionalised, showing that the natural substrates of the TGT were retained, making this derivatisation to a minimally invasive tool for the integration of synthetic derivatives, as only the specific Q positions are exchanged.

Located in the tRNA anticodon loop, the queuosine modification was reported to affect the translational speed and the decoding fidelity.[123,124] The present work provided further evidence for a crucial role of Q during translation since *E. coli* polysome preparations showed higher Q abundance on tRNAs isolated from the polysomal fraction compared to the cytosolic tRNA pool. The semi-synthetic analogue effectively mimics certain biological roles of Q, in particular it was also present on tRNAs actively involved in translation. In contrast to natural Q, the synthetic analogue did not show an increased abundance compared to the cytosolic tRNA pool. However, the synthetic analogue is functionally integrated into the tRNA, and these tRNAs are not excluded from translation, albeit Q-L1 cannot completely fulfil the role of Q in translation. Additionally, the derivate was shown to stimulate the methylation of cytosine at position 38 in $tRNA^{Asp}$ as it was reported for the natural Q.[134,135] This demonstrates the functional integration of the semi-synthetic analogue into a tRNA modification circuit in which the presence of one modification influences the introduction of another.

This study not only examined the integration of the synthetic $preQ_1$-analogue, which has been extensively studied for other derivatives *in vitro* and *in cellulo*,[128–132] but also its physiological impact *in vivo*. These findings could serve as pioneering work for the adaptation of such derivatisation methods for medical applications. Q-dependent implications in diseases, including multiple sclerosis, schizophrenia and Parkinson's disease, have been described, but the underlying mechanism has not been identified yet, although Tuorto *et al.* were able to link

the Q modification to brain function in a mouse model.[127,128,300,301] Thus, the functional integration of Q-L1 *in cellulo* into polysome-bound tRNAs in HeLa cells revealed new opportunities for further research in this field, including experiments with normal and pathogenic cell lines, to further investigate the role of Q in diseases.

6 Material and Methods

This chapter describes the materials and methods for the experiments discussed in chapter 4.1. Materials and methods for chapter 4.2 are included in the material and methods section of the enclosed publication.

6.1 Material

6.1.1 Chemicals

acetic acid (LC-MS grade)	Honeywell (Charlotte, North Carolina, USA)
acetonitrile (LC-MS grade)	Honeywell (Charlotte, North Carolina, USA)
acidic phenol	Merck (Darmstadt, Germany)
acrylamide mix (19:1), Rotiphorese Gel 40%	Carl Roth (Karlsruhe, Germany)
ammonium acetate	Carl Roth (Karlsruhe, Germany)
ammonium acetate (LC-MS grade)	Merck (Darmstadt, Germany)
ammonium chloride	Merck (Darmstadt, Germany)
ammonium persulfate (APS)	Carl Roth (Karlsruhe, Germany)
bacteriological agar	Merck (Darmstadt, Germany)
chloramphenicol	Carl Roth (Karlsruhe, Germany)
chloroform (HPLC grade)	Merck (Darmstadt, Germany)
deoxycholate	Merck (Darmstadt, Germany)
dithiothreitol (DTT)	Thermo Fisher Scientific (Waltham, USA)
ethanol (99.9%)	Carl Roth (Karlsruhe, Germany)
GelRed (3x)	Biotium (Hayward, USA)
glycerol	Merck (Darmstadt, Germany)
glycogen (RNA grade)	Thermo Fisher Scientific (Waltham, USA)
HEPES (≥99.5%)	Carl Roth (Karlsruhe, Germany)
kanamycin	Carl Roth (Karlsruhe, Germany)
LB broth with agar (Lennox)	Merck (Darmstadt, Germany)
LB broth (Lennox)	Carl Roth (Karlsruhe, Germany)
magnesium chloride hexahydrate	Merck (Darmstadt, Germany)
2-mercaptoethanol	Merck (Darmstadt, Germany)
paraquat dichloride hydrate	Merck (Darmstadt, Germany)
pentostatine (≥95%)	Merck (Darmstadt, Germany)
2-propanol	Carl Roth (Karlsruhe, Germany)
sodium chloride (≥99%)	Carl Roth (Karlsruhe, Germany)
sucrose (D(+)-Saccharose)	Carl Roth (Karlsruhe, Germany)
TBE buffer (10x)	Merck (Darmstadt, Germany)
TEMED (≥99%)	Carl Roth (Karlsruhe, Germany)

TRI reagent	Merck (Darmstadt, Germany)
Tris-HCl	Carl Roth (Karlsruhe, Germany)

6.1.2 Solutions, buffers and culture media

Solutions, buffers and media were prepared with MilliQ water unless otherwise stated.

agar plates	20 g/L LB broth with agar (Lennox), 15 g/L bacteriological agar
APS solution	10% APS (w/v)
chloramphenicol solution	100 mg/mL chloramphenicol in ethanol
deoxycholate solution	0.1 g/mL deoxycholate
digestion buffer	25 mM ammonium acetate, pH 7.5
kanamycin solution	25 mg/mL kanamycin
kinetic buffer n.1	50 mM HEPES pH 7.5, 150 mM NaCl and 15% glycerol (v/v)
kinetic buffer n.2	100 mM Tris HCl (pH 8), 150 mM ammonium acetate, 2 mM dithiothreitol (DTT), 10 mM $MgCl_2$, and 250 µM FMN
LB medium	20 g/L LB broth (Lennox)
0.5x LB medium	10 g/L LB broth (Lennox)
LC-MS solvent A	5 mM ammonium acetate, pH 5.3-5.4 (adjusted with acetic acid), 1% acetonitrile (v/v)
lysozyme solution	50 mg/mL lysozyme
polysome buffer	100 mM NH_4Cl, 10 mM $MgCl_2$, 20 mM Tris, 14 µL 2-mercaptoethanol/100 mL buffer, pH 7.5
polysome lysis buffer	100 mM NH_4Cl, 10 mM $MgCl_2$, 20 mM Tris, pH 7.5
5% sucrose solution	5% sucrose (w/v) in polysome buffer
40% sucrose solution	40% sucrose (w/v) in polysome buffer
TBE buffer (10x)	1 M tris boric acid, 20 mM EDTA

6.1.3 Enzymes

benzonase nuclease (<250 U/µL)	Merck (Darmstadt, Germany)
FastAP thermosensitive alkaline phosphatase (1 U/µL)	Thermo Fisher Scientific (Waltham, USA)
lysozyme	Carl Roth (Karlsruhe, Germany)
NEBNext Small RNA Library Prep Set for Illumina	New England Biolabs (Ipswich, USA)
nuclease P1 from *Penicillium citrinum* (lyophilised)	Merck (Darmstadt, Germany)
snake venom phospodiesterase from *Crotalus adamanteus venom* (lyophilised)	Worthington Biochemical Corporation (Lakewood, USA)

6.1.4 Bacteria strains

The *E. coli* wildtype strain (Keio parent, BW25113) and the Dus single knockouts (*ΔdusA*, *ΔdusB* and *ΔdusC*) were purchased from the *E. coli* Keio knockout collection (GE Healthcare (Dharmacon™), England). The triple knockout strain (*ΔdusA,B,C*) was generated by the group of [redacted] as described in Faivre *et al*.[302] The knockout strains carry a kanamycin resistance, whereas the wildtype strain does not. To culture the knockouts, kanamycin was added to the culture medium to a final concentration of 25 µg/mL.

6.1.5 Disposables

eppendorf tubes (1.5 mL)	Carl Roth (Karlsruhe, Germany)
falcon tubes (15 mL, 50 mL)	Sarstedt (Nümbrecht, Germany)
filter top vacuum bottles, PES, 0.2 µm (250 mL, 500 mL)	Sarstedt (Nümbrecht, Germany)
inserts, conical, clear glass (0.1 mL)	neoLab (Heidelberg, Germany)
MicroSpin G-25 column	GE Healthcare (Chicago, USA)
Multiflex Round Tips	Sorenson Bioscience (Murray, USA)
Nanosep MF Centrifugal Devices (0.45 µM)	Pall (New York, USA)
needles	Braun (Melsungen, Germany)
parafilm	VWR (Darmstadt, Germany)
PCR softtubes	Biozym (Hessisch Oldendorf, Germany)
petri dishes	Sarstedt (Nümbrecht, Germany)
pipette tips (with filter, sterile, RNase/DNase-free)	Greiner Bio-One (Frickenhausen, Germany)
polyclear open-top centrifugation tubes (14 x 89 mm)	Seton (Milwaukee, USA)
polypropylene centrifugation tubes (50 mL)	Sarstedt (Nümbrecht, Germany)
reaction tubes with screw cap (1.5 mL)	Carl Roth (Karlsruhe, Germany)
screw-cap ND9 (septum red rubber/PTFFE beige)	neoLab (Heidelberg, Germany)
serological pipettes (2 mL, 5 mL, 10 mL, 25 mL, 50 mL)	Sarstedt (Nümbrecht, Germany)
semi-micro cuvette, PS, transparent (3 mL)	Sarstedt (Nümbrecht, Germany)
short thread vials ND9 (1.5 mL)	neoLab (Heidelberg, Germany)
syringes (1 mL, 2 mL, 20 mL)	Braun (Melsungen, Germany)

6.1.6 Instruments

Analytical balances:

Mettler Toledo PM460	Mettler Toledo (Gießen, Germany)
Sartorius cubis analytical balance	Sartorius (Göttingen, Germany)

Centrifuges:

Beckman Avanti J25	Beckman Coulter (Krefeld, Germany)
Beckman ultracentrifuge Optima LE-80K	Beckman Coulter (Krefeld, Germany)
Eppendorf centrifuge 5810R	Eppendorf (Hamburg, Germany)
Eppendorf centrifuge 5430R	Eppendorf (Hamburg, Germany)
Heraeus megafuge 8R	Thermo Fisher Scientific (Waltham, USA)
Sprout mini centrifuge	Biozym (Hessisch Oldendorf, Germany)
SW40 Ti rotor	Beckman Coulter (Krefeld, Germany)

Bacterial cultures:

Biochrom ultrospec cell density meter	Thermo Fisher Scientific (Waltham, USA)
Duran GLS 80 stirred bottle reactor	Fisher Scientific (Waltham, USA)
Heraeus BB15 incubator	Thermo Fisher Scientific (Waltham, USA)
IKA RTC classic magnetic stirrer	IKA (Staufen, Germany)
IKA ETS-5D electronic contact thermometer	IKA (Staufen, Germany)
InFors Ecotron	InFors HT (Basel, Switzerland)
oxygen electrode VISIFERM DO ARC 160 H0	Hamilton (Bonaduz, Switzerland)
pH electrode EASYFERM PLUS HB ARC 160	Hamilton (Bonaduz, Switzerland)

Polysome preparations:

Biocomp Gradient Station model 108	Biocomp (New Brunswick, USA)
Gilson Fraction Collector FC203B	Gilson (Middleton, USA)

Polyacrylamide gel electrophoresis:

electrophoresis power supply (EPS 3500XL)	GE Healthcare (Chicago, USA)
LSG-400-20 NA vertical chamber	C.B.S. Scientific (San Diego, USA)
power supply model 250/2.5	BioRad (Munich, Germany)
shaker (DOS-10L)	neoLab (Heidelberg, Germany)
Typhoon 9400	GE Healthcare (Chicago, USA)

High performance liquid chromatography and columns:

Agilent 1260 Infinity (II) LC	Agilent Technologies (Waldbronn, Germany)
Synergy Fusion RP18 column (4 µM particle size, 80 Å pore size, 250 × 2.0 mm)	Phenomenex (Aschaffenburg, Germany)

Mass spectrometry:

Agilent 6460A triple quadrupole ESI parameters: gas temperature 350 °C, gas flow 8 L/min, nebulizer pressure 50 psi, sheath gas temperature 350 °C, sheath gas flow 12 L/min, capillary voltage 3000 V and nozzle voltage 500 V	Agilent Technologies (Waldbronn, Germany)
Agilent 6470B triple quadrupole ESI parameters: gas temperature 300 °C, gas flow 7 L/min, nebulizer pressure 60 psi, sheath gas temperature 400 °C, sheath gas flow 12 L/min, capillary voltage 3000 V and nozzle voltage 0 V	Agilent Technologies (Waldbronn, Germany)
Genius XE-70 nitrogen generator	PEAK Scientific (Düren, Germany)

Next Generation sequencing:

NextSeq2000 with a 50-bp single-end read mode	Illumina (San Diego, USA)

Further lab equipment:

digital heatblock	VWR International (Radnor, USA)
MilliQ ultrapure water purification system	Millipore (Schwalbach, Germany)
NanoDrop ND-2000	PeqLab (Erlangen, Germany)
pH meter FiveEasy FE20	Mettler Toledo (Gießen, Germany)
pipette boy Integra	VWR (Darmstadt, Germany)
thermomixer comfort Eppendorf	Eppendorf (Hamburg, Germany)
variable micropipettes Discovery Comfort (2 µL, 10 µL, 20 µL, 100 µL, 200 µL, 1000 µL)	Abimed (Langenfeld, Germany)
vortex mixer 7-2020	neoLab (Heidelberg, Germany)

6.1.7 Software

Adobe Illustrator 2022	Adobe Inc. (San José, USA)
awk command	developed by Alfred Aho, Peter Weinberger und Brian Kernighan
ArcAir software version 3.6.0	Hamilton (Bonaduz, Switzerland)
Bowtie2 version 2.4.4	developed by Ben Langmead, Cole Trapnell, Mihai Pop und Steven L. Salzberg
Citavi 6	Swiss Academic Software (Wädenswil, Switzerland)
Irfan View	made by Irfan Skiljan
FlowCell version 1.97A	FlowMetric (Doylestown, USA)
MassHunter Qualitative Analysis version 10.0	Agilent Technologies (Waldbronn, Germany)
MassHunter Quantitative Analysis version 10.0	Agilent Technologies (Waldbronn, Germany)
Microsoft Office 365	Microsoft (Redmont, USA)
R-Studio 1.0.143 with R version 3.4.4	R-Studio Inc. (Boston, USA)
samtools mpileup command	developed by Heng Li und Bob Handsaker
Typhoon scanner software	GE Healthcare (Chicago, USA)
Trimmomatic-0.32	developed by Anthony M. Bolger, Marc Lohse und Bjoern Usadel

6.2 Methods

6.2.1 Cultivation of *E. coli* bacteria and paraquat treatment

In principle, bacterial cultivation was started by plating the *E. coli* strain of interest on an agar plate for overnight incubation at 37 °C. A single cell colony was used to inoculate the pre-culture, which was incubated overnight in a shaker incubator at 37 °C and 190 rpm.

The *E. coli* cultures described in sections 4.1.1 and 4.1.2 were grown conventionally in flasks in LB medium in a shaker incubator at 190 rpm and 37 °C. To treat the culture with paraquat, paraquat dichloride hydrate was either added at an optical density (OD_{600}) of 0.4 and the cultures were grown for a further 3 hours, or the addition was made directly at the beginning of the culture to study the bacterial growth behaviour after treatment (growth curves).

In sections 4.1.3 and 4.1.4, bacterial cultures were grown under defined aerobic or anaerobic conditions, which was enabled by using a Duran glass reactor in combination with a magnetic stirrer (300 rpm). A water bath was used to keep the temperature constant at 37 °C. 0.5x LB medium was used as the growth medium, paraquat was added at an optical density of 0.1 and

growth was continued until the bacteria reached an OD_{600} of 0.3 respectively 0.6 for the polysome preparations.

6.2.2 Extraction of total tRNA from *E. coli* cultures

After bacterial cultivation, the cells were harvested by centrifugation at 10 000 g for 10 min at 4 °C and the cell pellets were resuspended in TRI Reagent (2-5 mL, depending on the culture volume). Subsequently, total tRNA was isolated following the instructions of the manufacturer. Briefly, two chloroform extractions were performed, including centrifugation at 13 000 g and 4 °C for 15 min, with the aqueous phase transferred to a fresh tube each time. The RNA was then precipitated with isopropanol (centrifugation at 15 000 g, -4 °C, 45 min) and washed with 70% ethanol. The RNA pellets were dried and then dissolved in MilliQ water.

6.2.3 Polysome preparations

In the case of polysome preparations, 100 µg chloramphenicol per mL culture was added to culture before harvesting and followed by a 3-minute incubation. The cells were then harvested (10 000 g, 4 °C, 10 min) and the cell pellets were resuspended in polysome lysis buffer. 5 µg lysozyme per mL of culture medium was added and freeze-thaw cycles were performed in liquid nitrogen. 10% deoxycholate was then added to complete cell lysis. To homogenise the cell lysate, it was passed through a 0.5 mm diameter needle several times. To separate the remaining cell wall debris, the lysate was centrifuged (12 000 g, 4 °C, 10 min) and the supernatant was stored at -80 °C before being loaded onto a sucrose gradient ranging from 5% to 40%. The gradient was prepared in open-top centrifuge tubes (14 x 89 mm) using the gradient station with the following settings: time 1.24 min, angle 81.5°, speed 21 rpm. The gradients were placed in a SW40 Ti rotor and centrifuged for 2.5 h at 150 000 g and 4 °C. Subsequently, the gradients were fractionated by measuring the absorbance at 260 nm and four different fractions were collected: F0 (free RNA fraction), F1 (ribosomal subunits), F2 (monosome fraction) and F3 (polysome fraction). For isolation of total RNA, two times the fraction volume of TRI reagent was added to the collected fractions and extraction was performed as described above (6.2.2).

6.2.4 tRNA isolation from polysome preparations

To isolate only the tRNA from the total RNA obtained after phenol-chloroform extraction, the total RNA was separated on a 10% denaturing polyacrylamide gel by gel electrophoresis. The RNA was stained with GelRed and visualised at an excitation wavelength of 532 nm, followed by excision of the corresponding tRNA bands from the gel. The tRNA was then eluted in 0.5 M ammonium acetate overnight (25 °C, 750 rpm). The gel pieces were subsequently removed by

filtration through NanoSep filters and the tRNA was precipitated in cold ethanol (15 000 g, -4 °C, 45 min). The tRNA pellets were washed with 70% ethanol, dried and dissolved in MilliQ water.

6.2.5 Quantification of dihydrouridine levels by LC-MS/MS

The RNA samples were digested to nucleoside level prior to LC-MS analysis, using an enzyme mixture containing 0.6 U nuclease P1, 0.2 U snake venom phosphodiesterase, 2 U FastAP, 10 U benzonase and 200 ng pentostatin, and incubated overnight at 37 °C in ammonium acetate buffer (25 mM).

300 ng of total tRNA, or 100 ng isolated tRNA in the case of polysome preparations, was subjected to LC-MS analysis and separated by liquid chromatography on a reversed-phase HPLC column. Aqueous ammonium acetate buffer (5 mM, solvent A) and acetonitrile (solvent B) were used as solvents to form a gradient. At a flow rate of 0.35 mL/min, the gradient started with 100% solvent A, followed by a linear gradient to 8% solvent B after 10 min. The gradient was then increased to 40% solvent B after 20 minutes and then returned to the initial conditions for 3 min, which were held for a further 10 min. The UV signal at 254 nm was recorded by a diode array detector (DAD). Following the chromatographic separation, the tandem mass spectrometry of the experiment described in 4.1.2 was performed on an Agilent 6460 Triple Quadrupole mass spectrometer. Further analysis was performed on an Agilent 6470 system described in 6.1.6. The analysis was operated in positive ion mode The mass spectrometer was run in the dynamic multiple reaction monitoring (dMRM) mode in positive ion mode, in particular searching for the mass transition of dihydrouridine (*m/z* = 247 → 115). Relative quantification was performed as described by Thüring *et al*.[178] Briefly, the detected signal for the mass transition corresponding to dihydrouridine was normalised to the UV signal of adenosine and related to one sample of the measured sample set, mostly the untreated wildtype which was set to 100%.

6.2.6 Detection of dihydrouridine by AlkAniline sequencing

The analysis by AlkAniline sequencing was performed by [redacted].

About 100 ng of gel purified tRNAs were subjected to the analysis, which was described in Marchand *et al*.[218,220] Briefly, tRNA was fragmented by a mild alkaline hydrolysis for 5 min at 96 °C. The non-aromatic dihydrouridine ring is instable under these conditions and is cleaved. The generated fragments were end-repaired by extensive treatment with alkaline phosphatase to remove the pre-existing 5'-phosphates as well as the 3'-phosphates resulting from alkaline hydrolysis. The tRNA fragments were then treated with aniline, leading to a

deprotection of a 5'-phosphate at the N_{+1} nucleotide, which serves as competent 5'-phosphate for selective ligation of sequencing adapters. Libraries were prepared using the NEBNext® Small RNA Library Prep Set for Illumina® according to the manufacturer's recommendations. Subsequently, the libraries were qualified, quantified and multiplexed for high-throughput sequencing using a NextSeq2000 with a 50-bp single-end read mode.

Initial trimming of the adapter sequence was performed with Trimmomatic-0.32 using default parameters.[303] Alignment to the reference tRNA sequence was done by Bowtie2 (version 2.4.4) in End-to-End mode and with 'sensitive parameter' set. The mapped reads were counted and the positioning of their 5'-extremities were performed by using awk command.[304] Coverage for the reference sequence was calculated using the samtools mpileup command. 5'-end count was directly used for calculation of AAS scores. Stop-ratio (ratio of reads starting at a given position and total number of passing reads) for every position of the reference sequence was calculated using 5'-end count and coverage data. All other steps of analysis were performed in R-Studio 1.0.143 with R version 3.4.4.

6.2.7 *In vitro* kinetic activity assay

The *in vitro* kinetic assays described here, were performed by [redacted].

The NADPH oxidation by *E. coli* dihydrouridine synthases were determined under aerobic steady state conditions in kinetic buffer n.1 by using various concentrations of NADPH. The decrease in absorbance at 343 nm (ε_{343} = 6.21 $mM^{-1} \cdot cm^{-1}$) was used to monitor the amount of NADPH oxidised. The initial rate versus the NADPH concentration was analysed according to Michaelis-Menten formalism. To determine the dihydrouridylation of the *E. coli* dihydrouridine synthases, the enzymes (5 µM) were incubated for the following different times 0 min, 1 min, 5 min, 15 min, 20 min, and 1 hour at 37 °C with non-dihydrouridylated tRNA (20 µM) that was isolated from the triple knockout strain in 100 µL kinetic buffer n.2. The reaction was initiated by the addition of 2 mM NADPH, while the reaction was quenched by adding 100 µL of acidic phenol, followed by centrifugation at 16 000 g for 10 minutes. tRNAs in the aqueous phase were ethanol-precipitated and further purified using a MicroSpin G-25 column. The dihydrouridine levels were then determined by LC-MS/MS as described in 6.2.5.

Bibliography

1. Crick, F. Central dogma of molecular biology. *Nature* **227,** 561–563; 10.1038/227561a0 (1970).
2. Steitz, T. A. A structural understanding of the dynamic ribosome machine. *Nature Reviews Molecular Cell Biology* **9,** 242–253; 10.1038/nrm2352 (2008).
3. Brenner, S., Jacob, F. & Meselson, M. An unstable intermediate carrying information from genes to ribosomes for protein synthesis. *Nature* **190,** 576–581; 10.1038/190576a0 (1961).
4. Cobb, M. 60 years ago, Francis Crick changed the logic of biology. *Public Library of Science Biology* **15,** e2003243; 10.1371/journal.pbio.2003243 (2017).
5. Clancy, S. Chemical structure of RNA. *Nature Education* **7** (2008).
6. Watson, J. D. & Crick, F. H. Molecular structure of nucleic acids; a structure for deoxyribose nucleic acid. *Nature* **171,** 737–738; 10.1038/171737a0 (1953).
7. Hoogsteen, K. The crystal and molecular structure of a hydrogen-bonded complex between 1-methylthymine and 9-methyladenine. *Acta Crystallographica* **16,** 907–916; 10.1107/S0365110X63002437 (1963).
8. Zhou, H. *et al.* Characterizing Watson-Crick versus Hoogsteen Base Pairing in a DNA-Protein Complex Using Nuclear Magnetic Resonance and Site-Specifically 13C- and 15N-Labeled DNA. *Biochemistry* **58,** 1963–1974; 10.1021/acs.biochem.9b00027 (2019).
9. Rich, A. & Davies, D. R. A new two stranded helical structure: polyadenylic acid and polyuridylic acid. *Journal of the American Chemical Society* **78,** 3548–3549; 10.1021/ja01595a086 (1956).
10. Leontis, N. B. & Westhof, E. Geometric nomenclature and classification of RNA base pairs. *RNA (New York, N.Y.)* **7,** 499–512; 10.1017/s1355838201002515 (2001).
11. Boccaletto, P. *et al.* MODOMICS: a database of RNA modification pathways. 2021 update. *Nucleic Acids Research* **50,** D231-D235; 10.1093/nar/gkab1083 (2022).
12. Kierzek, E. & Kierzek, R. The thermodynamic stability of RNA duplexes and hairpins containing N6-alkyladenosines and 2-methylthio-N6-alkyladenosines. *Nucleic Acids Research* **31,** 4472–4480; 10.1093/nar/gkg633 (2003).
13. Roost, C. *et al.* Structure and thermodynamics of N6-methyladenosine in RNA: a spring-loaded base modification. *Journal of the American Chemical Society* **137,** 2107–2115; 10.1021/ja513080v (2015).
14. Wright, D. J., Rice, J. L., Yanker, D. M. & Znosko, B. M. Nearest neighbor parameters for inosine x uridine pairs in RNA duplexes. *Biochemistry* **46,** 4625–4634; 10.1021/bi0616910 (2007).
15. Helm, M. & Alfonzo, J. D. Posttranscriptional RNA Modifications: playing metabolic games in a cell's chemical Legoland. *Chemistry & Biology* **21,** 174–185; 10.1016/j.chembiol.2013.10.015 (2014).

16. Nossent, A. Y. The epitranscriptome: RNA modifications in vascular remodelling. *Atherosclerosis* **374,** 24–33; 10.1016/j.atherosclerosis.2022.11.004 (2023).

17. Arzumanian, V. A., Dolgalev, G. V., Kurbatov, I. Y., Kiseleva, O. I. & Poverennaya, E. V. Epitranscriptome: Review of Top 25 Most-Studied RNA Modifications. *International Journal of Molecular Sciences* **23**; 10.3390/ijms232213851 (2022).

18. Carell, T. *et al.* Structure and function of noncanonical nucleobases. *Angewandte Chemie (International ed. in English)* **51,** 7110–7131; 10.1002/anie.201201193 (2012).

19. Pan, T. Modifications and functional genomics of human transfer RNA. *Cell Research* **28,** 395–404; 10.1038/s41422-018-0013-y (2018).

20. Zhang, W., Foo, M., Eren, A. M. & Pan, T. tRNA modification dynamics from individual organisms to metaepitranscriptomics of microbiomes. *Molecular Cell* **82,** 891–906; 10.1016/j.molcel.2021.12.007 (2022).

21. Machnicka, M. A., Olchowik, A., Grosjean, H. & Bujnicki, J. M. Distribution and frequencies of post-transcriptional modifications in tRNAs. *RNA Biology* **11,** 1619–1629; 10.4161/15476286.2014.992273 (2014).

22. Delaunay, S., Helm, M. & Frye, M. RNA modifications in physiology and disease: towards clinical applications. *Nature Reviews Genetics* **25,** 104–122; 10.1038/s41576-023-00645-2 (2024).

23. Li, X., Peng, J. & Yi, C. The epitranscriptome of small non-coding RNAs. *Non-coding RNA Research* **6,** 167–173; 10.1016/j.ncrna.2021.10.002 (2021).

24. Czerwoniec, A. *et al.* MODOMICS: a database of RNA modification pathways. 2008 update. *Nucleic Acids Research* **37,** D118-21; 10.1093/nar/gkn710 (2009).

25. Charette, M. & Gray, M. W. Pseudouridine in RNA: what, where, how, and why. *International Union of Biochemistry and Molecular Biology Life* **49,** 341–351; 10.1080/152165400410182 (2000).

26. Berg, M. D. & Brandl, C. J. Transfer RNAs: diversity in form and function. *RNA Biology* **18,** 316–339; 10.1080/15476286.2020.1809197 (2021).

27. Pak, D., Root-Bernstein, R. & Burton, Z. F. tRNA structure and evolution and standardization to the three nucleotide genetic code. *Transcription* **8,** 205–219; 10.1080/21541264.2017.1318811 (2017).

28. Holley, R. W. *et al.* Structure of a ribonucleic acid. *Science (New York, N.Y.)* **147,** 1462–1465; 10.1126/science.147.3664.1462 (1965).

29. Nissen, P., Kjeldgaard, M., Thirup, S., Clark, B. F. & Nyborg, J. The ternary complex of aminoacylated tRNA and EF-Tu-GTP. Recognition of a bond and a fold. *Biochimie* **78,** 921–933; 10.1016/s0300-9084(97)86714-4 (1996).

30. Sprinzl, M., Horn, C., Brown, M., Ioudovitch, A. & Steinberg, S. Compilation of tRNA sequences and sequences of tRNA genes. *Nucleic Acids Research* **26,** 148–153; 10.1093/nar/26.1.148 (1998).

31. Suzuki, T. The expanding world of tRNA modifications and their disease relevance. *Nature Reviews Molecular Cell Biology* **22,** 375–392; 10.1038/s41580-021-00342-0 (2021).

32. Lorenz, C., Lünse, C. E. & Mörl, M. tRNA Modifications: Impact on Structure and Thermal Adaptation. *Biomolecules* **7**; 10.3390/biom7020035 (2017).

33. Crécy-Lagard, V. de *et al.* Survey and Validation of tRNA Modifications and Their Corresponding Genes in Bacillus subtilis sp Subtilis Strain 168. *Biomolecules* **10**; 10.3390/biom10070977 (2020).

34. Phizicky, E. M. & Alfonzo, J. D. Do all modifications benefit all tRNAs? *Federation of European Biochemical Societies Letters* **584,** 265–271; 10.1016/j.febslet.2009.11.049 (2010).

35. Crick, F. H. Codon—anticodon pairing: the wobble hypothesis. *Journal of Molecular Biology* **19,** 548–555; 10.1016/s0022-2836(66)80022-0 (1966).

36. Agris, P. F. *et al.* Celebrating wobble decoding: Half a century and still much is new. *RNA Biology* **15,** 537–553; 10.1080/15476286.2017.1356562 (2018).

37. Rogalski, M., Karcher, D. & Bock, R. Superwobbling facilitates translation with reduced tRNA sets. *Nature Structural & Molecular Biology* **15,** 192–198; 10.1038/nsmb.1370 (2008).

38. Suzuki, T., Nagao, A. & Suzuki, T. Human mitochondrial tRNAs: biogenesis, function, structural aspects, and diseases. *Annual Review of Genetics* **45,** 299–329; 10.1146/annurev-genet-110410-132531 (2011).

39. Zinshteyn, B. & Gilbert, W. V. Loss of a conserved tRNA anticodon modification perturbs cellular signaling. *Public Library of Science Genetics* **9,** e1003675; 10.1371/journal.pgen.1003675 (2013).

40. Nedialkova, D. D. & Leidel, S. A. Optimization of Codon Translation Rates via tRNA Modifications Maintains Proteome Integrity. *Cell* **161,** 1606–1618; 10.1016/j.cell.2015.05.022 (2015).

41. Liu, F. *et al.* ALKBH1-Mediated tRNA Demethylation Regulates Translation. *Cell* **167,** 816-828.e16; 10.1016/j.cell.2016.09.038 (2016).

42. Madore, E. *et al.* Effect of modified nucleotides on Escherichia coli tRNAGlu structure and on its aminoacylation by glutamyl-tRNA synthetase. Predominant and distinct roles of the mnm5 and s2 modifications of U34. *European Journal of Biochemistry* **266,** 1128–1135; 10.1046/j.1432-1327.1999.00965.x (1999).

43. Pütz, J., Florentz, C., Benseler, F. & Giegé, R. A single methyl group prevents the mischarging of a tRNA. *Nature Structural Biology* **1,** 580–582; 10.1038/nsb0994-580 (1994).

44. Sylvers, L. A., Rogers, K. C., Shimizu, M., Ohtsuka, E. & Söll, D. A 2-thiouridine derivative in tRNAGlu is a positive determinant for aminoacylation by Escherichia coli glutamyl-tRNA synthetase. *Biochemistry* **32,** 3836–3841; 10.1021/bi00066a002 (1993).

45. Giegé, R., Sissler, M. & Florentz, C. Universal rules and idiosyncratic features in tRNA identity. *Nucleic Acids Research* **26,** 5017–5035; 10.1093/nar/26.22.5017 (1998).

46. Björk, G. R., Wikström, P. M. & Byström, A. S. Prevention of translational frameshifting by the modified nucleoside 1-methylguanosine. *Science (New York, N.Y.)* **244,** 986–989; 10.1126/science.2471265 (1989).

47. Agris, P. F., Vendeix, F. A. P. & Graham, W. D. tRNA's wobble decoding of the genome: 40 years of modification. *Journal of Molecular Biology* **366,** 1–13; 10.1016/j.jmb.2006.11.046 (2007).

48. Motorin, Y. & Helm, M. tRNA stabilization by modified nucleotides. *Biochemistry* **49,** 4934–4944; 10.1021/bi100408z (2010).

49. Alexandrov, A. *et al.* Rapid tRNA decay can result from lack of nonessential modifications. *Molecular Cell* **21,** 87–96; 10.1016/j.molcel.2005.10.036 (2006).

50. Chernyakov, I., Whipple, J. M., Kotelawala, L., Grayhack, E. J. & Phizicky, E. M. Degradation of several hypomodified mature tRNA species in Saccharomyces cerevisiae is mediated by Met22 and the 5'-3' exonucleases Rat1 and Xrn1. *Genes & Development* **22,** 1369–1380; 10.1101/gad.1654308 (2008).

51. Asano, K. *et al.* Metabolic and chemical regulation of tRNA modification associated with taurine deficiency and human disease. *Nucleic Acids Research* **46,** 1565–1583; 10.1093/nar/gky068 (2018).

52. Kirino, Y., Goto, Y.-I., Campos, Y., Arenas, J. & Suzuki, T. Specific correlation between the wobble modification deficiency in mutant tRNAs and the clinical features of a human mitochondrial disease. *Proceedings of the National Academy of Sciences of the United States of America* **102,** 7127–7132; 10.1073/pnas.0500563102 (2005).

53. Rikimaru, M. *et al.* Taurine ameliorates impaired the mitochondrial function and prevents stroke-like episodes in patients with MELAS. *Internal Medicine (Tokyo, Japan)* **51,** 3351–3357; 10.2169/internalmedicine.51.7529 (2012).

54. Ohsawa, Y. *et al.* Taurine supplementation for prevention of stroke-like episodes in MELAS: a multicentre, open-label, 52-week phase III trial. *Journal of Neurology, Neurosurgery and Psychiatry* **90,** 529–536; 10.1136/jnnp-2018-317964 (2019).

55. Tomoda, E. *et al.* Restoration of mitochondrial function through activation of hypomodified tRNAs with pathogenic mutations associated with mitochondrial diseases. *Nucleic Acids Research* **51,** 7563–7579; 10.1093/nar/gkad139 (2023).

56. Huang, B., Johansson, M. J. O. & Byström, A. S. An early step in wobble uridine tRNA modification requires the Elongator complex. *RNA (New York, N.Y.)* **11,** 424–436; 10.1261/rna.7247705 (2005).

57. Simpson, C. L. *et al.* Variants of the elongator protein 3 (ELP3) gene are associated with motor neuron degeneration. *Human Molecular Genetics* **18,** 472–481; 10.1093/hmg/ddn375 (2009).

58. Cheng, W., Gao, A., Lin, H. & Zhang, W. Novel roles of METTL1/WDR4 in tumor via m7G methylation. *Molecular Therapy Oncology* **26,** 27–34; 10.1016/j.omto.2022.05.009 (2022).

59. Lin, S. *et al.* Mettl1/Wdr4-Mediated m7G tRNA Methylome Is Required for Normal mRNA Translation and Embryonic Stem Cell Self-Renewal and Differentiation. *Molecular Cell* **71,** 244-255.e5; 10.1016/j.molcel.2018.06.001 (2018).

60. Zhang, G. *et al.* NSUN2 stimulates tumor progression via enhancing TIAM2 mRNA stability in pancreatic cancer. *Cell Death Discovery* **9,** 219; 10.1038/s41420-023-01521-y (2023).

61. Abbasi-Moheb, L. *et al.* Mutations in NSUN2 cause autosomal-recessive intellectual disability. *American Journal of Human Genetics* **90,** 847–855; 10.1016/j.ajhg.2012.03.021 (2012).

62. Khan, M. A. *et al.* Mutation in NSUN2, which encodes an RNA methyltransferase, causes autosomal-recessive intellectual disability. *American Journal of Human Genetics* **90,** 856–863; 10.1016/j.ajhg.2012.03.023 (2012).

63. Blanco, S. *et al.* Aberrant methylation of tRNAs links cellular stress to neuro-developmental disorders. *The European Molecular Biology Organization Journal* **33,** 2020–2039; 10.15252/embj.201489282 (2014).

64. Kowalak, J. A., Bruenger, E. & McCloskey, J. A. Posttranscriptional modification of the central loop of domain V in Escherichia coli 23 S ribosomal RNA. *The Journal of Biological Chemistry* **270,** 17758–17764; 10.1074/jbc.270.30.17758 (1995).

65. O'Connor, M., Lee, W. M., Mankad, A., Squires, C. L. & Dahlberg, A. E. Mutagenesis of the peptidyltransferase center of 23S rRNA: the invariant U2449 is dispensable. *Nucleic Acids Research* **29,** 710–715; 10.1093/nar/29.3.710 (2001).

66. Draycott, A. S. *et al.* Transcriptome-wide mapping reveals a diverse dihydrouridine landscape including mRNA. *Public Library of Science Biology* **20,** e3001622; 10.1371/journal.pbio.3001622 (2022).

67. Finet, O. *et al.* Transcription-wide mapping of dihydrouridine reveals that mRNA dihydrouridylation is required for meiotic chromosome segregation. *Molecular Cell* **82,** 404-419.e9; 10.1016/j.molcel.2021.11.003 (2022).

68. Yamada, Y. & Ishikura, H. Nucleotide sequence of non-initiator methionine tRNA from Bacillus subtilis. *Nucleic Acids Research* **8,** 4517–4520; 10.1093/nar/8.19.4517 (1980).

69. Kirpekar, F. *et al.* Mapping of ribosomal 23S ribosomal RNA modifications in Clostridium sporogenes. *RNA Biology* **15,** 1060–1070; 10.1080/15476286.2018.1486662 (2018).

70. Bou-Nader, C. *et al.* Unveiling structural and functional divergences of bacterial tRNA dihydrouridine synthases: perspectives on the evolution scenario. *Nucleic Acids Research* **46,** 1386–1394; 10.1093/nar/gkx1294 (2018).

71. Byrne, R. T. *et al.* Major reorientation of tRNA substrates defines specificity of dihydrouridine synthases. *Proceedings of the National Academy of Sciences of the United States of America* **112,** 6033–6037; 10.1073/pnas.1500161112 (2015).

72. Bishop, A. C., Xu, J., Johnson, R. C., Schimmel, P. & Crécy-Lagard, V. de. Identification of the tRNA-dihydrouridine synthase family. *Journal of Biological Chemistry* **277,** 25090–25095; 10.1074/jbc.M203208200 (2002).

73. Xing, F., Hiley, S. L., Hughes, T. R. & Phizicky, E. M. The specificities of four yeast dihydrouridine synthases for cytoplasmic tRNAs. *The Journal of Biological Chemistry* **279,** 17850–17860; 10.1074/jbc.M401221200 (2004).

74. Xing, F., Martzen, M. R. & Phizicky, E. M. A conserved family of Saccharomyces cerevisiae synthases effects dihydrouridine modification of tRNA. *RNA (New York, N.Y.)* **8,** 370–381; 10.1017/s1355838202029825 (2002).

75. Rider, L. W., Ottosen, M. B., Gattis, S. G. & Palfey, B. A. Mechanism of dihydrouridine synthase 2 from yeast and the importance of modifications for efficient tRNA reduction. *The Journal of Biological Chemistry* **284,** 10324–10333; 10.1074/jbc.M806137200 (2009).

76. Yu, F. *et al.* Molecular basis of dihydrouridine formation on tRNA. *Proceedings of the National Academy of Sciences of the United States of America* **108,** 19593–19598; 10.1073/pnas.1112352108 (2011).

77. Savage, D. F., Crécy-Lagard, V. de & Bishop, A. C. Molecular determinants of dihydrouridine synthase activity. *Federation of European Biochemical Society Letters* **580,** 5198–5202; 10.1016/j.febslet.2006.08.062 (2006).

78. Bansal, A., Kaushik, S. & Kukreti, S. Non-canonical DNA structures: Diversity and disease association. *Frontiers in Genetics* **13,** 959258; 10.3389/fgene.2022.959258 (2022).

79. Rohrer, D. C. & Sundaralingam, M. Stereochemistry of nucleic acids and their constituents. VI. The crystal structure and conformation of dihydrouracil: a minor base of transfer-ribonucleic acid. *Acta Crystallographica. Section B: Structural Crystallography and Crystal Chemistry* **26,** 546–553; 10.1107/s0567740870002789 (1970).

80. Suck, D., Saenger, W. & Zechmeister, K. Conformation of the tRNA minor constituent dihydrouridine. *Federation of European Biochemical Society Letters* **12,** 257–259; 10.1016/0014-5793(71)80191-6 (1971).

81. Dyubankova, N. *et al.* Contribution of dihydrouridine in folding of the D-arm in tRNA. *Organic & Biomolecular Chemistry* **13,** 4960–4966; 10.1039/C5OB00164A (2015).

82. Chujo, T. & Tomizawa, K. Human transfer RNA modopathies: diseases caused by aberrations in transfer RNA modifications. *The Federation of European Biochemical Society Journal* **288,** 7096–7122; 10.1111/febs.15736 (2021).

83. Yokoyama, S., Watanabe, K. & Miyazawa, T. Dynamic structures and functions of transfer ribonucleic acids from extreme thermophiles. *Advances in Biophysics* **23,** 115–147 (1987).

84. Davis, D. R. Stabilization of RNA stacking by pseudouridine. *Nucleic Acids Research* **23,** 5020–5026; 10.1093/nar/23.24.5020 (1995).

85. Emerson, J. & Sundaralingam, M. Structure of the potassium salt of the modified nucleotide dihydrouridine 3’-monophosphate hemihydrate: correlation between the base pucker and sugar pucker and models for metal interactions with ribonucleic acid loops. *Acta Crystallographica. Section B: Structural Crystallography and Crystal Chemistry* **36,** 537–543; 10.1107/S0567740880003780 (1980).

86. Stuart, J. W. *et al.* Structure of the Trinucleotide D-acp 3 U-A with Coordinated Mg 2+ Demonstrates that Modified Nucleosides Contribute to Regional Conformations of RNA. *Nucleosides and Nucleotides* **15,** 1009–1028; 10.1080/07328319608002031 (1996).

87. Dalluge, J. J., Hashizume, T., Sopchik, A. E., McCloskey, J. A. & Davis, D. R. Conformational flexibility in RNA: the role of dihydrouridine. *Nucleic Acids Research* **24,** 1073–1079; 10.1093/nar/24.6.1073 (1996).

88. Kligun, E. & Mandel-Gutfreund, Y. The role of RNA conformation in RNA-protein recognition. *RNA Biology* **12,** 720–727; 10.1080/15476286.2015.1040977 (2015).

89. Nomura, Y., Ohno, S., Nishikawa, K. & Yokogawa, T. Correlation between the stability of tRNA tertiary structure and the catalytic efficiency of a tRNA-modifying enzyme, archaeal tRNA-guanine transglycosylase. *Genes to Cells* **21,** 41–52; 10.1111/gtc.12317 (2016).

90. Dalluge, J. J. *et al.* Posttranscriptional modification of tRNA in psychrophilic bacteria. *Journal of Bacteriology* **179,** 1918–1923; 10.1128/jb.179.6.1918-1923.1997 (1997).

91. Liang, W.-D. *et al.* Gene expression profiling of Clostridium botulinum under heat shock stress. *BioMed Research International* **2013,** 760904; 10.1155/2013/760904 (2013).

92. Sun, Q.-L. *et al.* High temperature-induced proteomic and metabolomic profiles of a thermophilic Bacillus manusensis isolated from the deep-sea hydrothermal field of Manus Basin. *Journal of Proteomics* **203,** 103380; 10.1016/j.jprot.2019.103380 (2019).

93. Wang, H. *et al.* Epitranscriptomic profile of Lactobacillus agilis and its adaptation to growth on inulin. *BMC Research Notes* **14,** 154; 10.1186/s13104-021-05563-2 (2021).

94. Finet, O., Yague-Sanz, C., Marchand, F. & Hermand, D. The Dihydrouridine landscape from tRNA to mRNA: a perspective on synthesis, structural impact and function. *RNA Biology* **19,** 735–750; 10.1080/15476286.2022.2078094 (2022).

95. Kuchino, Y. & Borek, E. Tumour-specific phenylalanine tRNA contains two supernumerary methylated bases. *Nature* **271,** 126–129; 10.1038/271126a0 (1978).

96. Borek, E. *et al.* High turnover rate of transfer RNA in tumor tissue. *Cancer Research* **37,** 3362–3366 (1977).

97. Sridharan, G., Ramani, P. & Patankar, S. Serum metabolomics in oral leukoplakia and oral squamous cell carcinoma. *Journal of Cancer Research and Therapeutics* **13,** 556–561; 10.4103/jcrt.JCRT_1233_16 (2017).

98. Licha, D. *et al.* Untargeted Metabolomics Reveals Molecular Effects of Ketogenic Diet on Healthy and Tumor Xenograft Mouse Models. *International Journal of Molecular Sciences* **20**; 10.3390/ijms20163873 (2019).

99. Kato, T. *et al.* A novel human tRNA-dihydrouridine synthase involved in pulmonary carcinogenesis. *Cancer Research* **65,** 5638–5646; 10.1158/0008-5472.CAN-05-0600 (2005).

100. Huang, J. *et al.* Prospective serum metabolomic profiling of lethal prostate cancer. *International Journal of Cancer* **145,** 3231–3243; 10.1002/ijc.32218 (2019).

101. Mittelstadt, M. *et al.* Interaction of human tRNA-dihydrouridine synthase-2 with interferon-induced protein kinase PKR. *Nucleic Acids Research* **36,** 998–1008; 10.1093/nar/gkm1129 (2008).

102. Dai, W. *et al.* Activity-based RNA-modifying enzyme probing reveals DUS3L-mediated dihydrouridylation. *Nature Chemical Biology* **17,** 1178–1187; 10.1038/s41589-021-00874-8 (2021).

103. Rottman, F. & Cerutti, P. Template activity of uridylic acid-dihydrouridylic acid copolymers. *Proceedings of the National Academy of Sciences of the United States of America* **55,** 960–966; 10.1073/pnas.55.4.960 (1966).

104. Smrt, J., Skoda, J., Lisý, V. & Sorm, F. Loss of coding properties of the trinucleotide guanylyl-uridylyl-uridine on replacement of uridylic by dihydrouridylic acid. *Biochimica et Biophysica Acta* **129,** 210–211; 10.1016/0005-2787(66)90025-6 (1966).

105. Lee, S., Brown, G. L. & Kosinski, Z. Loss of coding properties of the oligonucleotide adenylyluridylylguanosine after photoreduction or hydration. *The Biochemical Journal* **103,** 25C-27C; 10.1042/bj1030025c (1967).

106. Smrt, J., Kemper, W., Caskey, T. & Nirenberg, M. Template Activity of Modified Terminator Codons. *Journal of Biological Chemistry* **245,** 2753–2757; 10.1016/S0021-9258(18)63132-1 (1970).

107. Cochella, L. & Green, R. An active role for tRNA in decoding beyond codon:anticodon pairing. *Science (New York, N.Y.)* **308,** 1178–1180; 10.1126/science.1111408 (2005).

108. Harada, F. & Nishimura, S. Possible anticodon sequences of tRNA His, tRNA Asm, and tRNA Asp from Escherichia coli B. Universal presence of nucleoside Q in the first position of the anticondons of these transfer ribonucleic acids. *Biochemistry* **11,** 301–308; 10.1021/bi00752a024 (1972).

109. Kasai, H. *et al.* Structure of the modified nucleoside Q isolated from Escherichia coli transfer ribonucleic acid. 7-(4,5-cis-Dihydroxy-1-cyclopenten-3-ylaminomethyl)-7-deazaguanosine. *Biochemistry* **14,** 4198–4208; 10.1021/bi00690a008 (1975).

110. Fergus, C., Barnes, D., Alqasem, M. A. & Kelly, V. P. The queuine micronutrient: charting a course from microbe to man. *Nutrients* **7,** 2897–2929; 10.3390/nu7042897 (2015).

111. Phillips, G. *et al.* Biosynthesis of 7-deazaguanosine-modified tRNA nucleosides: a new role for GTP cyclohydrolase I. *Journal of Bacteriology* **190,** 7876–7884; 10.1128/JB.00874-08 (2008).

112. van Lanen, S. G. *et al.* From cyclohydrolase to oxidoreductase: discovery of nitrile reductase activity in a common fold. *Proceedings of the National Academy of Sciences of the United States of America* **102,** 4264–4269; 10.1073/pnas.0408056102 (2005).

113. Lee, B. W. K., van Lanen, S. G. & Iwata-Reuyl, D. Mechanistic studies of Bacillus subtilis QueF, the nitrile oxidoreductase involved in queuosine biosynthesis. *Biochemistry* **46,** 12844–12854; 10.1021/bi701265r (2007).

114. Slany, R. K., Bösl, M. & Kersten, H. Transfer and isomerization of the ribose moiety of AdoMet during the biosynthesis of queuosine tRNAs, a new unique reaction catalyzed by

the QueA protein from Escherichia coli. *Biochimie* **76,** 389–393; 10.1016/0300-9084(94)90113-9 (1994).

115. Miles, Z. D., McCarty, R. M., Molnar, G. & Bandarian, V. Discovery of epoxyqueuosine (oQ) reductase reveals parallels between halorespiration and tRNA modification. *Proceedings of the National Academy of Sciences of the United States of America* **108,** 7368–7372; 10.1073/pnas.1018636108 (2011).

116. Farkas, W. R., Jacobson, K. B. & Katze, J. R. Substrate and inhibitor specificity of tRNA-guanine ribosyltransferase. *Biochimica et Biophysica Acta* **781,** 64–75; 10.1016/0167-4781(84)90124-6 (1984).

117. Boland, C., Hayes, P., Santa-Maria, I., Nishimura, S. & Kelly, V. P. Queuosine formation in eukaryotic tRNA occurs via a mitochondria-localized heteromeric transglycosylase. *The Journal of Biological Chemistry* **284,** 18218–18227; 10.1074/jbc.M109.002477 (2009).

118. Chen, Y.-C., Kelly, V. P., Stachura, S. V. & Garcia, G. A. Characterization of the human tRNA-guanine transglycosylase: confirmation of the heterodimeric subunit structure. *RNA (New York, N.Y.)* **16,** 958–968; 10.1261/rna.1997610 (2010).

119. Johannsson, S., Neumann, P. & Ficner, R. Crystal Structure of the Human tRNA Guanine Transglycosylase Catalytic Subunit QTRT1. *Biomolecules* **8**; 10.3390/biom8030081 (2018).

120. Yuan, Y. *et al.* Discovery of novel bacterial queuine salvage enzymes and pathways in human pathogens. *Proceedings of the National Academy of Sciences of the United States of America* **116,** 19126–19135; 10.1073/pnas.1909604116 (2019).

121. Morris, R. C., Brown, K. G. & Elliott, M. S. The effect of queuosine on tRNA structure and function. *Journal of Biomolecular Structure & Dynamics* **16,** 757–774; 10.1080/07391102.1999.10508291 (1999).

122. Grosjean, H. & Westhof, E. An integrated, structure- and energy-based view of the genetic code. *Nucleic Acids Research* **44,** 8020–8040; 10.1093/nar/gkw608 (2016).

123. Müller, M. *et al.* Queuine links translational control in eukaryotes to a micronutrient from bacteria. *Nucleic Acids Research* **47,** 3711–3727; 10.1093/nar/gkz063 (2019).

124. Tuorto, F. *et al.* Queuosine-modified tRNAs confer nutritional control of protein translation. *The European Molecular Biology Organization Journal* **37**; 10.15252/embj.201899777 (2018).

125. Dowling, D. P. *et al.* Molecular basis of cobalamin-dependent RNA modification. *Nucleic Acids Research* **44,** 9965–9976; 10.1093/nar/gkw806 (2016).

126. Cirzi, C. *et al.* Queuosine-tRNA promotes sex-dependent learning and memory formation by maintaining codon-biased translation elongation speed. *The European Molecular Biology Organization Journal,* e112507; 10.15252/embj.2022112507 (2023).

127. Richard, P. *et al.* Queuine, a bacterial-derived hypermodified nucleobase, shows protection in in vitro models of neurodegeneration. *Public Library of Science One* **16,** e0253216; 10.1371/journal.pone.0253216 (2021).

128. Varghese, S. *et al.* In vivo modification of tRNA with an artificial nucleobase leads to full disease remission in an animal model of multiple sclerosis. *Nucleic Acids Research* **45,** 2029–2039; 10.1093/nar/gkw847 (2017).

129. Fergus, C. *et al.* The human tRNA-guanine transglycosylase displays promiscuous nucleobase preference but strict tRNA specificity. *Nucleic Acids Research* **49,** 4877–4890; 10.1093/nar/gkab289 (2021).

130. Alexander, S. C., Busby, K. N., Cole, C. M., Zhou, C. Y. & Devaraj, N. K. Site-Specific Covalent Labeling of RNA by Enzymatic Transglycosylation. *Journal of the American Chemical Society* **137,** 12756–12759; 10.1021/jacs.5b07286 (2015).

131. Zhang, D., Zhou, C. Y., Busby, K. N., Alexander, S. C. & Devaraj, N. K. Light-Activated Control of Translation by Enzymatic Covalent mRNA Labeling. *Angewandte Chemie (International ed. in English)* **57,** 2822–2826; 10.1002/anie.201710917 (2018).

132. Ehret, F., Zhou, C. Y., Alexander, S. C., Zhang, D. & Devaraj, N. K. Site-Specific Covalent Conjugation of Modified mRNA by tRNA Guanine Transglycosylase. *Molecular Pharmaceutics* **15,** 737–742; 10.1021/acs.molpharmaceut.7b00356 (2018).

133. Zhang, D. *et al.* Site-Specific and Enzymatic Cross-Linking of sgRNA Enables Wavelength-Selectable Photoactivated Control of CRISPR Gene Editing. *Journal of the American Chemical Society* **144,** 4487–4495; 10.1021/jacs.1c12166 (2022).

134. Müller, M. *et al.* Dynamic modulation of Dnmt2-dependent tRNA methylation by the micronutrient queuine. *Nucleic Acids Research* **43,** 10952–10962; 10.1093/nar/gkv980 (2015).

135. Ehrenhofer-Murray, A. E. Cross-Talk between Dnmt2-Dependent tRNA Methylation and Queuosine Modification. *Biomolecules* **7**; 10.3390/biom7010014 (2017).

136. Johannsson, S. *et al.* Structural insights into the stimulation of S. pombe Dnmt2 catalytic efficiency by the tRNA nucleoside queuosine. *Scientific Reports* **8,** 8880; 10.1038/s41598-018-27118-5 (2018).

137. Mignone, F., Gissi, C., Liuni, S. & Pesole, G. Untranslated regions of mRNAs. *Genome Biology* **3,** reviews0004; 10.1186/gb-2002-3-3-reviews0004 (2002).

138. Daffis, S. *et al.* 2'-O methylation of the viral mRNA cap evades host restriction by IFIT family members. *Nature* **468,** 452–456; 10.1038/nature09489 (2010).

139. Züst, R. *et al.* Ribose 2'-O-methylation provides a molecular signature for the distinction of self and non-self mRNA dependent on the RNA sensor Mda5. *Nature Immunology* **12,** 137–143; 10.1038/ni.1979 (2011).

140. Galloway, A. & Cowling, V. H. mRNA cap regulation in mammalian cell function and fate. *Biochimica et Biophysica Acta. Gene Regulatory Mechanisms* **1862,** 270–279; 10.1016/j.bbagrm.2018.09.011 (2019).

141. Despic, V. & Jaffrey, S. R. mRNA ageing shapes the Cap2 methylome in mammalian mRNA. *Nature* **614,** 358–366; 10.1038/s41586-022-05668-z (2023).

142. Doamekpor, S. K., Sharma, S., Kiledjian, M. & Tong, L. Recent insights into noncanonical 5’ capping and decapping of RNA. *The Journal of Biological Chemistry* **298,** 102171; 10.1016/j.jbc.2022.102171 (2022).

143. Wolfram-Schauerte, M. *et al.* T4 phage RNA is NAD-capped and alters the NAD-cap epitranscriptome of Escherichia coli during infection through a phage-encoded decapping enzyme. *bioRxiv* 2024.04.04.588121; 10.1101/2024.04.04.588121 (2024), preprint: not peer reviewed.

144. Hubacek, J. A., Pitha, J., Adamkova, V., Lanska, V. & Poledne, R. A common variant in the FTO gene is associated with body mass index in males and postmenopausal females but not in premenopausal females. Czech post-MONICA and 3PMFs studies. *Clinical Chemistry and Laboratory Medicine* **47,** 387–390; 10.1515/CCLM.2009.109 (2009).

145. Dina, C. *et al.* Variation in FTO contributes to childhood obesity and severe adult obesity. *Nature Genetics* **39,** 724–726; 10.1038/ng2048 (2007).

146. Wells, S. E., Hillner, P. E., Vale, R. D. & Sachs, A. B. Circularization of mRNA by eukaryotic translation initiation factors. *Molecular Cell* **2,** 135–140; 10.1016/s1097-2765(00)80122-7 (1998).

147. Schütz, P. *et al.* Crystal structure of the yeast eIF4A-eIF4G complex: an RNA-helicase controlled by protein-protein interactions. *Proceedings of the National Academy of Sciences of the United States of America* **105,** 9564–9569; 10.1073/pnas.0800418105 (2008).

148. Boulias, K. & Greer, E. L. Biological roles of adenine methylation in RNA. *Nature Reviews Genetics* **24,** 143–160; 10.1038/s41576-022-00534-0 (2023).

149. Esteve-Puig, R. *et al.* Epigenetic loss of m1A RNA demethylase ALKBH3 in Hodgkin lymphoma targets collagen, conferring poor clinical outcome. *Blood* **137,** 994–999; 10.1182/blood.2020005823 (2021).

150. Chen, X. *et al.* 5-methylcytosine promotes pathogenesis of bladder cancer through stabilizing mRNAs. *Nature Cell Biology* **21,** 978–990; 10.1038/s41556-019-0361-y (2019).

151. Echaide, M. *et al.* mRNA Vaccines against SARS-CoV-2: Advantages and Caveats. *International Journal of Molecular Sciences* **24**; 10.3390/ijms24065944 (2023).

152. Janowski, M. & Andrzejewska, A. The legacy of mRNA engineering: A lineup of pioneers for the Nobel Prize. *Molecular Therapy Nucleic Acids* **29,** 272–284; 10.1016/j.omtn.2022.07.003 (2022).

153. Miao, L., Zhang, Y. & Huang, L. mRNA vaccine for cancer immunotherapy. *Molecular Cancer* **20,** 41; 10.1186/s12943-021-01335-5 (2021).

154. Pardi, N., Hogan, M. J., Porter, F. W. & Weissman, D. mRNA vaccines - a new era in vaccinology. *Nature Reviews Drug Discovery* **17,** 261–279; 10.1038/nrd.2017.243 (2018).

155. Sahin, U. *et al.* Personalized RNA mutanome vaccines mobilize poly-specific therapeutic immunity against cancer. *Nature* **547,** 222–226; 10.1038/nature23003 (2017).

156. Sharma, S. & Lafontaine, D. L. J. 'View From A Bridge': A New Perspective on Eukaryotic rRNA Base Modification. *Trends in Biochemical Sciences* **40,** 560–575; 10.1016/j.tibs.2015.07.008 (2015).

157. Birkedal, U. *et al.* Profiling of ribose methylations in RNA by high-throughput sequencing. *Angewandte Chemie (International ed. in English)* **54,** 451–455; 10.1002/anie.201408362 (2015).

158. Kiss, T. Small nucleolar RNAs: an abundant group of noncoding RNAs with diverse cellular functions. *Cell* **109,** 145–148; 10.1016/S0092-8674(02)00718-3 (2002).

159. Sloan, K. E. *et al.* Tuning the ribosome: The influence of rRNA modification on eukaryotic ribosome biogenesis and function. *RNA Biology* **14,** 1138–1152; 10.1080/15476286.2016.1259781 (2017).

160. Cech, T. R. Structural biology. The ribosome is a ribozyme. *Science (New York, N.Y.)* **289,** 878–879; 10.1126/science.289.5481.878 (2000).

161. Lafontaine, D. L. & Tollervey, D. The function and synthesis of ribosomes. *Nature Reviews Molecular Cell Biology* **2,** 514–520; 10.1038/35080045 (2001).

162. Baudin-Baillieu, A. *et al.* Nucleotide modifications in three functionally important regions of the Saccharomyces cerevisiae ribosome affect translation accuracy. *Nucleic Acids Research* **37,** 7665–7677; 10.1093/nar/gkp816 (2009).

163. King, T. H., Liu, B., McCully, R. R. & Fournier, M. J. Ribosome structure and activity are altered in cells lacking snoRNPs that form pseudouridines in the peptidyl transferase center. *Molecular Cell* **11,** 425–435; 10.1016/s1097-2765(03)00040-6 (2003).

164. Liang, X.-H., Liu, Q. & Fournier, M. J. Loss of rRNA modifications in the decoding center of the ribosome impairs translation and strongly delays pre-rRNA processing. *RNA (New York, N.Y.)* **15,** 1716–1728; 10.1261/rna.1724409 (2009).

165. Gigova, A., Duggimpudi, S., Pollex, T., Schaefer, M. & Koš, M. A cluster of methylations in the domain IV of 25S rRNA is required for ribosome stability. *RNA (New York, N.Y.)* **20,** 1632–1644; 10.1261/rna.043398.113 (2014).

166. Polikanov, Y. S., Melnikov, S. V., Söll, D. & Steitz, T. A. Structural insights into the role of rRNA modifications in protein synthesis and ribosome assembly. *Nature Structural & Molecular Biology* **22,** 342–344; 10.1038/nsmb.2992 (2015).

167. Thüring, K., Schmid, K., Keller, P. & Helm, M. LC-MS Analysis of Methylated RNA. *Methods in Molecular Biology (Clifton, N.J.)* **1562,** 3–18; 10.1007/978-1-4939-6807-7_1 (2017).

168. Wiener, D. & Schwartz, S. The epitranscriptome beyond m6A. *Nature Reviews Genetics* **22,** 119–131; 10.1038/s41576-020-00295-8 (2021).

169. Wetzel, C. & Limbach, P. A. Mass spectrometry of modified RNAs: recent developments. *The Analyst* **141,** 16–23; 10.1039/c5an01797a (2016).

170. Ammann, G., Berg, M., Dalwigk, J. F. & Kaiser, S. M. Pitfalls in RNA Modification Quantification Using Nucleoside Mass Spectrometry. *Accounts of Chemical Research* **56,** 3121–3131; 10.1021/acs.accounts.3c00402 (2023).

171. Cai, W. M. *et al.* A Platform for Discovery and Quantification of Modified Ribonucleosides in RNA: Application to Stress-Induced Reprogramming of tRNA Modifications. *Methods in Enzymology* **560,** 29–71; 10.1016/bs.mie.2015.03.004 (2015).

172. Bessler, L. *et al.* Esterification of Cyclic N6-threonylcarbamoyladenosine during RNA Sample Preparation. *ChemMedChem,* e202400115; 10.1002/cmdc.202400115 (2024).

173. Pomerantz, S. C. & McCloskey, J. A. Analysis of RNA hydrolyzates by liquid chromatography-mass spectrometry. *Methods in Enzymology* **193,** 796–824; 10.1016/0076-6879(90)93452-q (1990).

174. Gehrke, C. W. & Kuo, K. C. Ribonucleoside analysis by reversed-phase high-performance liquid chromatography. *Journal of Chromatography* **471,** 3–36; 10.1016/s0021-9673(00)94152-9 (1989).

175. Crain, P. F. Preparation and enzymatic hydrolysis of DNA and RNA for mass spectrometry. *Methods in Enzymology* **193,** 782–790; 10.1016/0076-6879(90)93450-y (1990).

176. Gehrke, C. W., Kuo, K. C., McCune, R. A., Gerhardt, K. O. & Agris, P. F. Quantitative enzymatic hydrolysis of tRNAs: reversed-phase high-performance liquid chromatography of tRNA nucleosides. *Journal of Chromatography* **230,** 297–308 (1982).

177. Kellner, S., Burhenne, J. & Helm, M. Detection of RNA modifications. *RNA Biology* **7,** 237–247; 10.4161/rna.7.2.11468 (2010).

178. Thüring, K., Schmid, K., Keller, P. & Helm, M. Analysis of RNA modifications by liquid chromatography-tandem mass spectrometry. *Methods (San Diego, Calif.)* **107,** 48–56; 10.1016/j.ymeth.2016.03.019 (2016).

179. Su, D. *et al.* Quantitative analysis of ribonucleoside modifications in tRNA by HPLC-coupled mass spectrometry. *Nature Protocols* **9,** 828–841; 10.1038/nprot.2014.047 (2014).

180. Yoluç, Y. *et al.* Instrumental analysis of RNA modifications. *Critical Reviews in Biochemistry and Molecular Biology* **56,** 178–204; 10.1080/10409238.2021.1887807 (2021).

181. Kellner, S. *et al.* Profiling of RNA modifications by multiplexed stable isotope labelling. *Chemical Communications (Cambridge, England)* **50,** 3516–3518; 10.1039/c3cc49114e (2014).

182. Dal Magro, C. *et al.* A Vastly Increased Chemical Variety of RNA Modifications Containing a Thioacetal Structure. *Angewandte Chemie (International ed. in English)* **57,** 7893–7897; 10.1002/anie.201713188 (2018).

183. Bessler, L. *et al.* A New Bacterial Adenosine-Derived Nucleoside as an Example of RNA Modification Damage. *Angewandte Chemie (International ed. in English)* **62,** e202217128; 10.1002/anie.202217128 (2023).

184. Bessler, L., Groß, J., Kampf, C. J., Opatz, T. & Helm, M. Reversible oxidative dimerization of 4-thiouridines in tRNA isolates. *Royal Society of Chemistry Chemical Biology* **5,** 216–224; 10.1039/D3CB00221G (2024).

185. Ohira, T. *et al.* Reversible RNA phosphorylation stabilizes tRNA for cellular thermotolerance. *Nature* **605,** 372–379; 10.1038/s41586-022-04677-2 (2022).

186. Kellner, S. *et al.* Absolute and relative quantification of RNA modifications via biosynthetic isotopomers. *Nucleic Acids Research* **42,** e142; 10.1093/nar/gku733 (2014).

187. Brandmayr, C. *et al.* Isotope-based analysis of modified tRNA nucleosides correlates modification density with translational efficiency. *Angewandte Chemie (International ed. in English)* **51,** 11162–11165; 10.1002/anie.201203769 (2012).

188. Borland, K. *et al.* Production and Application of Stable Isotope-Labeled Internal Standards for RNA Modification Analysis. *Genes* **10**; 10.3390/genes10010026 (2019).

189. Globisch, D. *et al.* Systems-based analysis of modified tRNA bases. *Angewandte Chemie (International ed. in English)* **50,** 9739–9742; 10.1002/anie.201103229 (2011).

190. Heiss, M., Borland, K., Yoluç, Y. & Kellner, S. Quantification of Modified Nucleosides in the Context of NAIL-MS. *Methods in Molecular Biology (Clifton, N.J.)* **2298,** 279–306; 10.1007/978-1-0716-1374-0_18 (2021).

191. Heiss, M., Reichle, V. F. & Kellner, S. Observing the fate of tRNA and its modifications by nucleic acid isotope labeling mass spectrometry: NAIL-MS. *RNA Biology* **14,** 1260–1268; 10.1080/15476286.2017.1325063 (2017).

192. Heiss, M., Hagelskamp, F., Marchand, V., Motorin, Y. & Kellner, S. Cell culture NAIL-MS allows insight into human tRNA and rRNA modification dynamics in vivo. *Nature Communications* **12,** 389; 10.1038/s41467-020-20576-4 (2021).

193. Reichle, V. F., Petrov, D. P., Weber, V., Jung, K. & Kellner, S. NAIL-MS reveals the repair of 2-methylthiocytidine by AlkB in E. coli. *Nature Communications* **10,** 5600; 10.1038/s41467-019-13565-9 (2019).

194. Motorin, Y. & Helm, M. General Principles and Limitations for Detection of RNA Modifications by Sequencing. *Accounts of Chemical Research* **57,** 275–288; 10.1021/acs.accounts.3c00529 (2024).

195. Cozen, A. E. *et al.* ARM-seq: AlkB-facilitated RNA methylation sequencing reveals a complex landscape of modified tRNA fragments. *Nature Methods* **12,** 879–884; 10.1038/nmeth.3508 (2015).

196. Zheng, G. *et al.* Efficient and quantitative high-throughput tRNA sequencing. *Nature Methods* **12,** 835–837; 10.1038/nmeth.3478 (2015).

197. Liu, H. *et al.* Accurate detection of m6A RNA modifications in native RNA sequences. *Nature Communications* **10,** 4079; 10.1038/s41467-019-11713-9 (2019).

198. Begik, O. *et al.* Quantitative profiling of pseudouridylation dynamics in native RNAs with nanopore sequencing. *Nature Biotechnology* **39,** 1278–1291; 10.1038/s41587-021-00915-6 (2021).

199. Jain, M., Olsen, H. E., Akeson, M. & Abu-Shumays, R. Adaptation of Human Ribosomal RNA for Nanopore Sequencing of Canonical and Modified Nucleotides. *Methods in Molecular Biology (Clifton, N.J.)* **2298,** 53–74; 10.1007/978-1-0716-1374-0_4 (2021).

200. Leger, A. *et al.* RNA modifications detection by comparative Nanopore direct RNA sequencing. *Nature Communications* **12,** 7198; 10.1038/s41467-021-27393-3 (2021).

201. Aschenbrenner, J. & Marx, A. Direct and site-specific quantification of RNA 2'-O-methylation by PCR with an engineered DNA polymerase. *Nucleic Acids Research* **44,** 3495–3502; 10.1093/nar/gkw200 (2016).

202. Aschenbrenner, J. *et al.* Engineering of a DNA Polymerase for Direct m6A Sequencing. *Angewandte Chemie (International ed. in English)* **57,** 417–421; 10.1002/anie.201710209 (2018).

203. Huber, L. B. *et al.* A dual-purpose polymerase engineered for direct sequencing of pseudouridine and queuosine. *Nucleic Acids Research* **51,** 3971–3987; 10.1093/nar/gkad177 (2023).

204. Incarnato, D. *et al.* High-throughput single-base resolution mapping of RNA 2′-O-methylated residues. *Nucleic Acids Research* **45,** 1433–1441; 10.1093/nar/gkw810 (2017).

205. Edelheit, S., Schwartz, S., Mumbach, M. R., Wurtzel, O. & Sorek, R. Transcriptome-wide mapping of 5-methylcytidine RNA modifications in bacteria, archaea, and yeast reveals m5C within archaeal mRNAs. *Public Library of Science Genetics* **9,** e1003602; 10.1371/journal.pgen.1003602 (2013).

206. Schaefer, M., Pollex, T., Hanna, K. & Lyko, F. RNA cytosine methylation analysis by bisulfite sequencing. *Nucleic Acids Research* **37,** e12; 10.1093/nar/gkn954 (2009).

207. Dai, Q. *et al.* Ultrafast bisulfite sequencing detection of 5-methylcytosine in DNA and RNA. *Nature Biotechnology,* 1–12; 10.1038/s41587-023-02034-w (2024).

208. Lovejoy, A. F., Riordan, D. P. & Brown, P. O. Transcriptome-wide mapping of pseudouridines: pseudouridine synthases modify specific mRNAs in S. cerevisiae. *Public Library of Science One* **9,** e110799; 10.1371/journal.pone.0110799 (2014).

209. Chang, S. E. & Ish-Horowicz, D. Selective modification of cytidine, uridine, guanosine and pseudouridine residues in Escherichia coli leucine transfer ribonucleic acid. *Journal of Molecular Biology* **84,** 375–388; 10.1016/0022-2836(74)90446-X (1974).

210. Bakin, A. & Ofengand, J. Four newly located pseudouridylate residues in Escherichia coli 23S ribosomal RNA are all at the peptidyltransferase center: analysis by the application of a new sequencing technique. *Biochemistry* **32,** 9754–9762; 10.1021/bi00088a030 (1993).

211. Marchand, V., Bourguignon-Igel, V., Helm, M. & Motorin, Y. Analysis of pseudouridines and other RNA modifications using HydraPsiSeq protocol. *Methods (San Diego, Calif.)* **203,** 383–391; 10.1016/j.ymeth.2021.08.008 (2022).

212. Werner, S. *et al.* NOseq: amplicon sequencing evaluation method for RNA m6A sites after chemical deamination. *Nucleic Acids Research* **49,** e23; 10.1093/nar/gkaa1173 (2021).

213. Liu, C. *et al.* Absolute quantification of single-base m6A methylation in the mammalian transcriptome using GLORI. *Nature Biotechnology* **41,** 355–366; 10.1038/s41587-022-01487-9 (2023).

214. Finet, O., Yague-Sanz, C. & Hermand, D. Epitranscriptomic mapping of RNA modifications at single-nucleotide resolution using rhodamine sequencing (Rho-seq). *STAR Protocols* **3,** 101369; 10.1016/j.xpro.2022.101369 (2022).

215. Peattie, D. A. Direct chemical method for sequencing RNA. *Proceedings of the National Academy of Sciences of the United States of America* **76,** 1760–1764; 10.1073/pnas.76.4.1760 (1979).

216. Küpfer, P. A. & Leumann, C. J. The chemical stability of abasic RNA compared to abasic DNA. *Nucleic Acids Research* **35,** 58–68; 10.1093/nar/gkl948 (2007).

217. Zueva, V. S., Mankin, A. S., Bogdanov, A. A. & Baratova, L. A. Specific fragmentation of tRNA and rRNA at a 7-methylguanine residue in the presence of methylated carrier RNA. *European Journal of Biochemistry* **146,** 679–687; 10.1111/j.1432-1033.1985.tb08704.x (1985).

218. Marchand, V. *et al.* AlkAniline-Seq: Profiling of m7 G and m3 C RNA Modifications at Single Nucleotide Resolution. *Angewandte Chemie (International ed. in English)* **57,** 16785–16790; 10.1002/anie.201810946 (2018).

219. Marchand, V., Ayadi, L., Bourguignon-Igel, V., Helm, M. & Motorin, Y. AlkAniline-Seq: A Highly Sensitive and Specific Method for Simultaneous Mapping of 7-Methyl-guanosine (m7G) and 3-Methyl-cytosine (m3C) in RNAs by High-Throughput Sequencing. *Methods in Molecular Biology (Clifton, N.J.)* **2298,** 77–95; 10.1007/978-1-0716-1374-0_5 (2021).

220. Marchand, V., Bourguignon-Igel, V., Helm, M. & Motorin, Y. Mapping of 7-methylguanosine (m7G), 3-methylcytidine (m3C), dihydrouridine (D) and 5-hydroxycytidine (ho5C) RNA modifications by AlkAniline-Seq. *Methods in Enzymology* **658,** 25–47; 10.1016/bs.mie.2021.06.001 (2021).

221. Molinaro, M., Sheiner, L. B., Neelon, F. A. & Cantoni, G. L. Effect of Chemical Modification of Dihydrouridine in Yeast Transfer Ribonucleic Acid on Amino Acid Acceptor Activity and Ribosomal Binding. *The Journal of Biological Chemistry* **243,** 1277–1282; 10.1016/S0021-9258(19)56983-6 (1968).

222. Bhavsar, R. B., Makley, L. N. & Tsonis, P. A. The other lives of ribosomal proteins. *Human Genomics* **4,** 327–344; 10.1186/1479-7364-4-5-327 (2010).

223. Catalanotto, C., Barbato, C., Cogoni, C. & Benelli, D. The RNA-Binding Function of Ribosomal Proteins and Ribosome Biogenesis Factors in Human Health and Disease. *Biomedicines* **11**; 10.3390/biomedicines11112969 (2023).

224. Ramakrishnan, V. Ribosome structure and the mechanism of translation. *Cell* **108,** 557–572; 10.1016/S0092-8674(02)00619-0 (2002).

225. Kohler, R., Mooney, R. A., Mills, D. J., Landick, R. & Cramer, P. Architecture of a transcribing-translating expressome. *Science (New York, N.Y.)* **356,** 194–197; 10.1126/science.aal3059 (2017).

226. Rodnina, M. V. Translation in Prokaryotes. *Cold Spring Harbor Perspectives in Biology* **10**; 10.1101/cshperspect.a032664 (2018).

227. Grigoriadou, C., Marzi, S., Kirillov, S., Gualerzi, C. O. & Cooperman, B. S. A quantitative kinetic scheme for 70 S translation initiation complex formation. *Journal of Molecular Biology* **373,** 562–572; 10.1016/j.jmb.2007.07.032 (2007).

228. Allen, G. S., Zavialov, A., Gursky, R., Ehrenberg, M. & Frank, J. The cryo-EM structure of a translation initiation complex from Escherichia coli. *Cell* **121,** 703–712; 10.1016/j.cell.2005.03.023 (2005).

229. Fabbretti, A. *et al.* The real-time path of translation factor IF3 onto and off the ribosome. *Molecular Cell* **25,** 285–296; 10.1016/j.molcel.2006.12.011 (2007).

230. Ibba, M. & Soll, D. Aminoacyl-tRNA synthesis. *Annual Review of Biochemistry* **69,** 617–650; 10.1146/annurev.biochem.69.1.617 (2000).

231. Agris, P. F. Bringing order to translation: the contributions of transfer RNA anticodon-domain modifications. *European Molecular Biology Organization Reports* **9,** 629–635; 10.1038/embor.2008.104 (2008).

232. Fukunaga, R. & Yokoyama, S. Aminoacylation complex structures of leucyl-tRNA synthetase and tRNALeu reveal two modes of discriminator-base recognition. *Nature Structural & Molecular Biology* **12,** 915–922; 10.1038/nsmb985 (2005).

233. Ogle, J. M. *et al.* Recognition of cognate transfer RNA by the 30S ribosomal subunit. *Science (New York, N.Y.)* **292,** 897–902; 10.1126/science.1060612 (2001).

234. Rodnina, M. V., Pape, T., Fricke, R., Kuhn, L. & Wintermeyer, W. Initial binding of the elongation factor Tu.GTP.aminoacyl-tRNA complex preceding codon recognition on the ribosome. *Journal of Biological Chemistry* **271,** 646–652; 10.1074/jbc.271.2.646 (1996).

235. Voorhees, R. M. & Ramakrishnan, V. Structural basis of the translational elongation cycle. *Annual Review of Biochemistry* **82,** 203–236; 10.1146/annurev-biochem-113009-092313 (2013).

236. Kothe, U., Wieden, H.-J., Mohr, D. & Rodnina, M. V. Interaction of helix D of elongation factor Tu with helices 4 and 5 of protein L7/12 on the ribosome. *Journal of Molecular Biology* **336,** 1011–1021; 10.1016/j.jmb.2003.12.080 (2004).

237. Gromadski, K. B. & Rodnina, M. V. Kinetic determinants of high-fidelity tRNA discrimination on the ribosome. *Molecular Cell* **13,** 191–200; 10.1016/s1097-2765(04)00005-x (2004).

238. Voorhees, R. M., Schmeing, T. M., Kelley, A. C. & Ramakrishnan, V. The mechanism for activation of GTP hydrolysis on the ribosome. *Science (New York, N.Y.)* **330,** 835–838; 10.1126/science.1194460 (2010).

239. Pang, L., Weeks, S. D. & van Aerschot, A. Aminoacyl-tRNA Synthetases as Valuable Targets for Antimicrobial Drug Discovery. *International Journal of Molecular Sciences* **22**; 10.3390/ijms22041750 (2021).

240. Voss, N. R., Gerstein, M., Steitz, T. A. & Moore, P. B. The geometry of the ribosomal polypeptide exit tunnel. *Journal of Molecular Biology* **360,** 893–906; 10.1016/j.jmb.2006.05.023 (2006).

241. Gong, F. & Yanofsky, C. Instruction of translating ribosome by nascent peptide. *Science (New York, N.Y.)* **297,** 1864–1867; 10.1126/science.1073997 (2002).

242. Seixas, A. F. *et al.* Bacterial Response to Oxidative Stress and RNA Oxidation. *Frontiers in Genetics* **12,** 821535; 10.3389/fgene.2021.821535 (2021).

243. Dubbs, J. M. & Mongkolsuk, S. Peroxide-sensing transcriptional regulators in bacteria. *Journal of Bacteriology* **194,** 5495–5503; 10.1128/jb.00304-12 (2012).

244. Fasnacht, M. & Polacek, N. Oxidative Stress in Bacteria and the Central Dogma of Molecular Biology. *Frontiers in Molecular Biosciences* **8,** 671037; 10.3389/fmolb.2021.671037 (2021).

245. Farr, S. B., Natvig, D. O. & Kogoma, T. Toxicity and mutagenicity of plumbagin and the induction of a possible new DNA repair pathway in Escherichia coli. *Journal of Bacteriology* **164,** 1309–1316; 10.1128/jb.164.3.1309-1316.1985 (1985).

246. Hassan, H. M. & Fridovich, I. Intracellular production of superoxide radical and of hydrogen peroxide by redox active compounds. *Archives of Biochemistry and Biophysics* **196,** 385–395; 10.1016/0003-9861(79)90289-3 (1979).

247. Farr, S. B. & Kogoma, T. Oxidative stress responses in Escherichia coli and Salmonella typhimurium. *Microbiological Reviews* **55,** 561–585; 10.1128/mr.55.4.561-585.1991 (1991).

248. Imlay, J. A. & Fridovich, I. Assay of metabolic superoxide production in Escherichia coli. *Journal of Biological Chemistry* **266,** 6957–6965; 10.1016/S0021-9258(20)89596-9 (1991).

249. Turrens, J. F. & Boveris, A. Generation of superoxide anion by the NADH dehydrogenase of bovine heart mitochondria. *The Biochemical Journal* **191,** 421–427; 10.1042/bj1910421 (1980).

250. Fridovich, I. Superoxide dismutases. *Journal of Biological Chemistry* **264,** 7761–7764; 10.1016/S0021-9258(18)83102-7 (1989).

251. Fenton, H. J. H. LXXIII.—Oxidation of tartaric acid in presence of iron. *Journal of the Chemical Society, Transactions* **65,** 899–910; 10.1039/CT8946500899 (1894).

252. Walling, C. Fenton's reagent revisited. *Accounts of Chemical Research* **8,** 125–131; 10.1021/ar50088a003 (1975).

253. Kremer, M. L. Mechanism of the Fenton reaction. Evidence for a new intermediate. *Physical Chemistry Chemical Physics* **1,** 3595–3605; 10.1039/a903915e (1999).

254. Reiter, R. J. *et al.* A review of the evidence supporting melatonin's role as an antioxidant. *Journal of Pineal Research* **18,** 1–11; 10.1111/j.1600-079x.1995.tb00133.x (1995).

255. Dalle-Donne, I. *et al.* Protein carbonylation, cellular dysfunction, and disease progression. *Journal of Cellular and Molecular Medicine* **10,** 389–406; 10.1111/j.1582-4934.2006.tb00407.x (2006).

256. Morzel, M., Gatellier, P., Sayd, T., Renerre, M. & Laville, E. Chemical oxidation decreases proteolytic susceptibility of skeletal muscle myofibrillar proteins. *Meat Science* **73,** 536–543; 10.1016/j.meatsci.2006.02.005 (2006).

257. Dobretsov, G. E., Borschevskaya, T. A., Petrov, V. A. & Vladimirov, Y. A. The increase of phospholipid bilayer rigidity after lipid peroxidation. *Federation of European Biochemical Society Letters* **84,** 125–128; 10.1016/0014-5793(77)81071-5 (1977).

258. Niki, E. Lipid peroxidation: physiological levels and dual biological effects. *Free Radical Biology & Medicine* **47,** 469–484; 10.1016/j.freeradbiomed.2009.05.032 (2009).

259. Su, L.-J. *et al.* Reactive Oxygen Species-Induced Lipid Peroxidation in Apoptosis, Autophagy, and Ferroptosis. *Oxidative Medicine and Cellular Longevity* **2019,** 5080843; 10.1155/2019/5080843 (2019).

260. Simms, C. L. & Zaher, H. S. Quality control of chemically damaged RNA. *Cellular and Molecular Life Sciences* **73,** 3639–3653; 10.1007/s00018-016-2261-7 (2016).

261. Lee, T.-H. & Kang, T.-H. DNA Oxidation and Excision Repair Pathways. *International Journal of Molecular Sciences* **20**; 10.3390/ijms20236092 (2019).

262. Malla, S. & Kwakye, A. RNA oxidation: Role of polynucleotide phosphorylase in the quality control of oxidized RNA. *Journal of Life Sciences* **3,** 43-60; 10.36069/jols/20210603 (2021).

263. Li, Z. *et al.* Recent Advances: Molecular Mechanism of RNA Oxidation and Its Role in Various Diseases. *Frontiers in Molecular Biosciences* **7,** 184; 10.3389/fmolb.2020.00184 (2020).

264. Nunomura, A. *et al.* RNA oxidation is a prominent feature of vulnerable neurons in Alzheimer's disease. *The Journal of Neuroscience* **19,** 1959–1964; 10.1523/JNEUROSCI.19-06-01959.1999 (1999).

265. Zhang, J. *et al.* Parkinson's disease is associated with oxidative damage to cytoplasmic DNA and RNA in substantia nigra neurons. *The American Journal of Pathology* **154,** 1423–1429; 10.1016/S0002-9440(10)65396-5 (1999).

266. Willi, J. *et al.* Oxidative stress damages rRNA inside the ribosome and differentially affects the catalytic center. *Nucleic Acids Research* **46,** 1945–1957; 10.1093/nar/gkx1308 (2018).

267. Estevez, M., Valesyan, S., Jora, M., Limbach, P. A. & Addepalli, B. Oxidative Damage to RNA is Altered by the Presence of Interacting Proteins or Modified Nucleosides. *Frontiers in Molecular Biosciences* **8,** 697149; 10.3389/fmolb.2021.697149 (2021).

268. Leiva, L. E. *et al.* Modulation of Escherichia coli Translation by the Specific Inactivation of tRNAGly Under Oxidative Stress. *Frontiers in Genetics* **11,** 856; 10.3389/fgene.2020.00856 (2020).

269. Leiva, L. E. *et al.* Oxidative stress strongly restricts the effect of codon choice on the efficiency of protein synthesis in Escherichia coli. *Frontiers in Microbiology* **13,** 1042675; 10.3389/fmicb.2022.1042675 (2022).

270. Steenken, S. & Jovanovic, S. V. How Easily Oxidizable Is DNA? One-Electron Reduction Potentials of Adenosine and Guanosine Radicals in Aqueous Solution. *Journal of the American Chemical Society* **119,** 617–618; 10.1021/ja962255b (1997).

271. Radak, Z. & Boldogh, I. 8-Oxo-7,8-dihydroguanine: links to gene expression, aging, and defense against oxidative stress. *Free Radical Biology & Medicine* **49,** 587–596; 10.1016/j.freeradbiomed.2010.05.008 (2010).

272. Simms, C. L., Hudson, B. H., Mosior, J. W., Rangwala, A. S. & Zaher, H. S. An active role for the ribosome in determining the fate of oxidized mRNA. *Cell Reports* **9,** 1256–1264; 10.1016/j.celrep.2014.10.042 (2014).

273. Thomas, E. N., Simms, C. L., Keedy, H. E. & Zaher, H. S. Insights into the base-pairing preferences of 8-oxoguanosine on the ribosome. *Nucleic Acids Research* **47,** 9857–9870; 10.1093/nar/gkz701 (2019).

274. Taddei, F. *et al.* Counteraction by MutT protein of transcriptional errors caused by oxidative damage. *Science (New York, N.Y.)* **278,** 128–130; 10.1126/science.278.5335.128 (1997).

275. Patil, A. G. G., Sang, P. B., Govindan, A. & Varshney, U. Mycobacterium tuberculosis MutT1 (Rv2985) and ADPRase (Rv1700) proteins constitute a two-stage mechanism of 8-oxo-dGTP and 8-oxo-GTP detoxification and adenosine to cytidine mutation avoidance. *The Journal of Biological Chemistry* **288,** 11252–11262; 10.1074/jbc.M112.442566 (2013).

276. Hayakawa, H., Kuwano, M. & Sekiguchi, M. Specific binding of 8-oxoguanine-containing RNA to polynucleotide phosphorylase protein. *Biochemistry* **40,** 9977–9982; 10.1021/bi010595q (2001).

277. Wu, J. *et al.* Polynucleotide phosphorylase protects Escherichia coli against oxidative stress. *Biochemistry* **48,** 2012–2020; 10.1021/bi801752p (2009).

278. Hayakawa, H. *et al.* Binding capacity of human YB-1 protein for RNA containing 8-oxoguanine. *Biochemistry* **41,** 12739–12744; 10.1021/bi0201872 (2002).

279. Seaver, L. C. & Imlay, J. A. Hydrogen peroxide fluxes and compartmentalization inside growing Escherichia coli. *Journal of Bacteriology* **183,** 7182–7189; 10.1128/JB.183.24.7182-7189.2001 (2001).

280. Steinman, H. M. Bacterial superoxide dismutases. *Basic Life Sciences* **49,** 641–646; 10.1007/978-1-4684-5568-7_101 (1988).

281. Partridge, J. D., Poole, R. K. & Green, J. The Escherichia coli yhjA gene, encoding a predicted cytochrome c peroxidase, is regulated by FNR and OxyR. *Microbiology (Reading, England)* **153,** 1499–1509; 10.1099/mic.0.2006/004838-0 (2007).

282. Khademian, M. & Imlay, J. A. Escherichia coli cytochrome c peroxidase is a respiratory oxidase that enables the use of hydrogen peroxide as a terminal electron acceptor. *Proceedings of the National Academy of Sciences of the United States of America* **114,** E6922-E6931; 10.1073/pnas.1701587114 (2017).

283. Day, B. J., Patel, M., Calavetta, L., Chang, L. Y. & Stamler, J. S. A mechanism of paraquat toxicity involving nitric oxide synthase. *Proceedings of the National Academy of Sciences of the United States of America* **96,** 12760–12765; 10.1073/pnas.96.22.12760 (1999).

284. Clejan, L. A. & Cederbaum, A. I. Stimulation by paraquat of microsomal and cytochrome P-450-dependent oxidation of glycerol to formaldehyde. *The Biochemical Journal* **295 (Pt 3),** 781–786; 10.1042/bj2950781 (1993).

285. Gray, J. P. *et al.* Paraquat increases cyanide-insensitive respiration in murine lung epithelial cells by activating an NAD(P)H:paraquat oxidoreductase: identification of the

enzyme as thioredoxin reductase. *The Journal of Biological Chemistry* **282,** 7939–7949; 10.1074/jbc.M611817200 (2007).

286. Smith, L. L., Rose, M. S. & Wyatt, I. The pathology and biochemistry of paraquat. *Ciba Foundation Symposium,* 321–341; 10.1002/9780470715413.ch18 (1978).

287. Bismuth, C., Garnier, R., Baud, F. J., Muszynski, J. & Keyes, C. Paraquat poisoning. An overview of the current status. *Drug-Safety* **5,** 243–251; 10.2165/00002018-199005040-00002 (1990).

288. Yang, H. *et al.* LncRNA NR_030777 Alleviates Paraquat-Induced Neurotoxicity by Regulating Zfp326 and Cpne5. *Toxicological Sciences* **178,** 173–188; 10.1093/toxsci/kfaa121 (2020).

289. Xiong, G. *et al.* Single-cell RNA sequencing reveals adverse effects of paraquat on the fate commitment of murine neural stem cells. *Science of The Total Environment* **785,** 147386; 10.1016/j.scitotenv.2021.147386 (2021).

290. Chen, N. *et al.* Paraquat-induced oxidative stress regulates N6-methyladenosine (m6A) modification of circular RNAs. *Environmental Pollution (Barking, Essex : 1987)* **290,** 117816; 10.1016/j.envpol.2021.117816 (2021).

291. Kawai, S. & Murata, K. Structure and function of NAD kinase and NADP phosphatase: key enzymes that regulate the intracellular balance of NAD(H) and NADP(H). *Bioscience, Biotechnology, and Biochemistry* **72,** 919–930; 10.1271/bbb.70738 (2008).

292. Spaans, S. K., Weusthuis, R. A., van der Oost, J. & Kengen, S. W. M. NADPH-generating systems in bacteria and archaea. *Frontiers in Microbiology* **6,** 742; 10.3389/fmicb.2015.00742 (2015).

293. Singh, R., Lemire, J., Mailloux, R. J. & Appanna, V. D. A novel strategy involved in corrected anti-oxidative defense: the conversion of NADH into NADPH by a metabolic network. *Public Library of Science One* **3,** e2682; 10.1371/journal.pone.0002682 (2008).

294. Barbusinski, K. Fenton reaction-controversy concerning the chemistry. *Ecological Chemistry Engineering S* **16,** 347-358 (2009).

295. Kitzler, J. W., Minakami, H. & Fridovich, I. Effects of paraquat on Escherichia coli: differences between B and K-12 strains. *Journal of Bacteriology* **172,** 686–690; 10.1128/jb.172.2.686-690.1990 (1990).

296. El Yacoubi, B., Bailly, M. & Crécy-Lagard, V. de. Biosynthesis and function of posttranscriptional modifications of transfer RNAs. *Annual Review of Genetics* **46,** 69–95; 10.1146/annurev-genet-110711-155641 (2012).

297. Hartstock, K. *et al.* MePMe-seq: antibody-free simultaneous m6A and m5C mapping in mRNA by metabolic propargyl labeling and sequencing. *Nature Communications* **14,** 7154; 10.1038/s41467-023-42832-z (2023).

298. Shu, X. *et al.* A metabolic labeling method detects m6A transcriptome-wide at single base resolution. *Nature Chemical Biology* **16,** 887–895; 10.1038/s41589-020-0526-9 (2020).

299. Galvanin, A. *et al.* Bacterial tRNA 2'-O-methylation is dynamically regulated under stress conditions and modulates innate immune response. *Nucleic Acids Research* **48,** 12833–12844; 10.1093/nar/gkaa1123 (2020).

300. Bednářová, A. *et al.* Lost in Translation: Defects in Transfer RNA Modifications and Neurological Disorders. *Frontiers in Molecular Neuroscience* **10,** 135; 10.3389/fnmol.2017.00135 (2017).

301. Skolnick, S. D. & Greig, N. H. Microbes and Monoamines: Potential Neuropsychiatric Consequences of Dysbiosis. *Trends in Neurosciences* **42,** 151–163; 10.1016/j.tins.2018.12.005 (2019).

302. Faivre, B. *et al.* Dihydrouridine synthesis in tRNAs is under reductive evolution in Mollicutes. *RNA Biology* **18,** 2278–2289; 10.1080/15476286.2021.1899653 (2021).

303. Bolger, A. M., Lohse, M. & Usadel, B. Trimmomatic: a flexible trimmer for Illumina sequence data. *Bioinformatics (Oxford, England)* **30,** 2114–2120; 10.1093/bioinformatics/btu170 (2014).

304. Marchand, V. *et al.* Next-Generation Sequencing-Based RiboMethSeq Protocol for Analysis of tRNA 2'-O-Methylation. *Biomolecules* **7**; 10.3390/biom7010013 (2017).

Appendix

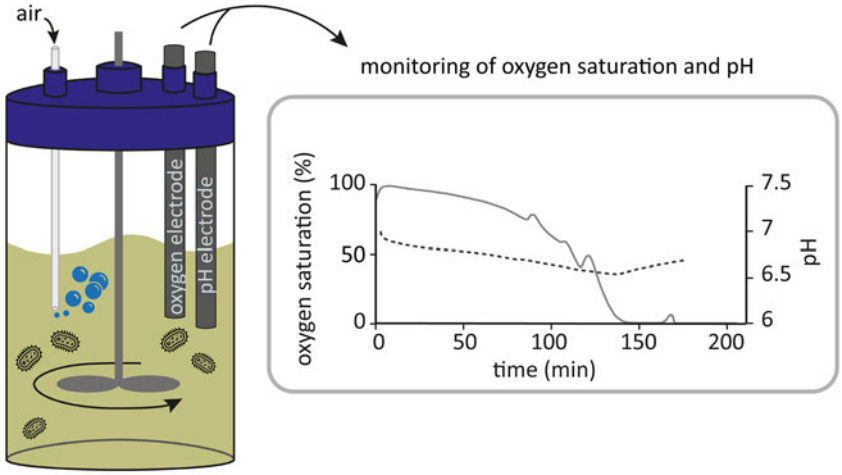

Figure A1: Monitoring of oxygen saturation and pH during bacterial growth. The attachment of oxygen and pH electrodes to the bioreactor allowed to continuously monitor the oxygen saturation (grey solid line) and the pH value (grey, dashed line) of the culture medium. Monitoring of a wildtype culture grown under aerobic conditions is shown.

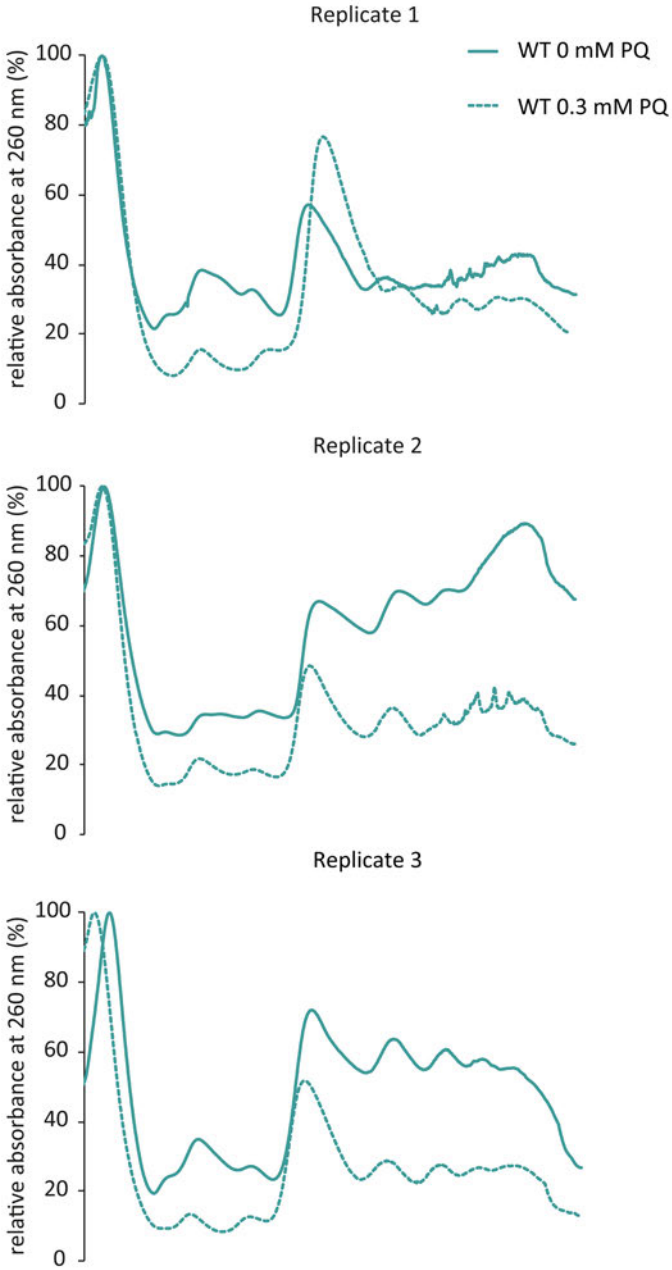

Figure A2: Absorbance curves during polysome preparations of wildtype cultures. The absorbance at 260 nm during fractionation was normalised to the first eluting peak corresponding to the free RNA fraction which was set to 100%. Absorbance curves of untreated (bluish green solid lines) and treated (0.3 mM PQ, bluish green dashed lines) wildtype cultures are shown for three biological replicates.

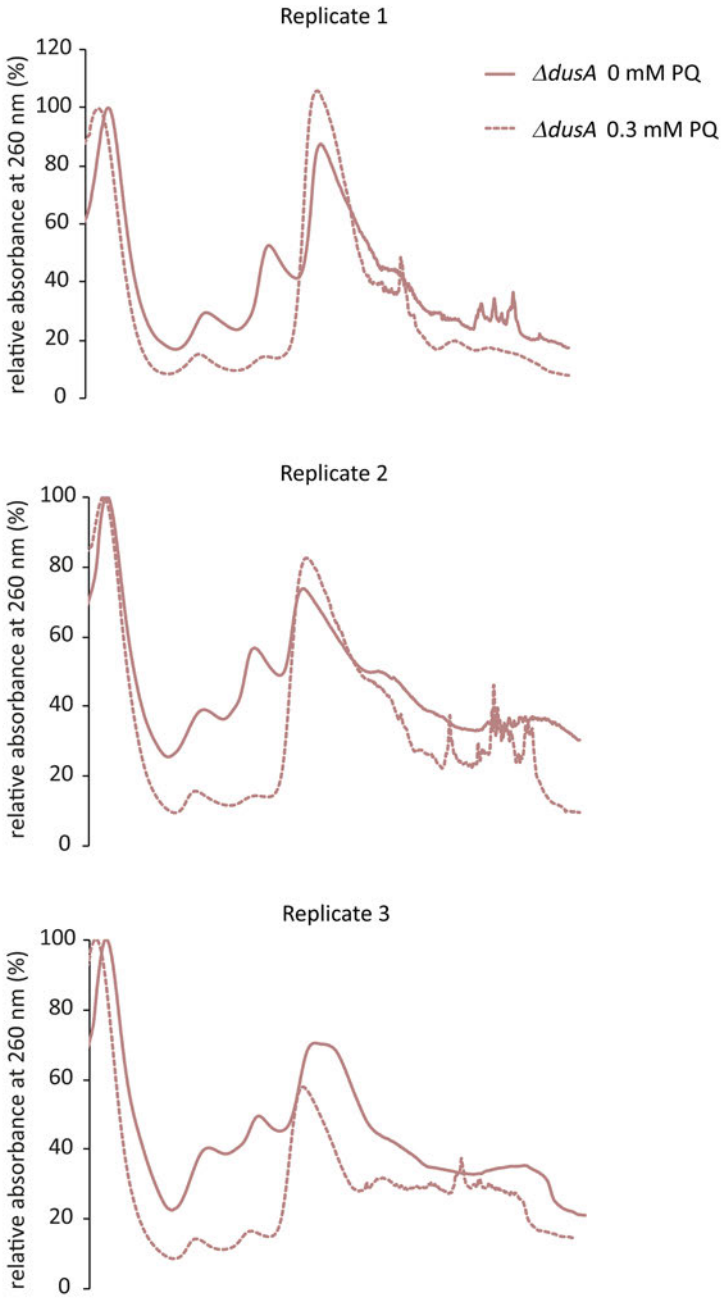

Figure A3: Absorbance curves during polysome preparations of DusA knockout cultures. The absorbance at 260 nm during fractionation was normalised to the first eluting peak corresponding to the free RNA fraction which was set to 100%. Absorbance curves of untreated (rose solid lines) and treated (0.3 mM PQ, rose dashed lines) *ΔdusA* cultures are shown for three biological replicates.

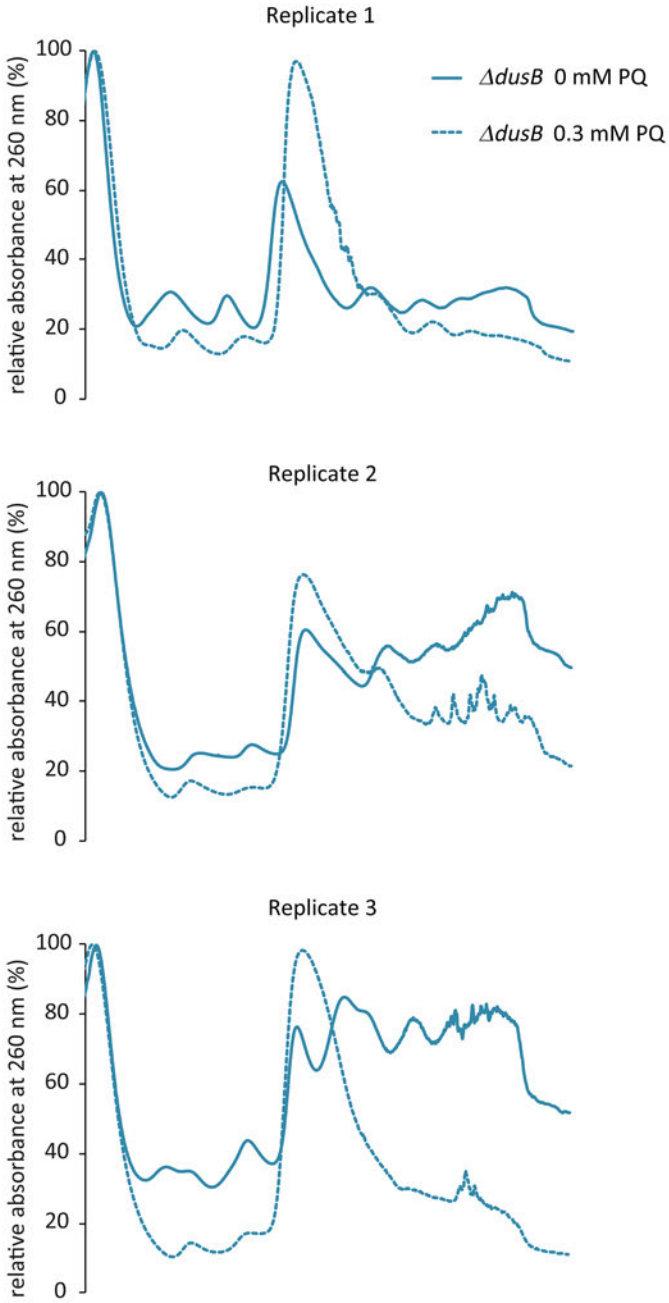

Figure A4: Absorbance curves during polysome preparations of DusB knockout cultures. The absorbance at 260 nm during fractionation was normalised to the first eluting peak corresponding to the free RNA fraction which was set to 100%. Absorbance curves of untreated (blue solid lines) and treated (0.3 mM PQ, blue dashed lines) *ΔdusB* cultures are shown for three biological replicates.

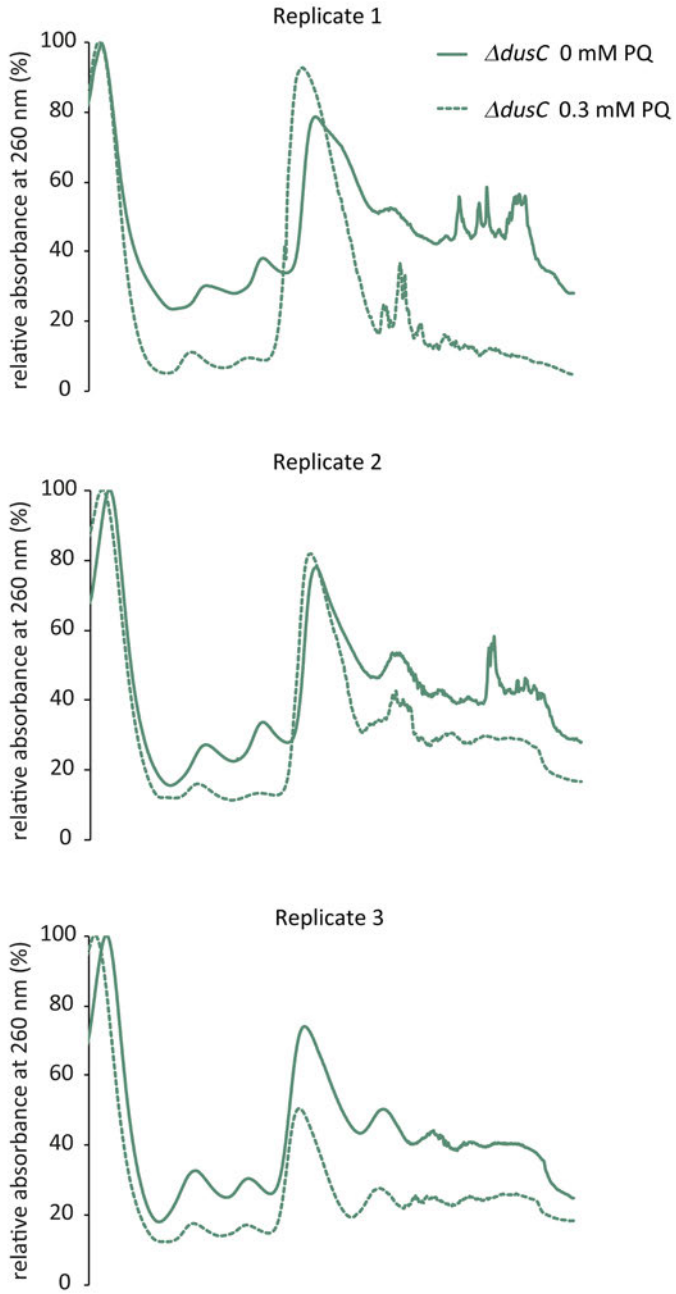

Figure A5: Absorbance curves during polysome preparations of DusC knockout cultures. The absorbance at 260 nm during fractionation was normalised to the first eluting peak corresponding to the free RNA fraction which was set to 100%. Absorbance curves of untreated (green solid lines) and treated (0.3 mM PQ, green dashed lines) *ΔdusC* cultures are shown for three biological replicates.

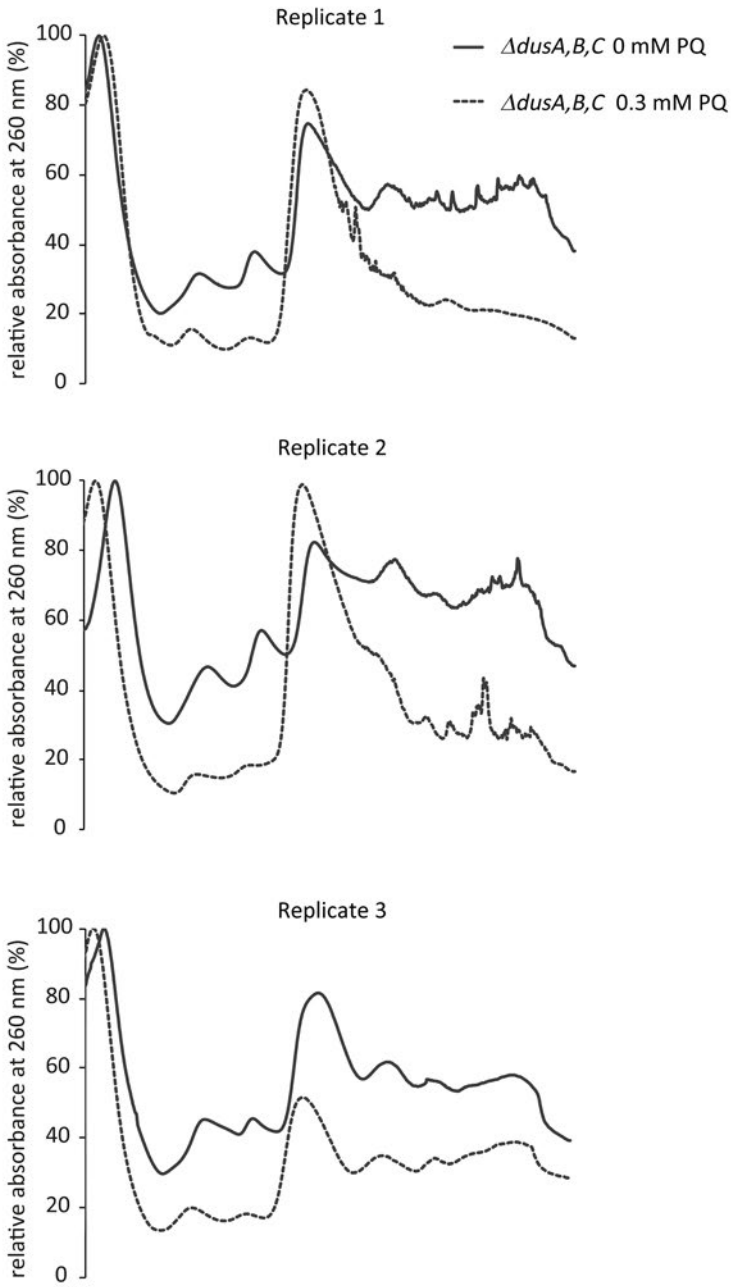

Figure A6: Absorbance curves during polysome preparations of triple knockout cultures. The absorbance at 260 nm during fractionation was normalised to the first eluting peak corresponding to the free RNA fraction which was set to 100%. Absorbance curves of untreated (black solid lines) and treated (0.3 mM PQ, black dashed lines) *ΔdusA,B,C* cultures are shown for three biological replicates.

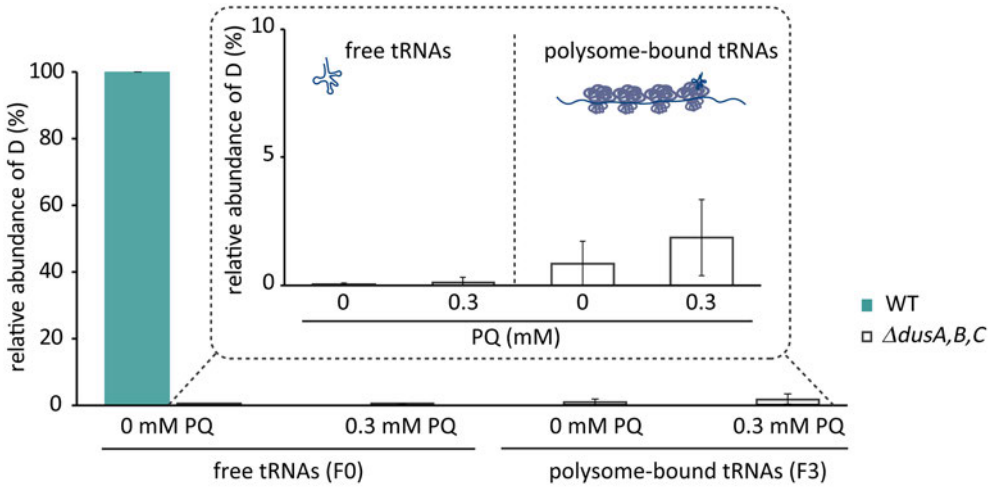

Figure A7: LC-MS/MS analysis of D modification levels in polysome-bound tRNAs. D levels in free tRNAs (F0) and polysome-bound tRNAs (F3) isolated from the untreated wildtype culture (bluish green) and treated and untreated triple Dus knockout cultures (*ΔdusA,B,C*, framed in grey). The detected signals with the mass transition *m/z* = 247 → 115 corresponding to D were normalised to the respective UV signal of adenosine and the normalised signals were related to the normalised D signal detected in the free tRNA fraction isolated from the untreated wildtype culture (WT 0 mM PQ F0). Results are shown as average of biological triplicates, the standard deviations are indicated as error bars.


F0: free tRNAs
F3: polysome-bound tRNAs
WT
ΔdusA
ΔdusB
ΔdusC
ΔdusA,B,C
0
0.3
PQ (mM)
F0 F3
no.
ec_tRNAArg_ACG-D20a/DusA
ec_tRNAArg_TCT-D20a/DusA
ec_tRNAAsn_GTT-D20/DusA
ec_tRNAAsp_GTC-D20/DusA
ec_tRNAAsp_GTC-D20a/DusA
ec_tRNACys_GCA-D20/DusA
ec_tRNACys_GCA-D20a/DusA
ec_tRNAGln_CTG_TTG-D20/DusA
ec_tRNAGly_CCC-D20/DusA
ec_tRNAGly_GCC-D20/DusA
ec_tRNAHis_GTG-D20/DusA
ec_tRNAIle_CAT-D20/DusA
ec_tRNAIle_CAT-D20a/DusA
ec_tRNAIle_GAT-D20/DusA
ec_tRNAIle_GAT-D20a/DusA
ec_tRNAiMet_CAT-D20/DusA
ec_tRNALeu_CAA-D20/DusA
ec_tRNALeu_CAG-D20/DusA
ec_tRNALeu_GAG-D20/DusA
ec_tRNALeu_TAA-D20/DusA
ec_tRNALeu_TAG-D20/DusA
ec_tRNAMet_CAT-D20/DusA
ec_tRNAMet_CAT-D20a/DusA
ec_tRNAPhe_GAA-D20/DusA
ec_tRNAPro_CGG-D20/DusA
ec_tRNAPro_GGG-D20/DusA
ec_tRNAPro_TGG-D20/DusA
ec_tRNASer_CGA-D20a/DusA
ec_tRNASer_GCT-D20a/DusA
ec_tRNASer_GGA-D20/DusA
ec_tRNASer_TGA-D20/DusA
ec_tRNASer_TGA-D20a/DusA
ec_tRNAThr_CGT1-D20/DusA
ec_tRNAThr_GGT-D20/DusA
ec_tRNAThr_TGT-D20/DusA
ec_tRNATrp_CCA-D20/DusA
ec_tRNAVal_GAC-D20/DusA
ec_tRNAVal_GAC-D20a/DusA
ec_tRNAAla_GGC_TGC-D17/DusB
ec_tRNAArg_ACG-D17/DusB
ec_tRNAGly_GCC-D17/DusB
ec_tRNAHis_GTG-D17/DusB
ec_tRNAIle_GAT-D17/DusB
ec_tRNALeu_CAG-D17/DusB
ec_tRNALeu_GAG-D17/DusB
ec_tRNALeu_TAG-D17/DusB
ec_tRNALys_TTT-D17/DusB
ec_tRNAMet_CAT-D17/DusB
ec_tRNAPro_TGG-D17/DusB
ec_tRNAThr_CGT1-D17/DusB
ec_tRNAThr_GGT-D17/DusB
ec_tRNATrp_CCA-D17/DusB
ec_tRNAVal_GAC-D17/DusB
ec_tRNAVal_TAC-D17/DusB
ec_tRNAAsn_GTT-D16/DusC
ec_tRNAAsp_GTC-D16/DusC
ec_tRNAGly_GCC-D16/DusC
ec_tRNAHis_GTG-D16/DusC
ec_tRNALeu_CAA-D16/DusC
ec_tRNALeu_CAG-D16/DusC
ec_tRNALeu_GAG-D16/DusC
ec_tRNALeu_TAA-D16/DusC
ec_tRNALeu_TAG-D16/DusC
ec_tRNALys_TTT-D16/DusC
ec_tRNAMet_CAT-D16/DusC
ec_tRNAPhe_GAA-D16/DusC
ec_tRNAThr_CGT1-D16/DusC
ec_tRNAThr_GGT-D16/DusC
ec_tRNAThr_TGT-D16/DusC
ec_tRNATrp_CCA-D16/DusC
ec_tRNAVal_GAC-D16/DusC
1
2
3
4
5
6
7
8
9
10
11
12
13
14
15
16
17
18
19
20
21
22
23
24
25
26
27
28
29
30
31
32
33
34
35
36
37
38
39
40
41
42
43
44
45
46
47
48
49
50
51
52
53
54
55
56
57
58
59
60
61
62
63
64
65
66
67
68
69
70
71
DusA
DusB
DusC
Colour Key and Histogram
Count
250
200
150
100
50
0
0
0.4
0.8
Value

Figure A8: Analysis of polysome-bound tRNAs by AlkAniline sequencing. Stop ratio score (ranging from 0 to 1) of signals detected in cytosolic (F0) and polysome-bound (F3) tRNA fractions isolated from non-treated and treated (0.3 mM PQ) wildtype and Dus knockout cultures. The various tRNAs and the corresponding D positions are shown on the left with the following code: organism_tRNA species_anticodon – position of D / modifying enzyme, while the numbering of tRNAs and modifying enzymes are indicated on the right (correspond to the numbering in Figure 19). Results of one of three biological replicates are shown.


F0: free tRNAs
F3: polysome-bound tRNAs
WT
ΔdusA
ΔdusB
ΔdusC
ΔdusA,B,C
0
0.3
PQ (mM)
F0 F3
no.
ec_tRNAArg_ACG-D20a/DusA
ec_tRNAArg_TCT-D20a/DusA
ec_tRNAAsn_GTT-D20/DusA
ec_tRNAAsp_GTC-D20/DusA
ec_tRNAAsp_GTC-D20a/DusA
ec_tRNACys_GCA-D20/DusA
ec_tRNACys_GCA-D20a/DusA
ec_tRNAGln_CTG_TTG-D20/DusA
ec_tRNAGly_CCC-D20/DusA
ec_tRNAGly_GCC-D20/DusA
ec_tRNAHis_GTG-D20/DusA
ec_tRNAIle_CAT-D20/DusA
ec_tRNAIle_CAT-D20a/DusA
ec_tRNAIle_GAT-D20/DusA
ec_tRNAIle_GAT-D20a/DusA
ec_tRNAiMet_CAT-D20/DusA
ec_tRNALeu_CAA-D20/DusA
ec_tRNALeu_CAG-D20/DusA
ec_tRNALeu_GAG-D20/DusA
ec_tRNALeu_TAA-D20/DusA
ec_tRNALeu_TAG-D20/DusA
ec_tRNAMet_CAT-D20/DusA
ec_tRNAMet_CAT-D20a/DusA
ec_tRNAPhe_GAA-D20/DusA
ec_tRNAPro_CGG-D20/DusA
ec_tRNAPro_GGG-D20/DusA
ec_tRNAPro_TGG-D20/DusA
ec_tRNASer_CGA-D20a/DusA
ec_tRNASer_GCT-D20a/DusA
ec_tRNASer_GGA-D20/DusA
ec_tRNASer_TGA-D20/DusA
ec_tRNASer_TGA-D20a/DusA
ec_tRNAThr_CGT1-D20/DusA
ec_tRNAThr_GGT-D20/DusA
ec_tRNAThr_TGT-D20/DusA
ec_tRNATrp_CCA-D20/DusA
ec_tRNAVal_GAC-D20/DusA
ec_tRNAVal_GAC-D20a/DusA
ec_tRNAAla_GGC_TGC-D17/DusB
ec_tRNAArg_ACG-D17/DusB
ec_tRNAGly_GCC-D17/DusB
ec_tRNAHis_GTG-D17/DusB
ec_tRNAIle_GAT-D17/DusB
ec_tRNALeu_CAG-D17/DusB
ec_tRNALeu_GAG-D17/DusB
ec_tRNALeu_TAG-D17/DusB
ec_tRNALys_TTT-D17/DusB
ec_tRNAMet_CAT-D17/DusB
ec_tRNAPro_TGG-D17/DusB
ec_tRNAThr_CGT1-D17/DusB
ec_tRNAThr_GGT-D17/DusB
ec_tRNATrp_CCA-D17/DusB
ec_tRNAVal_GAC-D17/DusB
ec_tRNAVal_TAC-D17/DusB
ec_tRNAAsn_GTT-D16/DusC
ec_tRNAAsp_GTC-D16/DusC
ec_tRNAGly_GCC-D16/DusC
ec_tRNAHis_GTG-D16/DusC
ec_tRNALeu_CAA-D16/DusC
ec_tRNALeu_CAG-D16/DusC
ec_tRNALeu_GAG-D16/DusC
ec_tRNALeu_TAA-D16/DusC
ec_tRNALeu_TAG-D16/DusC
ec_tRNALys_TTT-D16/DusC
ec_tRNAMet_CAT-D16/DusC
ec_tRNAPhe_GAA-D16/DusC
ec_tRNAThr_CGT1-D16/DusC
ec_tRNAThr_GGT-D16/DusC
ec_tRNAThr_TGT-D16/DusC
ec_tRNATrp_CCA-D16/DusC
ec_tRNAVal_GAC-D16/DusC
1 2 3 4 5 6 7 8 9 10 11 12 13 14 15 16 17 18 19 20 21 22 23 24 25 26 27 28 29 30 31 32 33 34 35 36 37 38 39 40 41 42 43 44 45 46 47 48 49 50 51 52 53 54 55 56 57 58 59 60 61 62 63 64 65 66 67 68 69 70 71
DusA
DusB
DusC
Colour Key and Histogram
Count
250
200
150
100
50
0
0 0.4 0.8
Value

Figure A9: Analysis of polysome-bound tRNAs by AlkAniline sequencing. Stop ratio score (ranging from 0 to 1) of signals detected in cytosolic (F0) and polysome-bound (F3) tRNA fractions isolated from non-treated and treated (0.3 mM PQ) wildtype and Dus knockout cultures. The various tRNAs and the corresponding D positions are shown on the left with the following code: organism_tRNA species_anticodon – position of D / modifying enzyme, while the numbering of tRNAs and modifying enzymes are indicated on the right (correspond to the numbering in Figure 19). Results of one of three biological replicates are shown.

Curriculum Vitae

[redacted]

[redacted]

[redacted]